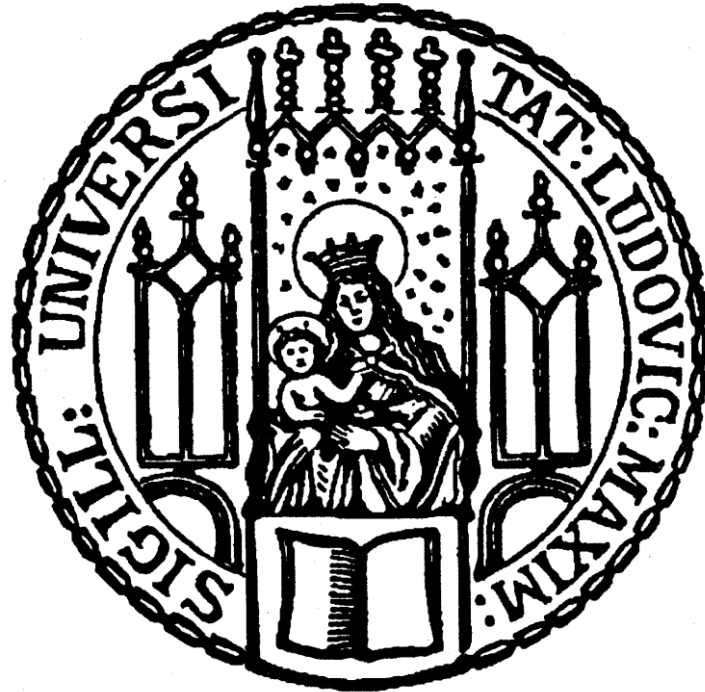


# Enhancing the Resolution of Cohesin Dynamics in Meiosis



Dissertation der Fakultät für Biologie  
der Ludwig-Maximilians-Universität München

Peter Andreas Graf

Mai 2018



Diese Dissertation wurde angefertigt  
unter der Leitung von Dr. Wolfgang Zachariae  
in der Arbeitsgruppe Chromosomenbiologie  
am Max-Planck-Institut für Biochemie in Martinsried, Deutschland.

1. Gutachter: Prof. Dr. Marc Bramkamp
2. Gutachter: Prof. Dr. Peter Becker
3. Gutachter: Prof. Dr. Christof Osman
4. Gutachter: Prof. Dr. Barbara Conradt
5. Gutachter: Prof. Dr. Nicolas Gompel
6. Gutachter: Prof. Dr. Michael Boshart

Tag der Abgabe: 15.05.2018

Tag der mündlichen Prüfung: 27.09.2018

## ERKLÄRUNG

Ich versichere hiermit an Eides statt, dass meine Dissertation selbständig und ohne unerlaubte Hilfsmittel angefertigt worden ist.

Die vorliegende Dissertation wurde weder ganz, noch teilweise bei einer anderen Prüfungskommission vorgelegt.

Ich habe noch zu keinem früheren Zeitpunkt versucht, eine Dissertation einzureichen oder an einer Doktorprüfung teilzunehmen.

München, den 15. Mai 2018

Peter Andreas Graf



*Für Gabi und Maja.*



## **Publications**

Argüello-Miranda, O., Zagoriy, I., Mengoli, V., Rojas, J., Jonak, K., Oz, T., Graf, P., and Zachariae, W. (2017). Casein Kinase 1 Coordinates Cohesin Cleavage, Gametogenesis, and Exit from M Phase in Meiosis II. *Developmental Cell* 40, 37–52.

Jonak, K., Zagoriy, I., Oz, T., Graf, P., Rojas, J., Mengoli, V., and Zachariae, W. (2017). APC/C-Cdc20 mediates deprotection of centromeric cohesin at meiosis II in yeast. *Cell Cycle* 16, 1145–1152.

Figure 46 of this thesis was published in this paper.



## **Abstract**

Meiosis is a specialized form of cell division in which one diploid mother cell is converted into four haploid daughter cells. Cohesin is a multi-protein complex, providing cohesion to replicated chromosomes. During meiosis, cohesin is removed from chromosomes in two steps. First, it is proteolytically cleaved from chromosome arms in anaphase I, whereas cohesin in the vicinity of the centromere is protected from cleavage. This pericentromeric cohesin is then removed in anaphase II. This stepwise loss of cohesin is part of the current model of meiotic chromosome segregation. Evidence for this kind of cohesin dynamics came originally from immunofluorescence experiments with very limited spatial resolution.

A new workflow was established by combining a novel synchronization system for budding yeast meiosis with a calibrated and optimized ChIP-Seq protocol. This workflow allows resolving the cohesin dynamics in the course of the two meiotic divisions with unprecedented temporal and spatial resolution.

With this new experimental system, we confirmed the existence of two cohesin fractions on chromosomes, a protected and an unprotected fraction. Contrary to the current model, we detected both fractions in the region around the centromere. This indicates that the distinction between arm cohesin and pericentromeric cohesin is not identical to the classification into unprotected cohesin and protected cohesin. These results suggest that the mechanism of protection is not only determined by the localization of the cohesin protein complex. Additionally, we discovered significant differences in the cohesin protection activity among individual chromosomes.

The protein Sgo1 is required for the centromeric protection of cohesin. Sgo1 was analyzed directly with the new workflow, and we generated novel insights into the loading of the protection machinery onto chromosomes and the establishment of centromeric protection in meiosis. The protection machinery is loaded onto chromosomes in a cohesin-dependent mechanism, and a novel model of a dynamic three-step loading mechanism of the protection machinery is presented. This model explains how the cells are able to provide a robust and reliable protection to cohesin located in very diverse patterns on different chromosomes. Moreover, the model suggests a new function of the protein Sgo1 in centromeric protection.

A last result is that the polo-like kinase of budding yeast, Cdc5, is involved in regulating the levels of the protection machinery, which are loaded onto chromosomes.



## Table of Contents

Table of Contents .....	11
1. Introduction .....	14
Meiosis.....	14
Cohesin .....	16
Meiotic cohesin .....	17
Topological binding of cohesin.....	19
Cohesin loading and sliding .....	20
Centromeric protection .....	22
Establishment of centromeric protection.....	24
Regulation of centromeric protection.....	26
Aim of the study .....	27
2. Results .....	28
Establishment of ChIP-qPCR for meiosis .....	28
ChIP-qPCR of meiotic cohesin.....	38
Application of a ChIP calibration system for meiosis .....	42
Establishment of calibrated ChIP-qPCR for meiosis .....	42
Establishment of calibrated ChIP-Seq for meiosis.....	45
Calibrated ChIP-Seq of a meiotic arrest/release time course.....	49
Two-step cohesin cleavage in meiosis.....	53
Quantification of calibrated ChIP-Seq data .....	60
Quantification of samples from a prolonged metaphase I arrest .....	65
Centromeric protection .....	66
Establishment of centromeric protection.....	66
Regulation of centromeric protection.....	80
3. Discussion.....	89
Experimental workflow .....	89

---

Characterization of meiotic cohesin .....	90
Recruitment of the protection machinery .....	95
Regulation of centromeric protection .....	100
4. Material and Methods .....	103
Yeast strains .....	103
Plasmid construction.....	104
<i>C. glabrata</i> tagging plasmid.....	104
Yeast transformation.....	104
<i>S. cerevisiae</i> transformation .....	104
<i>C. glabrata</i> transformation.....	105
Culture media.....	105
Induction of meiosis.....	106
Fixed-cell immunofluorescence.....	107
Live-cell imaging .....	107
Western blotting.....	108
Chromatin immunoprecipitation.....	109
qPCR.....	110
Next-generation sequencing .....	112
Bioinformatics .....	112
Short-read mapping.....	112
Calibration of ChIP-Seq profiles.....	113
calChIP-Seq quantification .....	113
Antibodies.....	113
List of strains .....	114
5. Contributions .....	117
6. Acknowledgements .....	118
7. References .....	119

---

8. Appendix .....	131
-------------------	-----

## 1. Introduction

### Meiosis

Meiosis is a specialized form of cell division in which two rounds of chromosome segregation follow one round of DNA replication. By duplicating the genome once and thereafter splitting it twice, one diploid mother cell is converted into four haploid daughter cells (Figure 1). This type of cell division can be found in almost all eukaryotic species. In unicellular eukaryotes, like Baker's yeast (*Saccharomyces cerevisiae*), meiosis allows forming haploid spores. These spores package the DNA in a tightly sealed environment and shield it from unfavorable environmental conditions and allow later mating of the haploid cells under more favorable conditions. In higher organisms like mammals, meiosis gives rise to gametes, i.e., sperm and egg cells. From Baker's yeast to mammals, many of the genes, which are relevant for meiosis, are conserved. Due to the ease of inducing meiosis and the number of available experimental tools, Baker's yeast is an ideal model organism to study meiosis on the cellular and molecular level and to provide hypothesis about meiotic mechanisms in higher organisms.

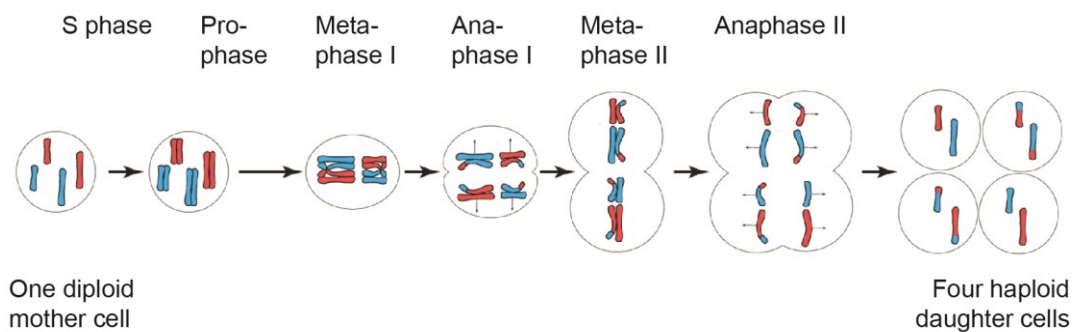


*Figure 1: Meiosis consists of two consecutive rounds of chromosome segregation after one round of DNA replication. Adapted from and modified: d'Erfurth, I., Jolivet, S., Froger, N., Catrice, O., Novatchkova, M., and Mercier, R. (2009). PLOS Biology 7, e1000124.*

In yeast, meiosis is induced as a response to nitrogen and carbon starvation. It starts with pre-meiotic S phase during which a meiosis-specific form of cohesin, containing the subunit Rec8 instead of Scc1, is loaded onto chromosomes (Klein et al., 1999; Watanabe and Nurse, 1999). After this, the DNA is replicated. Cohesin is a multi-subunit protein complex, which provides cohesion to replicated chromosomes by connecting sister chromatids (Nasmyth and Haering, 2009). Subsequently, recombination between non-

sister chromatids takes place, linking homologs together by the formation of chiasmata. After completion of recombination and satisfaction of the recombination checkpoint, the meiosis-specific transcription factor Ndt80 drives the cells into metaphase I by upregulating, among others, the genes for the polo-like kinase Cdc5 and the Cdk1-activating, B-type cyclins Clb1 and Clb4 (Chu et al., 1998). Upregulation of the kinases Cdc5 and Cdk1 shifts the cells into a high-kinase state, which triggers the formation of the meiotic spindle, the separation of spindle pole bodies (SPBs), and the attachment of sister kinetochores to microtubules originating from the same pole (mono-orientation). This process depends on the multi-protein complex monopolin, including the casein kinase 1 $\delta/\epsilon$  (CK1 $\delta/\epsilon$ ) (Hrr25 in budding yeast) (Tóth et al., 2000; Rabitsch et al., 2003; Petronczki et al., 2006). The anaphase-promoting complex/cyclosome (APC/C) together with its activator/substrate-recognition factor Cdc20 triggers the metaphase-to-anaphase transition. APC/C<sup>Cdc20</sup> activates the cysteine protease separase/Esp1 by marking the separase-inhibitor Pds1 for degradation by the proteasome (reviewed in Zachariae, 2004). Activated separase cleaves the Rec8 subunit of cohesin along chromosome arms, thereby allowing the separation of homologs (Buonomo et al., 2000). Sister chromatids remain attached to each other during anaphase I because cohesin at centromeres is protected from cleavage by separase. This protection is possible because Rec8 needs to be phosphorylated so that separase can efficiently recognize it as a substrate. The phosphorylation of Rec8 is performed by Hrr25 and Dbf4-dependent Cdc7 kinase (DDK) (Katis et al., 2010). At the centromeres, this phosphorylation is removed by the phosphatase PP2A, thus protecting centromeric Rec8 from cleavage by separase (Kitajima et al., 2006; Riedel et al., 2006). Concomitantly with the onset of anaphase I, the phosphatase Cdc14 is released from the nucleolus. The release is mediated by a non-proteolytic function of separase and the Cdc fourteen early anaphase release (FEAR) network (Buonomo et al., 2003; Marston et al., 2003). Cdc14 counteracts Cdk1 activity, bringing the cells back to a low-kinase state, which is a prerequisite for disassembly of the meiosis I spindle. After a very short prophase II, Cdk1 activity rises again, shifting the cells back to the high-kinase state, and metaphase II starts. The spindle pole bodies re-duplicate and meiosis II spindles are assembled. The sister kinetochores now attach to microtubules emanating from opposite poles (biorientation). As in meiosis I, APC/C<sup>Cdc20</sup> activates separase but now the centromeric Rec8 is cleaved, and the spindle apparatus pulls the sister chromatids to opposite poles (Figure 2).

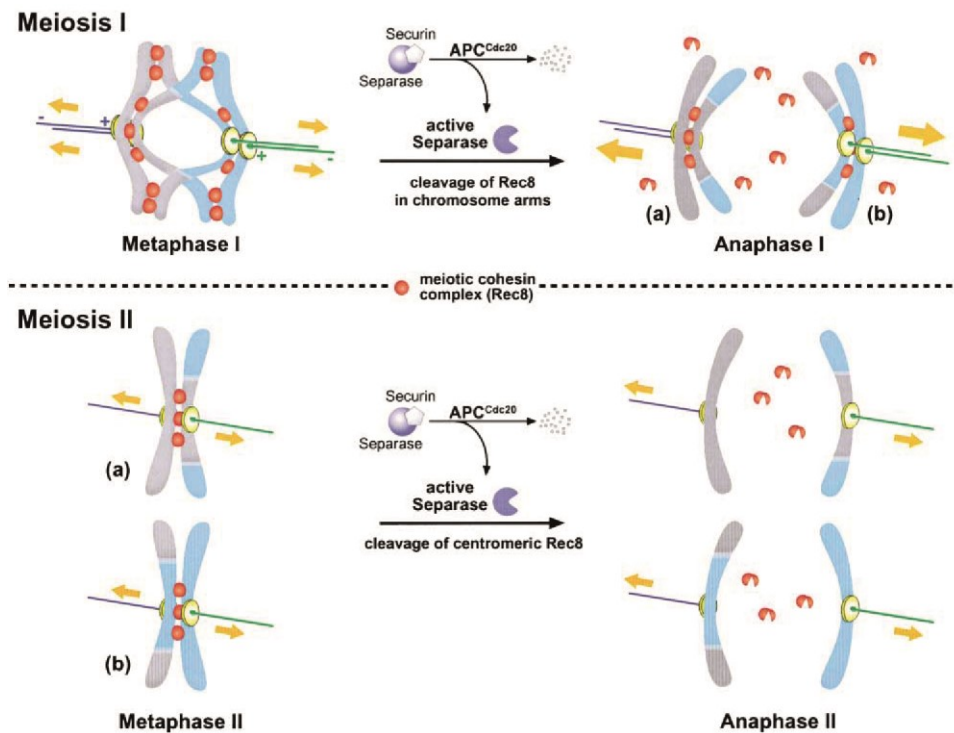


Figure 2: *In meiosis I, the reductional division separates the homologs, in meiosis II, the equational division separates the sister chromatids. The first division in anaphase I is elicited by cleavage of arm cohesin. The second division in anaphase II is elicited by cleavage of centromeric cohesin. Taken from: Petronczki, M., Siomos, M.F., and Nasmyth, K. (2003). Un Ménage à Quatre: The Molecular Biology of Chromosome Segregation in Meiosis. Cell 112, 423–440.*

## Cohesin

The cohesin protein complex is a multi-protein complex that is named after its most prominent function, which is to provide cohesion to newly replicated sister chromatids (Guacci et al., 1997; Michaelis et al., 1997). In budding yeast, it consists of five core subunits, and additional regulatory subunits bind to it (reviewed in Haering and Gruber, 2016). The five core subunits in budding yeast are named Smc1, Smc3,  $\alpha$ -kleisin, Scc3, and Pds5, with a total molecular weight of 626 kDa (Figure 3). Smc1 and Smc3 each consist of a large coiled-coil domain with a globular hinge domain at the outer ends, and both proteins form a heterodimer in the cohesin complex (Melby et al., 1998). Smc1 and Smc3 are bridged by the  $\alpha$ -kleisin subunit, which binds to the globular hinge domains of the Smc proteins (Haering et al., 2002).

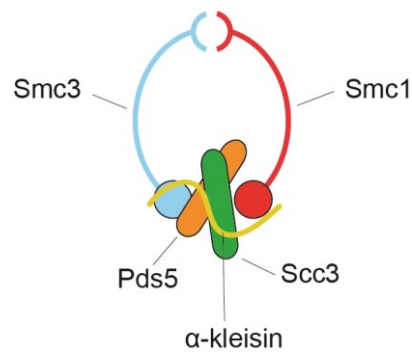


Figure 3: **Schematic representation of the cohesin protein complex from budding yeast.** Adapted from and modified: Nasmyth, K. (2011). Cohesin: a catenase with separate entry and exit gates? *Nature Cell Biology* 13, ncb2349.

### Meiotic cohesin

In mitosis, the cohesin complex provides cohesion of sister chromatids, until their segregation in anaphase. Meiosis, by contrast, consists of two consecutive rounds of chromosome segregation. In anaphase I of meiosis, homologs are segregated, in anaphase II sister chromatids are segregated. Hence, in meiosis, cohesion is lost in two steps. First, the cohesion of homologs is released in anaphase I, but the cohesion of sister chromatids is retained until meiosis II and is released in anaphase II. Therefore, it was unclear for a long time if two different mechanisms provide cohesion to homologs and sister chromatids or if the same mechanism is responsible for both (reviewed in Miyazaki and Orr-Weaver, 1994).

In meiosis, the protein Rec8 is required for chromosome cohesion (Molnar et al., 1995). Rec8 constitutes a meiosis-specific variant of the cohesin protein complex (Klein et al., 1999; Watanabe and Nurse, 1999), which provides cohesion to homologs and sister chromatids. Consequently, the same mechanism is responsible for both functions. Rec8, which is absent in mitosis, is the meiosis-specific version of the  $\alpha$ -kleisin subunit of the cohesin complex. The other four subunits of the cohesin complex are expressed in mitosis and meiosis. The mitotic version of the  $\alpha$ -kleisin subunit (Scc1 in *S. cerevisiae*), on the other hand, can also be found at low levels in meiotic cells (Klein et al., 1999), but several lines of evidence suggest that cohesion of chromosomes during meiosis occurs exclusively through Rec8 cohesin (Rankin, 2015). Moreover, various meiosis-specific functions, like the formation of axial elements, recombination during meiotic prophase or

centromeric protection at anaphase I require the meiosis-specific cohesin subunit Rec8. Whereas Scc1 cannot provide these functions (Petronczki et al., 2003). Thus, both paralogs deviate strongly concerning their function and regulation. The degree of sequence homology between the two proteins also reflects this difference. Both proteins are not identifiable as homologs by a standard BLAST search; only remote homology recognition techniques reveal their relationship. Crucial sites for regulation, like the separase cleavage site, are at very different positions in both proteins (Sullivan et al., 2004).

Rec8 co-localizes with chromosomes during meiotic prophase and disappears from chromosome arms in anaphase I, whereas a small fraction of Rec8 persists in the vicinity of the centromere until anaphase II (Klein et al., 1999; Watanabe and Nurse, 1999) (Figure 4). From these observations, which are based on immunofluorescence techniques, the current model of meiosis emerged. According to this model, cohesin comprises two fractions, one fraction on the chromosome arms and one fraction in the vicinity of the

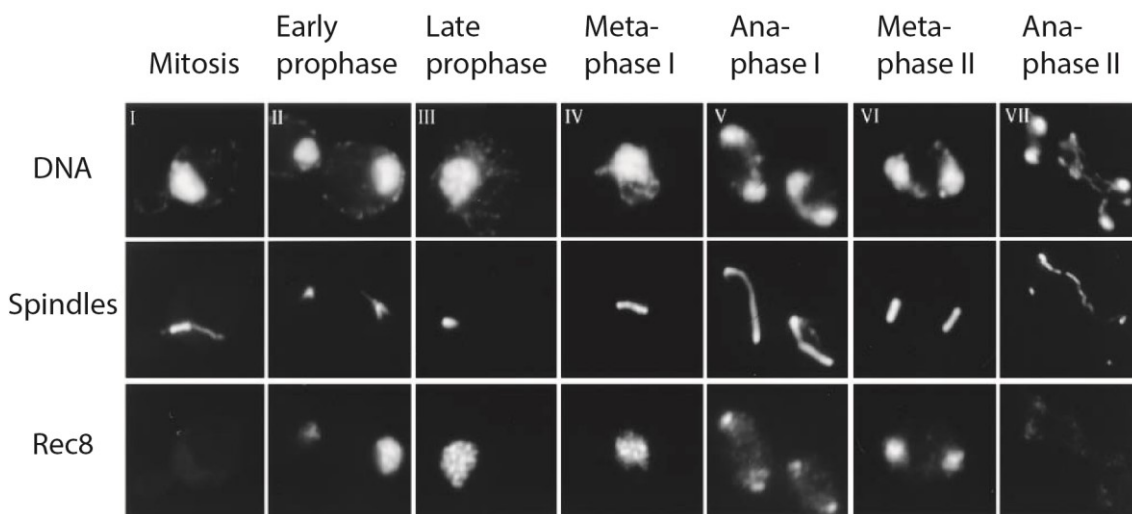


**Figure 4: Immunofluorescence staining of spindles and the meiosis-specific cohesin subunit Rec8 at representative meiotic stages.** The DNA was visualized by DAPI staining. Adapted from and modified: Klein, F., Mahr, P., Galova, M., Buonomo, S.B.C., Michaelis, C., Nairz, K., and Nasmyth, K. (1999). A Central Role for Cohesins in Sister Chromatid Cohesion, Formation of Axial Elements, and Recombination during Yeast Meiosis. *Cell* 98, 91–103.

centromere. Cohesin on the chromosome arms provides cohesion to homologs and is cleaved in meiosis I, cohesin in the vicinity of the centromere provides cohesion to sister chromatids and is cleaved in meiosis II (Orr-Weaver, 1999; Brar et al., 2006). A later study quantified the size of the region around the centromere in which cohesin is preserved in meiosis II indirectly, by correlating the position of Rec8 with chromatin

immunoprecipitation on a chip (ChIP-Chip) data of the cohesin protection machinery (Kiburz et al., 2005). This study estimated the size of the protected region, to be 50 kbp around the centromere for every chromosome.

In budding yeast mitosis, cohesin is removed from chromosomes at the metaphase-to-anaphase transition via the proteolytic activity of separase (Uhlmann et al., 1999; Uhlmann et al., 2000). For vertebrate mitosis, by contrast, it was shown that cohesin is removed from chromosomes in two steps, first by a separase-independent mechanism in prophase, followed by a separase-dependent step at the metaphase-to-anaphase transition (Darwiche et al., 1999; Sumara et al., 2000; Waizenegger et al., 2000). The separase-independent prophase pathway of cohesin removal is controlled by the Polo-like kinase (Sumara et al., 2002) and mediated by Wapl (Dobie et al., 2001; Gandhi et al., 2006). For budding yeast mitosis, no prophase-pathway of cohesin removal has been described to date (Lopez-Serra et al., 2013). For budding yeast meiosis, however, it was demonstrated using chromosome spreads that the overall cohesin levels are lower in metaphase I than in prophase, suggesting a prophase pathway-like mechanism might be in place in budding yeast meiosis (Yu and Koshland, 2005).

### **Topological binding of cohesin**

The protease separase is required for removing cohesin from chromosomes in anaphase. This dependency suggests that the cohesin complex needs to be proteolytically cleaved for its removal from chromosomes. The requirement for proteolytic cleavage was demonstrated in mitosis, where the mitotic  $\alpha$ -kleisin subunit Scc1 of cohesin needs to be cleaved by separase to allow chromosome segregation at anaphase (Uhlmann et al., 1999). For meiosis, the same mechanism was confirmed by showing that proteolytic cleavage of the meiosis-specific  $\alpha$ -kleisin subunit Rec8 is required for faithful chromosome segregation in anaphase I (Buonomo et al., 2000). Structural studies revealed that individual Smc subunits of the cohesin complex form rod-like structures, with interaction sites at their outer ends, which could easily be assembled into a proteinaceous loop, able to entrap a DNA molecule. It was shown that the rod-like cohesin subunits Smc1 and Smc3 directly interact at their out tips, whereas their other end is connected via the  $\alpha$ -kleisin subunit (Haering et al., 2002). Therefore, it was speculated that the cohesin protein complex might interact with DNA topologically. According to this model, the cohesin complex does not just interact with DNA, but it embraces the DNA molecule in a closed

ring-like structure (Figure 5). Over the course of several years, many studies have supported this model and collected evidence for its validity. By artificially cleaving the Smc3 subunit of the cohesin complex, it was demonstrated that not only cleavage of the  $\alpha$ -kleisin subunit, like it physiologically occurs in the cells, but cleavage of any cohesin subunit is sufficient to remove cohesin from chromatin (Gruber et al., 2003). This result is consistent with the ring model, according to which cohesin can only bind to DNA if

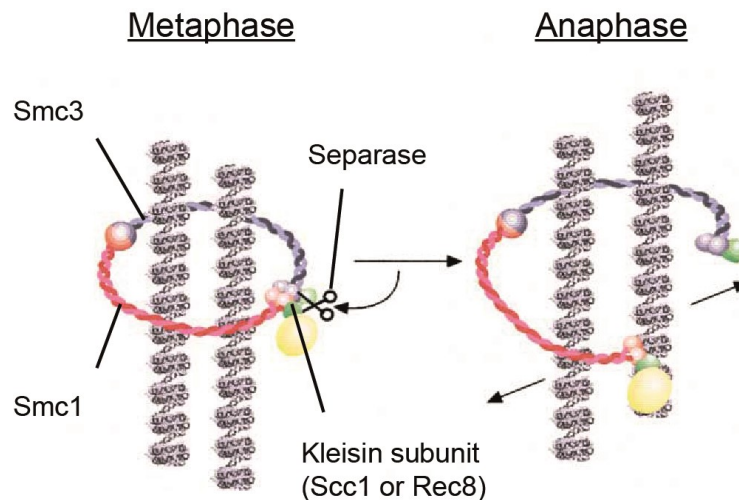


*Figure 5: Structure of the cohesin protein complex according to the ring model. Smc1, Smc3 and the kleisin subunit form a closed ring, embracing two strands of DNA. The kleisin subunit is cleaved by the protease separase, which triggers chromosome segregation at the metaphase-to-anaphase transition. Accessory proteins like Scc3, depicted in yellow, bind to the cohesin complex. Adapted from and modified: Haering, C.H., Löwe, J., Hochwagen, A., and Nasmyth, K. (2002). Molecular Architecture of SMC Proteins and the Yeast Cohesin Complex. Molecular Cell 9, 773–788.*

the ring is intact, but cohesin would detach if any link in the ring were lost as it occurs upon cleavage of Smc3. Moreover, it was demonstrated that it is feasible to generate stable SDS-resistant protein-DNA complexes by cysteine-crosslinking of the cohesin subunits Smc1, Smc3 and Scc1 (Haering et al., 2008). This result is consistent with the ring model because it shows that it is possible to establish a robust cohesin-DNA interaction just by cross-linking the cohesin subunits with each other, without cross-linking any cohesin subunit directly to DNA or another chromatin factor.

### Cohesin loading and sliding

In *S. cerevisiae*, loading of the cohesin complex onto chromosomes occurs in G1 and depends on the loader complex, comprising the subunits Scc2 and Scc4 (Ciosk et al., 2000). A conserved patch on the surface of Scc4 recruits the Scc2/Scc4 cohesin loader

complex to chromatin (Hinshaw et al., 2015). A mutation in this conserved patch (*scc4-m35*) eliminates the centromeric localization of the loader complex. The recruitment of the cohesin loader to chromosomes involves phosphorylation of the kinetochore protein complex Ctf19 by DDK, phosphorylated Ctf19 is in turn recognized by *Scs2/Scs4* (Ciosk et al., 2000; Hinshaw et al., 2017; Hu et al., 2011; Natsume et al., 2013). Another conserved function of DDK is to phosphorylate several subunits of the Mcm helicase complex, and thus, DDK is involved in the initiation of replication (reviewed in Rossbach and Sclafani, 2016). Hence, a DDK-dependent *Scs2/Scs4* cohesin loader recruitment couples the licensing of DNA replication to the initiation of cohesin loading (Gillepsie et al., 2004; Hinshaw et al., 2017). However, the cohesin loader complex does not detach from chromatin after S phase, as it can still be detected on chromatin in metaphase (Kogut et al., 2009). Maintenance of sister chromatid cohesion after S phase, on the other hand, is not dependent on the loader complex. The reason for this is that cohesin loading and establishment of cohesion are different functions, which are performed by different effectors. Once cohesin is loaded onto chromosomes, the establishment of cohesion occurs concomitant with replication and is mediated by replication fork-associated factors, independent of the *Scs2/Scs4* loader complex (Lengronne et al., 2006).

The pioneering works about cohesin localization in mitosis show that cohesin localizes to several sites along the whole chromosome axis. It displays a higher concentration around the centromere than on the chromosome arm. On chromosome arm sites, it preferentially enriches at AT-rich regions in intervals of approximately 15 kbp (Blat and Kleckner, 1999; Tanaka et al., 1999). The localization sites of cohesin along the chromosome axis are well defined, and the pattern of cohesin peaks is very reproducible. However, it is not known what defines these sites of cohesin localization. Interestingly, the *Scs2/Scs4* cohesin loader binding sites only poorly co-localize with the cohesin binding sites in *S. cerevisiae* (Hu et al., 2011; Lengronne et al., 2004; Lopez-Serra et al., 2014). The same was demonstrated for human cells (Zuin et al., 2014). Hence, the current hypothesis is that two consecutive functions define the cohesin localization. First, the *Scs2/Scs4* cohesin loader recruits cohesin to chromosomes topologically, followed by cohesin translocation to its sites of permanent residence. Some reports exist that oppose this model of loading and subsequent translocation. One study claims that in *S. cerevisiae* only the *Scs2/Scs4* cohesin loader determines the distribution of cohesin along the chromosome (Kogut et al., 2009). However, the data presented in this study shows that

the ratio of Scc2/Scc4 and cohesin deviates significantly, depending on the chromosomal locus, rendering the interpretation of the data highly speculative. For *Drosophila*, it was shown that the cohesin loader co-localizes with cohesin, raising the possibility that the localization of cohesin is solely defined by the binding sites of the cohesin loader in this organism (Misulovin et al., 2008). Hence, it is conceivable that different mechanisms control cohesin's localization in different species.

Concerning the mechanism that translocates cohesin from the sites of loading, it was demonstrated that cohesin preferentially enriches at intergenic regions between convergently transcribed genes, giving rise to the possibility that the transcription machinery is responsible for cohesin repositioning (Lengronne et al., 2004). Another study on this topic confirmed that cohesin responds to transcriptional activity and that transcript elongation into cohesin association sites results in the local disassociation of cohesin (Bausch et al., 2007). However, the precise translocation mechanism remained ambiguous, and two different models emerged. The relocation model proposes that cohesin might dissociate from sites of initial Scc2–Scc4 binding, presumably by transcriptional activity and then be newly reloaded further downstream. The sliding model proposes that cohesin relocates from its initial binding sites on chromosomes by sliding along chromatin while remaining bound topologically (reviewed in Ocampo-Hafalla and Uhlmann, 2011). Recent studies collected compelling evidence for the validity of the sliding model. It was confirmed, using single-molecule imaging, that *in vitro* individual molecules of cohesin form topologically bound complexes that diffuse on DNA, showing high mobility and a long association time (Stigler et al., 2016). Another study demonstrated by using chromatin immunoprecipitation (ChIP) that pre-existing cohesin is pushed downstream along the DNA in response to transcriptional gene activation, apparently without the need for intermittent dissociation or reloading (Ocampo-Hafalla et al., 2016). A third study further strengthened the sliding model by showing that mobilized cohesin complexes continue to provide cohesion, excluding their dissociation from chromosomes (Borrie et al., 2017).

### **Centromeric protection**

In the course of the two meiotic divisions, the cells remove cohesin from chromosomes in a step-wise manner. First, the cells remove arm cohesin in meiosis I, followed by

cohesin around the centromere in meiosis II. This step-wise loss of cohesin is possible because cohesin around the centromere is protected from cleavage in meiosis I (Brar et al., 2006; Orr-Weaver, 1999; Klein et al., 1999; Watanabe and Nurse, 1999). This protection is directly mediated by protein phosphatase 2A (PP2A), bound to its B' subunit (Rts1 in *S.cerevisiae*). Inactivation of PP2A leads to a premature loss of centromeric Rec8 in anaphase I (Kitajima et al., 2006; Riedel et al., 2006). PP2A fulfills its protective function by dephosphorylating the meiosis-specific cohesin subunit Rec8. Phosphorylation of Rec8 at multiple sites by DDK and CK1 $\delta/\epsilon$  is a prerequisite for cleavage by separase (Ishiguro et al., 2010; Katis et al., 2010). The mutation of 24 phosphosites into alanine residues on Rec8 prevents its cleavage by separase in anaphase I. Conversely, the phosphomimetic substitutions of 14 residues within the N-terminus of Rec8 caused the precocious separation of sister centromeres. (Katis et al., 2010).

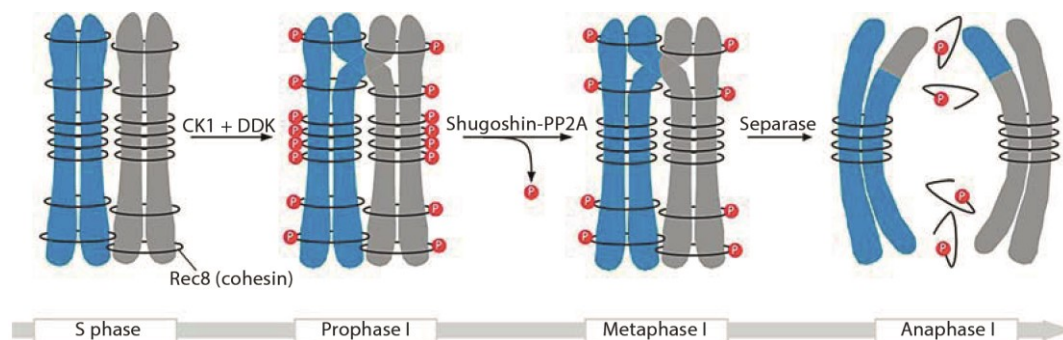


Figure 6: **Function of Shugoshin in centromeric protection of meiotic cohesin.** Taken from: Clift, D., and Marston, A.L. (2011). *The Role of Shugoshin in Meiotic Chromosome Segregation. Cytogenet Genome Res* 133, 234–242.

In addition to PP2A-B', it was shown that the protein Shugoshin (Sgo1 in *S.cerevisiae*) is required for protection of centromeric cohesin in meiosis I (Katis et al., 2004; Kerrebrock et al., 1995; Kitajima et al., 2004; Marston et al., 2004; Rabitsch et al., 2004). Sgo1's function is to recruit the phosphatase PP2A-B' to chromatin (Kitajima et al., 2006; Riedel et al., 2006). The stoichiometry of Sgo1 and PP2A is 2:1 (Xu et al., 2009). This function of Sgo1 is illustrated in Figure 6. Shugoshin exists as two paralogs, Sgo1 and Sgo2 in most organisms. Both paralogs have different functions and are regulated differently. In mammals, the protection of centromeric cohesin in meiosis via the recruitment of PP2A is carried out exclusively by Sgo2 (Lee et al., 2008). Sgo1, on the other hand, is required for maintaining sister chromatid cohesion in prophase of mammalian mitosis and does not counteract separase (Salic et al., 2004; Tang et al.,

2004). The degree of homology between Sgo1 and Sgo2 is very low (Yao and Dai, 2012). Together with *Drosophila*, budding yeast is an exception in this respect, as it only has one Shugoshin version (Sgo1), which fulfills all mitotic and meiotic functions.

### **Establishment of centromeric protection**

While it is well established that Shugoshin is required for centromeric protection and that it fulfills this role by recruiting PP2A-B' to chromatin, it is much less clear how the binding of Shugoshin to chromatin is regulated and which are the relevant binding partners. It was demonstrated that Sgo1's localization to chromatin depends on the kinase Bub1. Bub1 was originally described as a spindle assembly checkpoint kinase (Roberts et al., 1994). However, it was shown that it fulfills an additional function of regulating the recruitment of Shugoshin to chromatin. The centromeric localization of Shugoshin in yeast cells and mammalian cells depends on the presence of Bub1 (Kiburz et al., 2005; Kitajima et al., 2004; Kitajima et al., 2005; Tang et al., 2004). The relevant substrate for Bub1 phosphorylation is the histone H2A. Again, this substrate is conserved from yeast to humans. In human cells, hSgo1 is removed from chromosomes after treatment with hBub1 small interfering RNA. In yeast, mutation of the corresponding serine/threonine residues to alanine results in a complete loss of Shugoshin-chromatin interaction (Kawashima et al., 2010). Human and fission yeast Sgo1 additionally depend on the heterochromatin protein HP1 for their localization to chromosomes (Yamagishi et al., 2008). Budding yeast, by contrast, does not have pericentromeric heterochromatin. Nevertheless, it was reported that the budding yeast kinetochore proteins Iml3 and Chl4 contribute to the localization of Sgo1 (Kiburz et al., 2005). Iml3 and Chl4 are both subunits of the Ctf19 complex, which is required for the recruitment of the cohesin loader Scc2/Scc4 (Ciosk et al., 2000; Hinshaw et al., 2017; Hu et al., 2011; Natsume et al., 2013). Controversial reports exist about the role of cohesin in the recruitment of Shugoshin. Performing a ChIP analysis of yeast cells, Kitajima (2004) reported that they "found that Rec8 localization is not dependent on Sgo1 and vice versa [...]. This independence of localization ensures that the mechanism protects Rec8 only at centromeres and not along chromosome arm regions." If Sgo1 were recruited to chromosome arm sites, it would have catastrophic consequences, as it would protect arm cohesin from cleavage in meiosis I, thus, preventing the first meiotic division (Kitajima et al., 2006; Riedel et al., 2006). A similar result was reported for *Drosophila*. Lee et al. (2004) analyzed the recruitment of

the Shugoshin-homolog MEI-S332 to chromosomes, using immunofluorescence analysis of cells in which cohesin was depleted and reported that their “results demonstrate that the localization of MEI-S332 is independent of cohesin”. Using immunofluorescence analysis of mouse spermatocytes, Gómez et al. (2007) found that SGO2 and REC8 only weakly co-localize in metaphase I of meiosis (Figure 7). In this study, REC8 displayed an X-shaped pattern, whereas SGO2 displayed a triangular pattern. The sole area of co-localization was at the center of the SGO2 triangular, which overlapped with the outer ends of the REC8 X-pattern. Concerning a possible loading mechanism of SGO2 onto chromosomes, one would not consider REC8 to be a strong candidate for a loading factor,

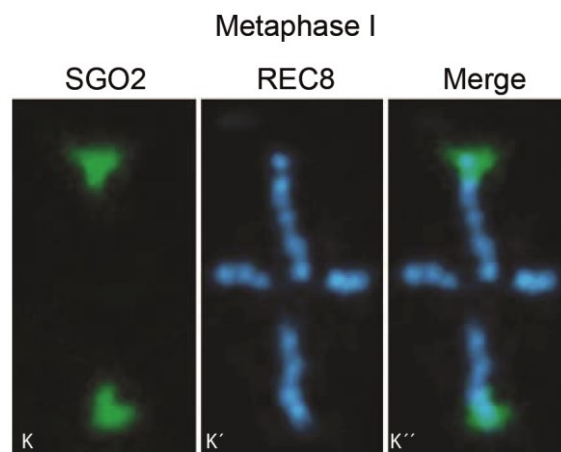


*Figure 7: Immunofluorescence images of SGO2 and REC8 in mouse spermatocytes. Both proteins were imaged in metaphase I and show a different distribution. The area of overlap is small. Taken from and modified: Gómez, R., Valdeolillos, A., Parra, M.T., Viera, A., Carreiro, C., Roncal, F., Rufas, J.S., Barbero, J.L., and Suja, J.A. (2007). Mammalian SGO2 appears at the inner centromere domain and redistributes depending on tension across centromeres during meiosis II and mitosis. *EMBO Rep* 8, 173–180.*

taking into account the weak co-localization of the two proteins.

On the other hand, using immunofluorescence analysis of mouse oocytes, Lister et al. (2010) showed that the localization of SGO2 depends on the presence of functional cohesin complexes. In oocytes of mice, in which the meiosis-specific cohesin subunit Smc1 $\beta$  was knocked-out, SGO2 failed to accumulate on chromosomes. Also in maize, recruitment of Sgo1 is Rec8-dependent (Hamant et al., 2005). Similarly, in budding yeast, Sgo1 is absent from chromosomes, if Rec8 is deleted (Kiburz et al., 2005). Finally, in humans, cohesin mediates the centromere localization of Sgo1 (Liu et al., 2013a; Liu et al., 2013b).

### Regulation of centromeric protection

If Sgo1 and with it PP2A were recruited to chromosome arm sites, it would have catastrophic consequences, as it would protect arm cohesin from cleavage in meiosis I, thus, preventing the first meiotic division (Kitajima et al., 2006; Riedel et al., 2006). Consequently, the most important question concerning the regulation of the recruitment of the centromeric protection machinery is how to exclude Sgo1 from chromosome arms. One effector reported to regulate Shugosin's recruitment to chromatin is the Chromosomal Passenger Complex (CPC). The CPC is a conserved protein complex, consisting of four subunits, called AuroraB/Ipl1, INCENP/Sli15, Survivin/Bir1, and Borealin/Nbl1 (Nakajima et al., 2009). It has been connected to various functions of the mitotic cell-cycle, including chromosome-microtubule interactions, sister chromatid cohesion and cytokinesis (Ruchaud et al., 2007). In fission yeast, *Drosophila* and humans, it was shown that inhibition of single components of the CPC leads to a loss of centromeric localization of Shugoshin (Resnick et al., 2006; Huang et al., 2007; Kawashima et al., 2007). However, it is unclear whether this function of the CPC is also conserved in *S. cerevisiae*. Another protein that was demonstrated to regulate the recruitment of Shugoshin to chromosomes is the polo-like kinase (Cdc5 in *S. cerevisiae*). For *Drosophila*, it was shown that the Shugosin-homolog MEI-S332 carries POLO binding sites and associates with this kinase *in vivo* (Clarke et al., 2005). POLO was further described in this paper as a major regulator and antagonist of MEI-S332 function. In human mitosis, only the Shugoshin paralog *SGO1* is expressed, but not the meiosis-specific *SGO2*. For the mitotic Shugoshin, it was shown that depletion of Plk1, the human polo homolog, stimulates the recruitment of Sgo1 to chromosomes, supporting a possibly antagonizing function of the polo-like kinase (Tang et al., 2006). A third reported regulator of Shugosin's recruitment to chromosomes is the phosphatase complex PP2A, which is known to mediate centromeric protection by dephosphorylating Rec8. By using chromosome spreads, Tang et al. (2006) found that in mammalian mitosis the Sgo1-PP2A interaction is required for centromeric localization of Sgo1.

Another important question concerning the regulation of centromeric protection is the inactivation of the centromeric protection machinery after meiosis I so that centromeric cohesin can be cleaved in meiosis II. This inactivation is also called "deprotection" of centromeric cohesin. Without deprotection, it would not be possible to segregate sister chromatids and thus, the cells would arrest in meiosis II. Several mechanisms for

deprotection have been proposed in the literature (Arguello et al., 2017; Clift and Marston 2011; Gómez et al., 2007; Kitajima et al., 2004; Lee et al., 2008). Recently, it was reported that in mice, deprotection occurs via an inhibitor of PP2A's enzymatic function. This inhibition of PP2A is mediated by the conserved histone chaperone SET/TAF-1b (Chambon et al., 2013). However, it is not known whether the same mechanism deprotects centromeric cohesin in yeast.

### **Aim of the study**

During meiosis, cohesin is first removed from chromosome arms in anaphase I, followed by removal of pericentromeric cohesin in anaphase II. This stepwise loss of cohesin is part of the current model of meiotic chromosome segregation. Evidence for this kind of cohesin dynamics came originally from immunofluorescence experiments with very limited temporal and spatial resolution (Klein et al., 1999; Watanabe and Nurse, 1999). These dynamics were later confirmed by live-cell imaging (Katis et al., 2010). Even though live-cell imaging provides an excellent temporal resolution of cellular events, its spatial resolution is very limited, especially in small yeast cells.

This study aims to overcome this limitation by combining a novel synchronization system for budding yeast meiosis with an optimized and calibrated chromatin immunoprecipitation followed by sequencing (ChIP-Seq) protocol to establish an assay with a yet unprecedented temporal and spatial resolution.

With this assay, we aim to analyze the behavior of meiotic cohesin in the course of the two meiotic divisions. Moreover, we aim to analyze the protein Sgo1, which is required to recruit the protection machinery to chromosomes to generate novel insights into the temporal-spatial dynamics of cohesin and its protector.

## 2. Results

Several critical steps of meiosis require the cohesin protein complex, like cohesion of sister chromatids after replication, DNA damage repair, recombination in prophase, and chromosome segregation. Cohesin interacts with DNA topologically, and it shows a meiosis-specific two-step cleavage behavior during the two meiotic divisions. However, most of what we know about the *in vivo* dynamics of meiotic cohesin comes from immunofluorescence experiments with limited spatial resolution. We therefore aimed to analyze the behavior of meiotic cohesin with almost single-nucleotide precision, using a biochemical ChIP assay. Biochemical methods analyze samples comprising from thousands to billions of individual cells. The measured signal thus represents an average of those cells. To study a physiological process in time, using a biochemical method, it is therefore crucial that the analyzed samples genuinely represent specific stages of this process. To achieve an enrichment of cells of a specific physiological stage in samples of a yeast meiotic time course, our lab has developed a new synchronization system, which allows generating highly synchronous meiotic cultures. This system was named CDC20-meiotic-arrest/release (*CDC20-mAR*) and is based on depletion of the APC/C activator/substrate-recognition factor Cdc20, which arrests the cells in metaphase I, followed by induction of Cdc20, which is controlled by the copper-inducible *CUPI* promoter (Arguello et al., 2017). Hence, by adding CuSO<sub>4</sub> to a culture of metaphase I-arrested cells, the cells are released from the arrest and synchronously undergo the two meiotic divisions. Having this system available, it is now possible to use biochemical methods like ChIP to analyze those samples with a sufficiently high temporal resolution.

### Establishment of ChIP-qPCR for meiosis

Our first attempts to analyze meiotic samples from *S. cerevisiae* cultures using existing ChIP protocols did not yield meaningful results. Therefore, we decided to establish a ChIP assay by systematically adjusting the experimental steps and thus, optimize the protocol specifically for our meiotic experimental conditions. ChIP is a method to determine the *in vivo* binding sites of a protein of interest on DNA (Park, 2009). The method comprises several consecutive experimental steps (Figure 8). It starts with treating a cell suspension with a cross-linking agent, to chemically stabilize the protein-DNA interactions at the

time of sampling. Subsequently, the cells are lysed, and the chromatin is fragmented and solubilized. The chromatin fragmentation can be performed via physical, enzymatic or chemical methods (Head et al., 2014). Then, the protein of interest is enriched together

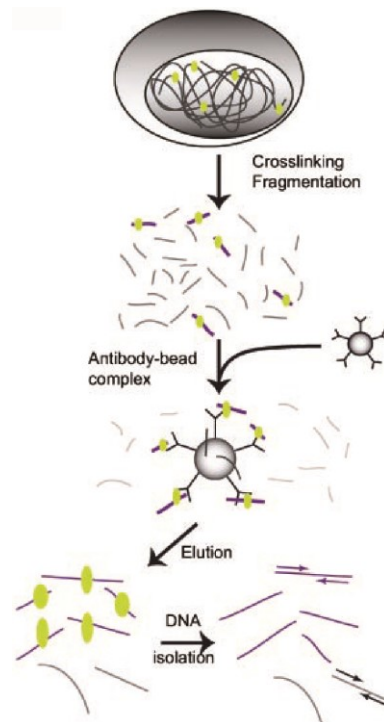


Figure 8: **ChIP workflow.** Taken from: Barski, A., and Zhao, K. (2009). *Genomic location analysis by ChIP-Seq.* *J. Cell. Biochem.* 107, 11–18.

with its cross-linked chromatin interactors by immunoprecipitation. Next, the obtained samples are purified to separate the DNA from all other cellular components like, e.g. proteins and RNA. Finally, the purified DNA samples are analyzed by either qPCR, to measure the concentration of specific DNA fragments or by next-generation sequencing (NGS) technologies, to generate a comprehensive, genome-wide map of protein-DNA interaction sites.

Thus, ChIP is a complex multi-step biochemical method. Adapting existing protocols to a new experimental setting is therefore not trivial, because of a large number of parameters that could be changed and might potentially influence the result. The problem becomes even more complicated, due to possible second or higher order effects between parameters: The optimal setting for one parameter might be dependent on the settings of other parameters. A systematic approach to addressing such a multi-parameter problem is statistical experiment planning a method known as design of experiments (DOE)

(Tanco et al., 2007). The concept of DOE is to design an experiment in such a way that it allows to vary multiple input factors (parameters) in one single experiment and still generate meaningful results (Grömping, 2014). The outcome of the experiment will be an estimate of the effect of each input factor on the result of the ChIP experiment, making it possible to identify the critical parameters. Manipulating several input factors in one experiment allows identifying the critical factors in a fast and efficient way. For the task of establishing a ChIP-qPCR workflow for *S. cerevisiae* meiosis, we defined two critical output parameters for optimization of the workflow. First, the center of mass of the chromatin fragment size distribution after sonication and second, the intensity of the ChIP-qPCR signal. Analyzing the DNA in the purified samples at the end of the ChIP workflow is a random sampling process. Therefore, efficient fragmentation is essential to allow an unbiased random sampling of DNA fragments, genuinely representing the distribution of *in vivo* protein binding sites. Too large chromatin fragments can negatively influence the data quality (O’Geen et al., 2011). It is recommended to aim for a chromatin fragment size not larger than 600 bp (Park, 2009). Evaluating the literature on chromatin fragmentation conditions shows that optimal conditions for chromatin fragmentation vary strongly, depending on the used cell type, the physiological conditions and the technical equipment for sonication. Bortz and Wamhoff (2011) recommend chromatin shearing by sonication for 30 minutes, for example, whereas Kugou and Ohta (2009) established 2 minutes of sonication in their protocol. Another problem in adapting published ChIP protocols arises from the fact that sonicators for chromatin shearing are available from different manufacturers and the settings of those machines cannot be compared directly, due to lack of technical standardization. Hence, it was unclear, which are the optimal chromatin shearing conditions for our meiotic experimental setting. We chose the ChIP-qPCR signal as a second output parameter, as we hypothesized that a high qPCR signal would allow detecting also small physiological changes in the cells, without losing those differences in the technical noise. Hence, we aimed to generate the highest possible ChIP-qPCR signal from our samples. The input factors we wanted to screen for their effect on those two output factors using DOE, were: Fixation time, time of chromatin shearing, cell density, shearing power, chromatin shearing duty factor, the concentration of fixative, cycles/burst during chromatin shearing and the shearing buffer type. We fixed the cells in an aqueous formaldehyde solution. The chromatin was sheared using an S220 Covaris water bath sonicator. Duty factor is the percentage of active treatment during the total run

time. Cycles/burst denote the number of acoustic oscillations in each burst; it is identical to the audio frequency. As shearing buffers, we tested the commercially available Covaris

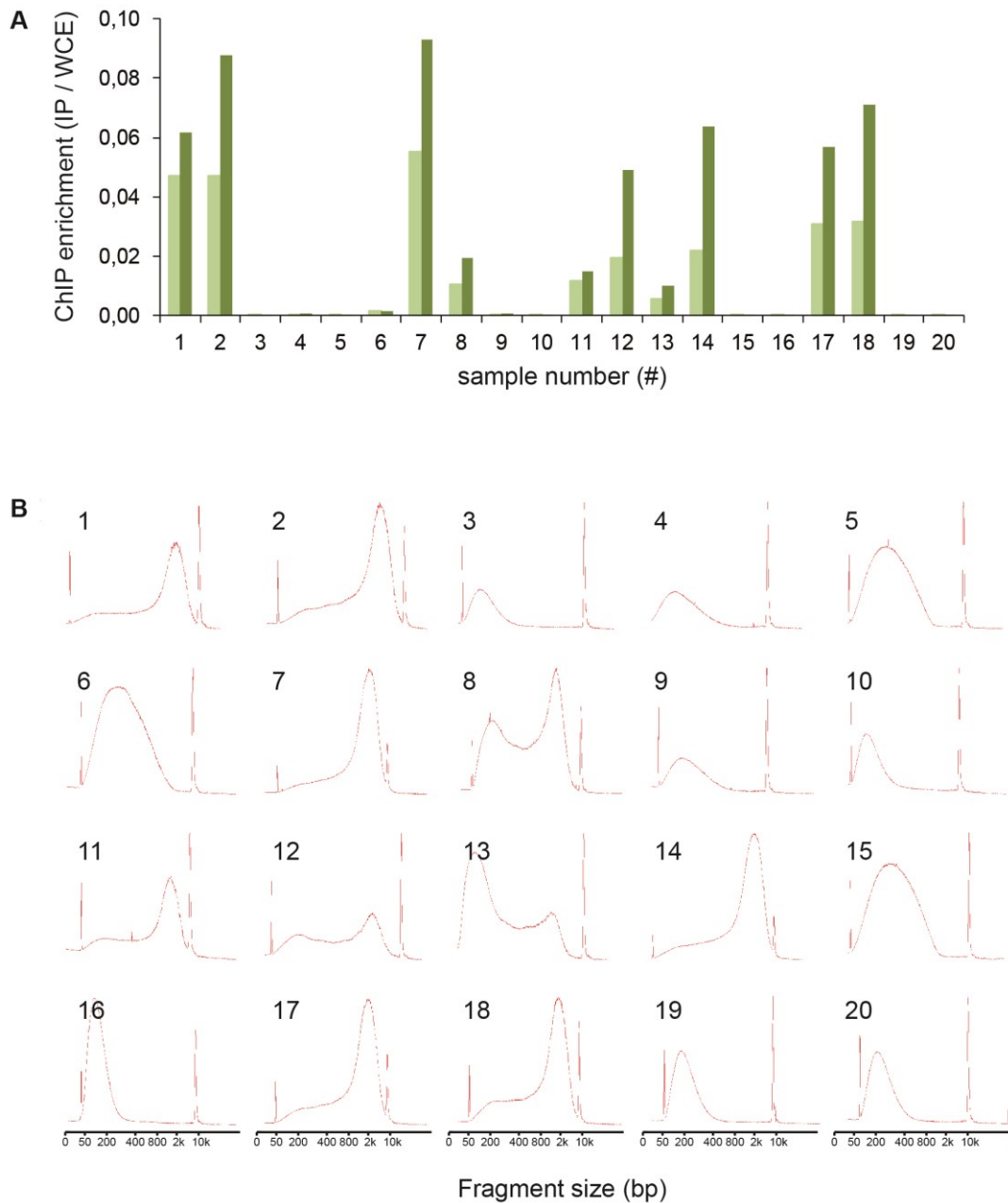


*Figure 9: Measured values of the output factors “ChIP-qPCR” and “Shearing” after realization of the fractional factorial design, comprising 16 runs and two sets of duplicates. (A) ChIP-qPCR values for 20 samples. For each sample the values of two different loci were measured in duplicates. The y-axis denotes the enrichment in the immunoprecipitation samples (IP) over the whole cell extract samples (WCE). Samples 1 to 16 are the experimental runs with changing input parameter values. Samples 17 and 18 are duplicates and define the center points for buffer 1, sample 19 and 20 are duplicates and define the center points for buffer 2. (B) Bioanalyzer profiles of the same 20 samples show the chromatin fragment size distributions after shearing on a Covaris water bath sonicator. The horizontal axis on the small diagrams denotes the fragment size in base pairs.*

truChIP Chromatin Shearing Reagent Kit against a self-mixed buffer according to the

protocol of Kugou and Ohta (2009). The experimental plan was calculated using the R Package FrF2 (Grömping, 2014). The chosen design was a two-level fractional factorial with resolution IV. Two level means that each input factor was represented by two values in the experiment. Resolution IV implies that the design allows estimating the main effect of each input factor in a linear regression model and allows to test its statistical significance. A fractional factorial design to examine eight input factors at resolution IV requires 16 experimental runs and two sets of replicates to define center points (Appendix A1). The final result comprises a total of 20 values (16 runs and two sets of duplicates) for each output factor (Figure 9 A and B). We transformed the 20 values into a data vector and used the *lm* function of R to fit a linear model to these data (Table 1).

*Table 1 Effect of eight different input factors on the two output factors ChIP-qPCR and shearing, estimated in a linear model. The first column lists the eight input factors. The columns labeled “coefficient estimate” contain the quantified effect on the output factors. Std Error denotes the standard deviation of the coefficient estimate and measures how precisely the unknown coefficient is modeled. The t-value is calculated dividing the coefficient estimate by the std. error; it allows calculating the p-value. The p-value indicates whether an input factor has a significant effect on the output factor*

	ChIP-qPCR				Shearing			
	Coefficient estimate	Std. Error	t value	Pr(> t )	Coefficient estimate	Std. Error	t value	Pr(> t )
tFix	0.002568	0.005665	0.453	0.66407	0.001257	0.009656	0.130	0.90008
tShear	-0.003030	0.005665	-0.535	0.60932	0.001973	0.009656	0.204	0.84391
density	-0.001653	0.005665	-0.292	0.77888	0.016280	0.009656	1.686	0.13565
power	-0.007883	0.005665	-1.392	0.20669	0.010817	0.009656	-1.120	0.29957
duty	-0.008597	0.005665	-1.518	0.17292	-0.010449	0.009656	-1.082	0.31505
cFix	0.005086	0.005665	0.898	0.39919	-0.006972	0.009656	-0.722	0.49369
cycles	0.007387	0.005665	1.304	0.23349	0.021365	0.009656	2.213	0.06255
buffer	-0.024734	0.005665	-4.366	<b>0.00329 **</b>	-0.040481	0.009656	-4.193	<b>0.00407 **</b>

For the output factor “ChIP-qPCR”, the p-value of the input factor “shearing buffer type” is 0.00329, indicating that it is highly statistically significant. The coefficient for this input factor is 0.024734, meaning that on average of all samples, the selection of the shearing buffer affects the ChIP-qPCR signal by 2.47 ChIP%. For ChIP-qPCR, an enrichment of 2.47 ChIP% is quite high, suggesting that the shearing buffer composition is a very critical factor. In this experiment, only the input factor “shearing buffer type” was identified to

be statistically significant because its effect on the ChIP-qPCR signal and the shearing is so dominant that it masks the potential effect of all other input factors. With an experiment comprising of 16 runs, it is not possible to detect smaller effects of different input factors if one input factor is very dominant.

Due to these results, we asked which are the critical components of the shearing buffer. To address this, we compared the composition of the Covaris truChIP shearing buffer to the buffer according to Kugou and Ohta (2009) and systematically tested the different components: Buffer system, salt concentration and type and concentration of detergents. We found that the salt concentration in the shearing buffer particularly affected the chromatin shearing pattern (Appendix A4). We conclude that no extra salt should be added to the shearing buffer. To investigate the effect of the buffer system, we performed

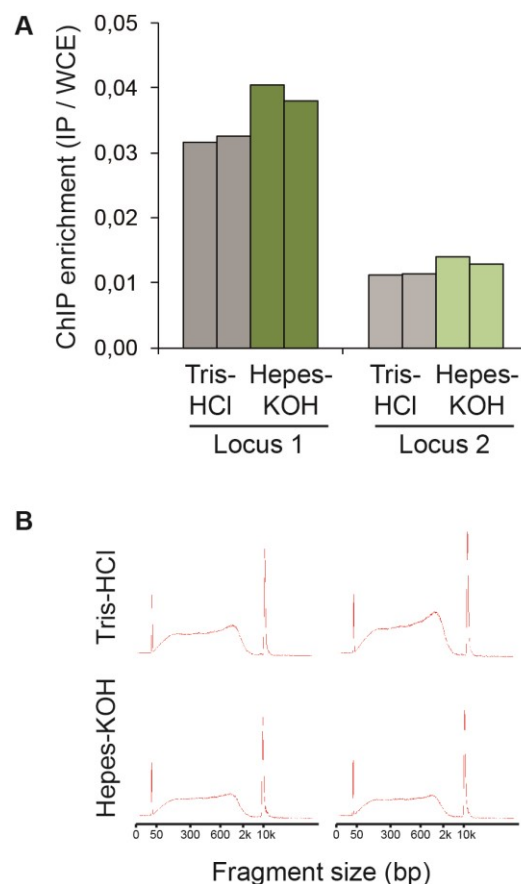


*Figure 10: Effect of the buffer system on ChIP-qPCR and the chromatin shearing. Tris-HCl-based shearing buffer (pH 7.5) was compared to Hepes-KOH-based shearing buffer (pH 7.5) under otherwise identical conditions. (A) ChIP-qPCR of duplicates for each buffer. For each sample the values of two different loci were measured. The y-axis denotes the enrichment in the immunoprecipitation samples (IP) over the whole cell extract samples (WCE). (B) Chromatin fragment size distribution after sonication of the same samples like in A. The horizontal axis on the small Bioanalyzer diagrams denotes the fragment size in base pairs.*

chromatin shearing in a buffer consisting of 10mM Tris-HCl (pH 7.5), 0.1 % Na-Deoxycholate, 1 % Triton X-100, 1mM EDTA versus a buffer consisting of 10mM Hepes-KOH (pH 7.5), 0.1 % Na-Deoxycholate, 1 % Triton X-100, 1mM EDTA. We found that the buffer system had a moderate, but reproducible effect on the ChIP-qPCR signal (Figure 10 A) and the chromatin shearing pattern (Figure 10 B). Shearing the samples in the Hepes-based buffer, generated a qPCR signal, which was on average 0.7 ChIP% higher, compared to shearing in the Tris-based buffer. We conclude that a shearing buffer should be composed of a Hepes-KOH-based buffer system.

Finally, we elucidated the effect of the detergent type and detergent concentration on the ChIP-qPCR signal (Figure 11 A) and the chromatin fragment size distribution after sonication (Figure 11 B). We sonicated samples in shearing buffers containing either 1 % Triton X-100, or 0.05 % SDS or none of the two detergents, respectively. Strikingly, the ChIP-qPCR signal of the Triton X-100 samples was almost 10-fold higher than that of the SDS samples (Figure 11 A). This difference of nearly one order of magnitude demonstrates that the most critical component in the shearing buffer is the detergent type

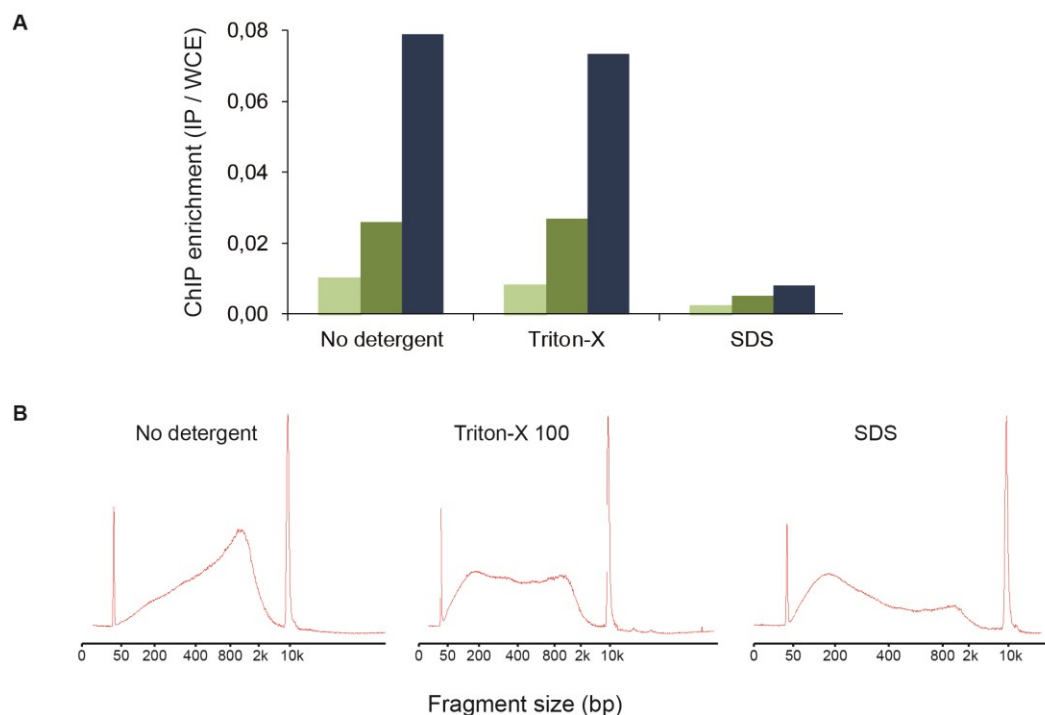


**Figure 11: Effect of different detergents on the qPCR signal and the chromatin shearing pattern.** (A) ChIP-qPCR of three different loci, each bar represents the mean of four samples. Control samples were sheared without detergent, In SDS+Dia samples SDS was dialyzed-out after the shearing and prior to the IP. (B) Size distribution of chromatin fragments after sonication. The horizontal axis on the small Bioanalyzer diagrams denotes the fragment size in base pairs., the vertical axis shows an arbitrary unit, correlated to the amount of input material. Detergents improve the chromatin shearing.

and concentration. We concluded that SDS should not be used as a shearing buffer component if a high qPCR signal is the goal. Instead, Triton X-100 is the preferred detergent.

Using the same optimized shearing buffer for all samples, we conducted a second fractional factorial experiment. The design and resolution were identical to the first one, only the input factor “shearing buffer” was substituted by the input factor “protease inhibitors”. This new input factor tested a standard protease inhibitor cocktail against a combination of two protease inhibitor cocktails and PMSF. Again, the ChIP-qPCR signal of two loci and the size distribution of the chromatin fragments after sonication were measured for every sample and used as output factors. Like in the previous factorial experiment, the results were converted into a data vector, and a linear model was fitted to those data using R (Table 2). By using the same shearing buffer for all samples, we identified two additional input factors as having a statistically significant effect on the ChIP-qPCR signal: The time of fixation and the time of shearing. The other input factors had minor or no impact.

*Table 2: Effect of eight different input factors on the two output factors ChIP-qPCR and shearing, estimated in a linear model. The first column lists the eight input factors. The columns labeled “coefficient estimate” contain the quantified effect on the output factors. Std Error denotes the standard deviation of the coefficient estimate and measures how precisely the unknown coefficient is modeled. The t-value is calculated dividing the coefficient estimate by the std. error, it allows calculating the p-value. The p-value indicates whether an input factor has a significant effect on the output factor.*

	ChIP-qPCR			Shearing		
	Coefficient estimate	t value	Pr(> t )	Coefficient estimate	t value	Pr(> t )
protInhib	0.0008924	0.309	0.76665	-0.0079294	-1.515	0.1735
tShear	-0.0075651	-2.616	<b>0.03464 *</b>	-0.0105199	-2.010	0.0843
density	0.0016922	0.585	0.57688	0.0076618	1.464	0.1866
power	-0.0002973	-0.103	0.92101	0.0003505	0.067	0.9485
duty	-0.0053879	-1.863	0.10478	-0.0110394	-2.109	0.0729
cFix	-0.0011303	-0.391	0.70759	0.0033991	0.650	0.5367
cycles	-0.0031364	-1.084	0.31413	0.0013369	0.255	0.8057
tFix	0.0119425	4.129	<b>0.00441 **</b>	0.0146945	2.808	<b>0.0262 *</b>

Having identified the time of fixation as a significant determinant out of our initial set of input factors suggests that the fixation conditions, in general, are likely to have a substantial effect on the results of a ChIP experiment. Reports in the literature indicate that apart from the time of fixation, the pH at which the fixation reaction takes place is a crucial factor for the reaction kinetics of a formaldehyde fixation reaction (Berod et al., 1981). To address this issue, we performed an experiment to test the formaldehyde fixation of meiotic yeast samples in different fixation solutions at different pH. To induce meiosis, we transferred the yeast cells into sporulation (SPO) medium, which only contains water and salts. Hence, no additional components, which are reactive towards formaldehyde are present in a meiotic yeast culture medium. This lack of competitive reaction partners makes it possible to perform the fixation directly in the meiotic culture medium. We tested this option against fixation in two different buffered fixation solutions. We buffered one solution to a pH of 8.0 using Hepes-KOH and the other

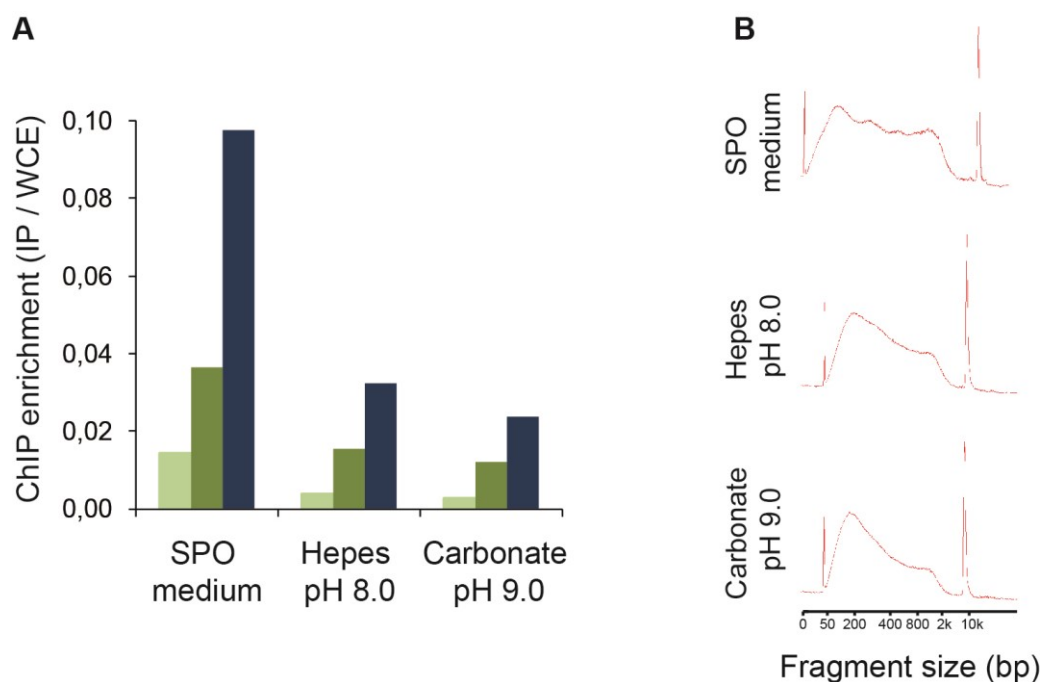


**Figure 12: Effect of the fixation conditions on the qPCR signal and the chromatin shearing pattern.** *S. cerevisiae* samples were fixed in different fixation solutions. Control samples were fixed in SPO culture medium without addition of buffer. Hepes and Carbonate samples were fixed in a buffered fixation solution at the indicated pH. (A) qPCR signal of three different loci for each condition. Each bar represents the mean of two samples. (B) The corresponding chromatin fragment size distributions after sonication of the same samples. The horizontal axis on the small Bioanalyzer diagrams denotes the fragment size in base pairs.

solution to a pH of 9.0 using a carbonate buffer system. Subsequently, we subjected the samples from all three fixation conditions to the same downstream ChIP protocol, with

qPCR and a Bioanalyzer measurement as the final readout. We observed that the samples, which we fixed directly in the meiotic culture SPO medium, generated the highest qPCR signal. In contrast to the samples, which we fixed in one of the buffered fixation solutions, for which we measured a reduced qPCR signal (Figure 12 A). Moreover, fixation in one of the buffered solutions shifts the Bioanalyzer curves slightly to the left, towards a smaller fragment size (Figure 12 B). The reduced fragment size in those samples suggests that the fixation reaction was less intense, as the shearing conditions were the same for all samples. Thus, we established that for a meiotic ChIP experiment, direct fixation in the meiotic culture medium is strongly favored.

Next, we performed a full factorial experiment with a reduced number of input factors to confirm all of the above findings and to reveal potential second-order effects between the input factors. The salt concentration of the IP reaction was included as an additional input factor in this factorial run and tested for its impact on the output factors. The shearing buffer was the same for all samples (Appendix A2). This experiment confirmed that the time of fixation and the time of shearing have both a statistically significant effect on the ChIP-qPCR signal and the shearing result. The other two tested factors had no significant

*Table 3: Effect of four different input factors on the two output factors ChIP-qPCR and shearing, estimated in a linear model. The first column lists the four input factors, as well as possible combinations of two-factor interactions. The columns labeled "coefficient estimate" contain the quantified effect on the output factors. Std Error denotes the standard deviation of the coefficient estimate and measures how precisely the unknown coefficient is modeled. The t-value is calculated dividing the coefficient estimate by the std. error, it allows calculating the p-value. The p-value indicates whether an input factor has a significant effect on the output factor.*

	ChIP-qPCR			Shearing		
	Coefficient estimate	t value	Pr(> t )	Coefficient estimate	t value	Pr(> t )
tShear	-0.008178	-2.941	<b>0.01343 *</b>	-0.076928	-9.297	<b>1.52e-06 ***</b>
NaCl	0.003037	1.092	0.29810	-0.008491	-1.026	0.3269
protInhib	-0.001930	-0.694	0.50199	0.004714	0.570	0.5803
tFix	0.009421	3.388	<b>0.00606 **</b>	0.018627	2.251	<b>0.0458 *</b>
tShear:NaCl	-0.0044626	-1.894	0.116783	-0.008479	-1.510	0.1914
tShear:protInhib	0.0028812	1.223	0.275920	0.009863	1.757	0.1393
tShear:tFix	-0.0034168	-1.450	0.206747	0.007412	1.320	0.2440
NaCl:protInhib	-0.0039956	-1.696	0.150719	-0.013592	-2.421	0.0601
NaCl:tFix	0.0011862	0.503	0.636073	-0.007736	-1.378	0.2267
protInhib:tFix	-0.0002085	-0.088	0.932917	0.011260	2.005	0.1012

effect. Moreover, no second-order effects could be detected among the input factors, implying that all input factors act independently on the output factors, regardless of the value of the other tested input factors (Table 3). The estimated coefficients for the shearing time and fixation time are -0.82 and 0.94, respectively, indicating that a reduced shearing time and an increased fixation time result in an increase of the ChIP-qPCR signal by approximately 1.76 ChIP% for the tested genomic locus.

Taken together, we show that the composition of the shearing buffer, the time of shearing and the time of fixation are the primary determinants of the chromatin shearing pattern and the qPCR signal in a meiotic ChIP experiment. No second-order effects exist among those factors, implying that they act independently on the results and that they can be modified and optimized separately. We identified the shearing buffer as the most crucial component for the result of a ChIP experiment, and particular care should be taken to optimize this often neglected factor. The buffer system, the salt concentration and in particular the detergents of the shearing buffer all affect the result. Of these components, the detergent type is the most important one. Concerning the fixation conditions, we established that for meiotic experiments, the fixation of the cells should be performed directly in the culture medium without using a special buffer.

For our meiotic ChIP-qPCR experiments, we established the following conditions: 40 min fixation at a final concentration of 3 % formaldehyde, which is added directly to the meiotic culture. 22 min sonication in a shearing buffer consisting of 10 mM Hepes-KOH (pH 7.5), 0.1 % Na-Deoxycholate, 1 % Triton X-100, 1mM EDTA.

### **ChIP-qPCR of meiotic cohesin**

Having established the optimal conditions for ChIP-qPCR in meiosis, we performed a meiotic time course experiment, using *CDC20-mAR* strains, in which the meiosis-specific cohesin subunit Rec8 was Ha3-tagged. Two *S. cerevisiae* cultures were induced to enter meiosis and arrested in metaphase I after eight hours. Then, we released one of the two cultures from the arrest by addition of CuSO<sub>4</sub>, which subsequently underwent the two meiotic divisions synchronously. The other culture was kept in a prolonged arrest. Starting from the time of release, we took samples every 20 minutes over a time of 2.5 hours, fixed them in formaldehyde, washed and stored them at -80°C. To assure that the two cultures arrested in metaphase I and that the release was highly synchronous, we first

subjected the samples to immunofluorescence analysis to assess the meiotic stage of the cells (Figure 13 A). For this purpose, we stained the meiotic spindles. The spindles can be used as meiotic stage markers. For each sample this meiotic stage marker and the nuclear division was assessed in 100 cells. In both cultures, the majority of cells arrested in metaphase I after eight hours. 40 minutes after the release, only a tiny fraction of the cells in the released culture still exhibited metaphase I spindles, contrary to the arrested culture, in which the fraction of metaphase I cells stays almost constant. Concomitant,

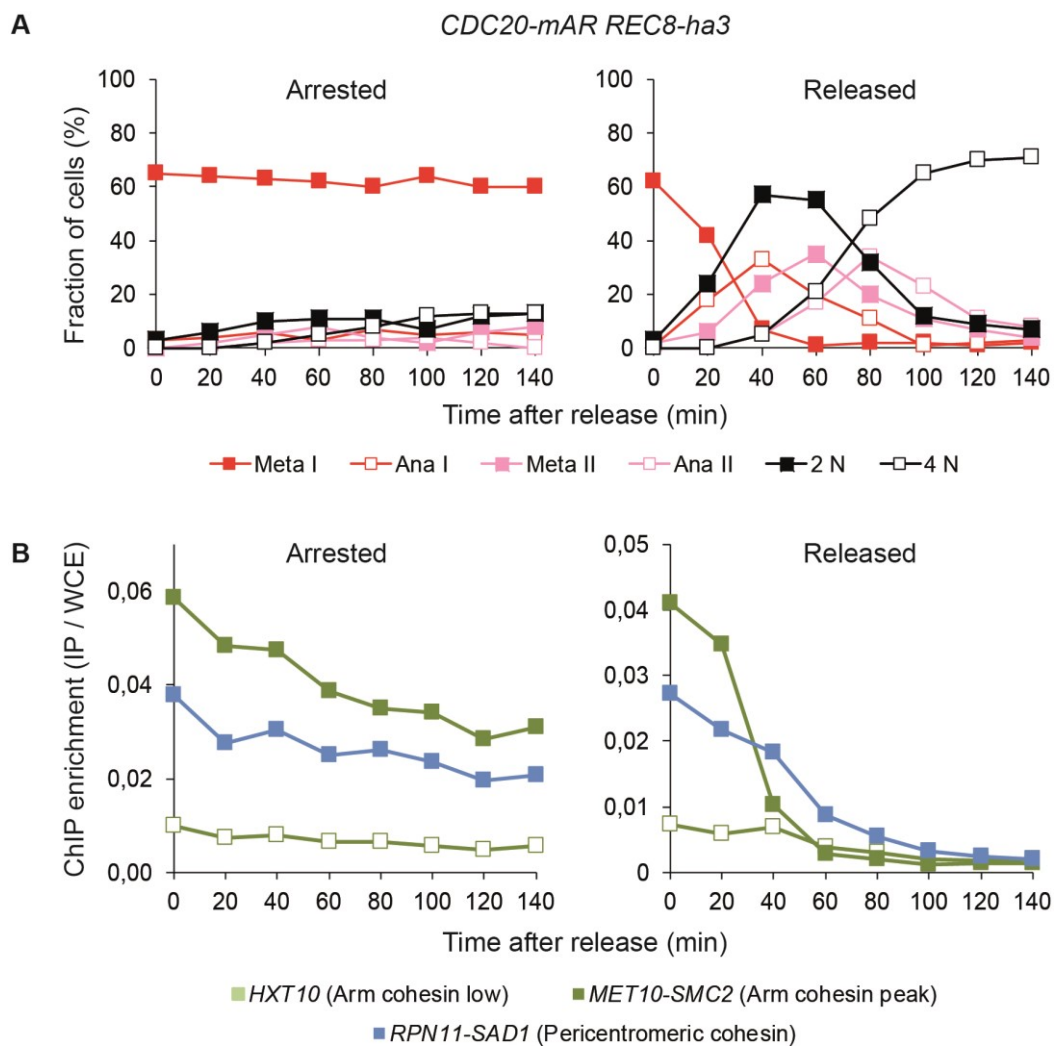


Figure 13: *ChIP analysis of the cohesin subunit Rec8-ha3 in a meiotic yeast culture synchronized by the CDC20-mAR system.* The culture was arrested in metaphase I and synchronously released from the arrest at 0 minutes (right diagram) or kept in a prolonged metaphase I arrest (left diagram). (A) Immunofluorescence countings of meiotic spindles and nuclear division to assess the meiotic stage of individual time point samples. Spindles were visualized by staining of tubulin with a specific antibody. Nuclei were visualized by DAPI staining of DNA. (B) ChIP-qPCR of the same meiotic samples. Three different loci on chromosome VI. were analyzed.

most of the cells in the released culture displayed two nuclei (2 N) after 40 minutes. The peak of anaphase I spindles occurs approximately 40 minutes after the release, the

maximum of metaphase II spindles after 60 minutes and that of anaphase II spindles after 80 minutes. 120 minutes after the release, the majority of cells in the released culture showed four nuclei (4 N), indicating completion of the two meiotic divisions. In the arrested culture, nearly three-quarter of cells still displayed intact undivided nuclei at this time point.

To analyze the behavior of meiotic cohesin during the two divisions, we subjected all the samples of this time course to our optimized ChIP-qPCR protocol (Figure 13 B). In the IP reaction, we enriched for the ha-tagged meiosis-specific Rec8 cohesin subunit. After purification of the ChIP samples, we analyzed the obtained DNA samples using qPCR primers specific for three different loci on chromosome VI. Each locus representing a distinct “class” of cohesin: The first locus is at the chromosome arm, with a very low enrichment of cohesin in a wildtype cell (“arm cohesin low”), as was determined by others (Lengronne et al., 2004). The second locus represents a cohesin peak region on the chromosome arm (“arm cohesin peak”). The third locus represents a cohesin peak region in the protected region close to the centromere (“pericentromeric cohesin”). As expected, in metaphase I (0 min), the qPCR signal at the cohesin peak sites at the chromosome arm and around the centromere are much higher than that of the arm site with low cohesin enrichment. 40 minutes after the release from the arrest, when most of the cells are in anaphase I, the qPCR signal of the “arm cohesin peak” site is almost as low as the signal of the “arm cohesin low” site, indicating the complete removal of arm cohesin. The qPCR signal of the “pericentromeric cohesin” site, on the other hand, is still at approximately 50 % of its initial level at this time. 100 minutes after the release, when most cells are post-anaphase II and completed the two meiotic divisions, the signal of all three loci collapse at a low level.

The qPCR signals of the arrested culture, on the other hand, display a slow decline over time, with no abrupt change between time points. This difference between the two cultures demonstrates that the qPCR pattern of the released culture is indeed a consequence of the release from the metaphase I arrest and reflects the behavior of cohesin during the two meiotic divisions.

To demonstrate the robustness of our approach and to show that the measured cohesin dynamics in the released culture is reproducible, we performed two additional experiments with several weeks in between. Again, we measured the qPCR signal of the same three loci as in the first experiment and calculated the mean for each time point and

each locus independently. We then plotted the calculated means as time course series. To assess the variation between the three experiments, we calculated the standard deviation and plotted one standard deviation as error bar for every data point (Figure 14 A). To correct for variations due to different amounts of input material or different IP efficiencies, we normalized the qPCR signals of individual time courses to the highest signal in the respective time course, which is the initial arm peak signal, before calculation of the mean. This transformation equals the starting level of each time course's signal. Thus, this transformation allows focussing solely on variations that reflect different temporal dynamics of the three investigated loci. However, it excludes variations that arise from different starting levels of the qPCR signal, demonstrating the robustness and

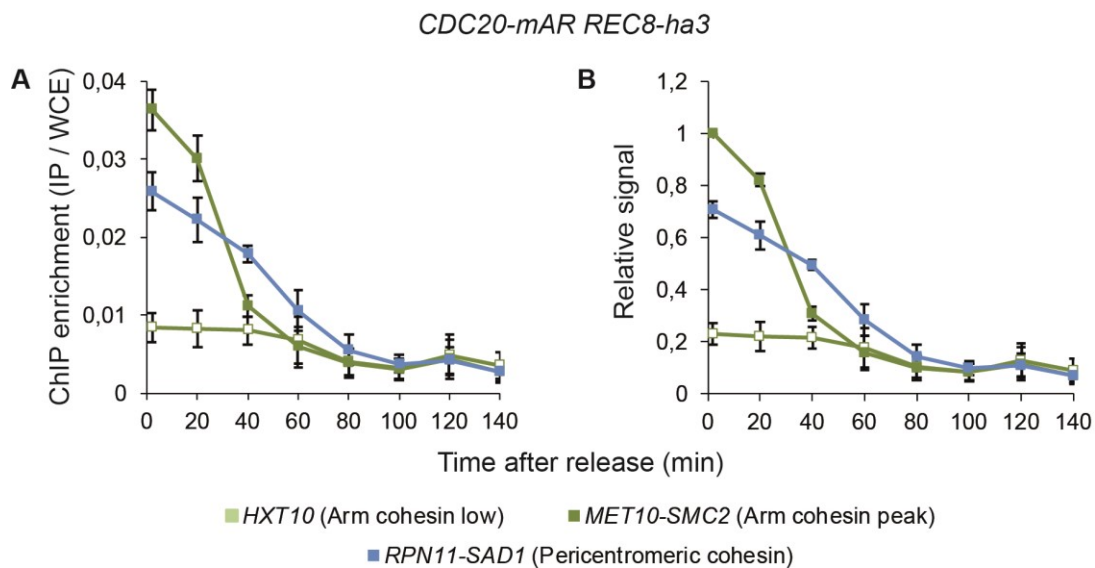


*Figure 14: Mean of three independent biological replicates of a ChIP-qPCR analysis of the meiosis-specific cohesin subunit Rec8-ha3 in CDC20-mAR strains. The measurement starts when the cells were released from the metaphase I arrest at 0 minutes. (A) Mean of the qPCR signal of three independent biological replicates. The error bars indicate one standard deviation. (B) Mean of the normalized qPCR signal of the same three biological replicates. The error bar again indicates one standard deviation. The vertical axis is the qPCR signal, relative to the arm cohesin peak signal.*

reproducibility of our approach (Figure 14 B). Forty minutes after the release from the metaphase I arrest, the signal at the “arm cohesin peak” locus almost collapses with the “arm cohesin low” signal, indicating completion of arm cohesin removal. At this time, the pericentromeric signal is still at approximately 50 % of its initial level. It takes 80 minutes after the release for the pericentromeric signal to fall to the same low level and almost collapse with the “arm cohesin low” signal.

Collectively, we show that once APC<sup>Cdc20</sup> is activated by addition of CuSO<sub>4</sub>, cohesin is removed from the chromosome arm as well as the pericentromeric region. However, the rate of reduction is different between the investigated loci. At the chromosome arm, the qPCR signal is reduced very abruptly, and most of the signal is lost within the first 40 minutes after the release. In the pericentromeric region, on the other hand, the rate of reduction is slower, and it takes more than 80 minutes for the signal to be reduced to the same level like at the other two loci.

### **Application of a ChIP calibration system for meiosis**

To resolve a physiological process in time, one needs to compare samples of the same experiment relative to each other. Therefore, the measured signals need to be quantitative. The prerequisite of a quantitative signal is a conceptual problem when using ChIP-Seq because only ChIP-qPCR generates quantitative data, whereas conventional ChIP-Seq does not. Recently, a method called Calibrated ChIP (calChIP) was developed that allows generating quantitative genome-wide data from mitotic cells (Hu et al., 2015). This calibration technique depends on the presence of a second yeast genome in the samples and is a bioinformatic method that uses the counts and statistics of short read mapping to convert conventional ChIP-Seq profiles into genuinely quantitative profiles. This genome-wide quantitative measurement makes it possible to not only determine the sites of protein binding but also changes in protein concentration over time.

### **Establishment of calibrated ChIP-qPCR for meiosis**

As described by Hu et al. (2015) we used *Candida glabrata* as our calibration strain. *C. glabrata* is a yeast species with a genome size of 12 million base pairs, organized in 13 chromosomes, which is very similar to the *S. cerevisiae* genome, consisting of 12 million base pairs, organized in 16 chromosomes. The phylogenetic distance between both species is not very high, indicating similar physiological characteristics. This similarity in physiology is essential because the cells from both strains need to react in a similar way to the treatment by the ChIP protocol. However, the phylogenetic distance is far enough for a sufficiently high genomic sequence diversity between both strains. This diversity is important, so that sequencing reads can be assigned to one of the genomes based on the DNA sequence. For the calibration system to work it must be possible to

enrich for a chromatin-bound protein by IP with the same antibody in both strains. In our experimental setting, we use an anti-ha-antibody to precipitate our protein of interest. Consequently, a suitable calibration strain for our ChIP workflow needs to express an ha-tagged chromatin-bound protein as well. However, *C. glabrata* is a haploid yeast species. No reports about diploid cells exist to date. Hence, it is not known if this species undergoes meiosis at all. Therefore, as described in the paper by Hu et al. (2015), we used

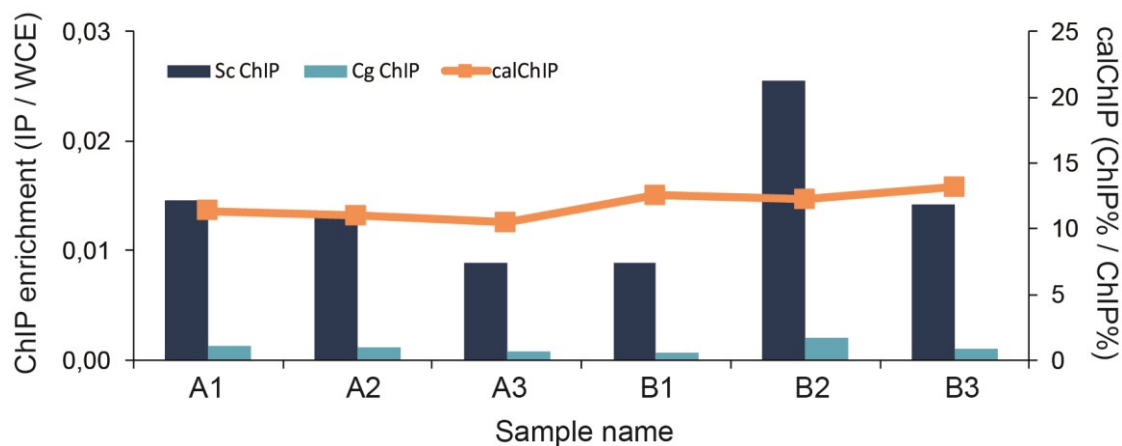


Figure 15: *C. glabrata* tagging plasmid map. The construct for tagging consists of a C-terminal CgSCC1 fragment, the epitope tag, a marker cassette and a CgSCC1 terminator fragment. Additionally, the vector backbone harbors a resistance cassette and ORI for propagation in *E. coli*.

the mitosis-specific cohesin subunit Scc1 as our IP target and aimed to ha3-tag Scc1 on the C-terminus. For this purpose, we designed a tagging plasmid, harboring the C-terminal part of the *C. glabrata* SCC1 gene, followed by the Ha3 epitope tag, a marker cassette conferring resistance to Nourseothricin (NatMX6), and the terminator of the CgSCC1 gene (Figure 15). Using this tagging plasmid, a *C. glabrata* wild-type strain,

obtained from the National Collection of Yeast Cultures (NCYC), was transformed according to the protocol described in the materials and methods section. To validate the expression of the epitope-tagged *SCCI* cohesin subunit, we performed a western blot of TCA samples prepared from a standard mitotic culture of the transformed *C. glabrata* strain. Using an anti-ha antibody, we detected a distinct band in the expected size range, whereas we detected no signal in the negative control, confirming successful epitope tagging.

To produce calibrated ChIP samples, one needs to mix cells from the experimental strain and the calibration strain and subjected this mixture to the same downstream treatment. Subsequently, the DNA amount of both genomic fractions needs to be measured separately in the obtained, purified DNA samples. This separate measurement is possible because the degree of sequence homology between both genomes is low. One possibility is to use genome-specific primers and perform a qPCR measurement for both genomes separately. The other option is to sequence the samples using NGS technology and assign individual reads to one of the two genomes based on sequence similarity. In both cases,



*Figure 16: Comparison of conventional ChIP-qPCR signals with calibrated ChIP-qPCR (calChIP-qPCR) signals of the same samples. The left vertical axis shows the conventional ChIP-qPCR enrichment: IP signal divided by the corresponding WCE signal. The right vertical axis shows the dimensionless calChIP signal. Two sets of triplicates, the sample set A and sample set B, were measured with both methods. Variation can be observed between the replicates of the same sample set, using conventional ChIP enrichment as readout, whereas the calChIP signal of the same replicates is almost free of variation.*

the calibration is done by first calculating the IP efficiency of the calibration genome in every sample, followed by using this value to calibrate the signal from the experimental genome. We tested the calibration system by first performing a ChIP-qPCR experiment on two sets of triplicates, comparing the conventional ChIP enrichment

immunoprecipitated fraction / whole cell extract (IP/WCE) to the calibrated ChIP signal (Figure 16). Each set of triplicates was generated by pooling samples of different time points of a meiotic time course and aliquoting them into equal volumes. The average ChIP enrichment (IP/WCE) of the sample A triplicate is 1.24 %, of the sample B triplicate 1.62 %. However, a substantial variation can be observed between the three replicates of one sample set. The calChIP signal of the same samples, on the other hand, is 10.9 and 12.6, confirming a slightly higher enrichment in sample set B. But the variation between the three replicates of one sample set is much lower. The calChIP signal is dimensionless because it is calculated by dividing the enrichment of the experimental genome by the enrichment of the calibration genome.  $(IP/WCE)_{exp} / (IP/WCE)_{cal}$ . The coefficient of variation (CV) of the conventional ChIP enrichment is 24 for sample set A and 52 for sample set B, compared to 4 for both calChIP signals, demonstrating the striking ability of the calibration system to correct for most of the technical variation in a meiotic experimental setting.

Taken together, we demonstrate that the calibration system is successfully established for ChIP-qPCR experiments, using meiotic samples. We further show that the calibration system is potent in reducing technical variation and hence, is not only useful for ChIP-Seq, but also for ChIP-qPCR experiments.

### **Establishment of calibrated ChIP-Seq for meiosis**

To test whether the ChIP samples produced by our calChIP-qPCR protocol were suitable for generating ChIP-Seq profiles, we subjected those samples to a NGS platform and mapped the obtained reads to the *S. cerevisiae* genome. Doing this, we realized that the DNA amount in our samples was close to the lower limit for preparation of a sequencing library. Nevertheless, the ChIP-Seq profile of the metaphase I-arrest experimental sample displayed several Rec8 cohesin peaks, distributed all along the chromosome, consistent with previously published results (Lengronne et al., 2004). The control sample, on the other hand, displayed one single central peak around the centromere region (Figure 17). We hypothesized that this central spike could be an artifact, generated by non-specific binding of the antibody during the IP enrichment step. Thus, analyzing a sample set with ChIP-Seq for the first time, revealed that the conditions for optimal ChIP-qPCR samples do not generate optimal ChIP-Seq samples. Consequently, we had to adapt the protocol for ChIP-Seq with respect to two parameters. First, we aimed to reduce the artefactual

enrichment in the centromere region. Second, we sought to increase the DNA amount in the ChIP samples, to ensure successful sequencing library preparation also for samples

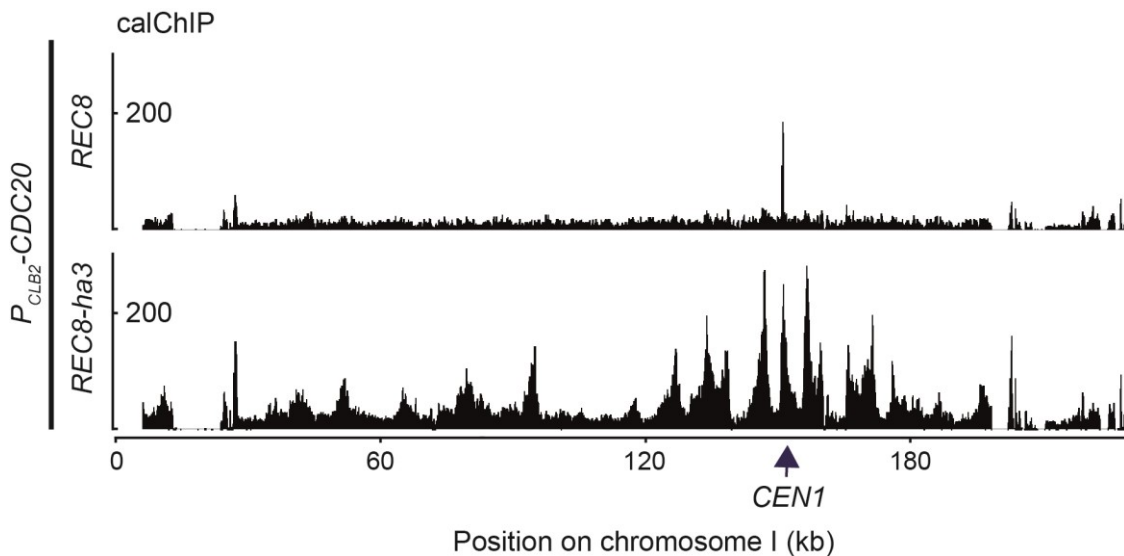


Figure 17: Calibrated ChIP-Seq profiles of the occupancy of the meiosis-specific cohesin subunit Rec8 on chromosome I of *S. cerevisiae*. The vertical axis shows dimensionless units and represents the quantitative calChIP signal.

with low protein occupancy.

### Antibody titration

As the most likely source of artefactual enrichment of signal is the IP step in the ChIP protocol, we optimized the antibody concentration in the IP reaction by performing a titration series (Figure 18 A). The ChIP enrichment of Rec8-ha3 at the centromere, as measured by ChIP-qPCR, increases with increasing antibody concentrations. Also, the DNA amount in the samples increased with increasing antibody concentrations. However, the curve depicting the relationship between the antibody concentration and DNA amount exhibits a declining slope, indicating that very high amounts of antibody only generate small amounts of additional DNA (Figure 18 C). Using a set of untagged samples as control revealed that with increasing antibody concentrations a ChIP signal also appeared in these samples. Therefore, we calculated the signal/noise ratio by dividing the signal of the tagged sample by the signal of the untagged sample and determined an antibody amount of 7  $\mu\text{g}/\text{sample}$  as optimal (Figure 18 B), because it maximizes the signal/noise ratio and still pulls-down enough DNA. In an attempt to identify the experimental conditions, which minimize the non-specific background in our experiments, we tested the 3F10  $\alpha$ -Ha antibody against the previously used 12CA5  $\alpha$ -Ha antibody. The

signal/noise ratio of 7  $\mu\text{g}$  12CA5 ChIP samples was on average 17. Strikingly, the signal/noise ratio of 7  $\mu\text{g}$  3F10 samples was on average 3995, with comparable levels of

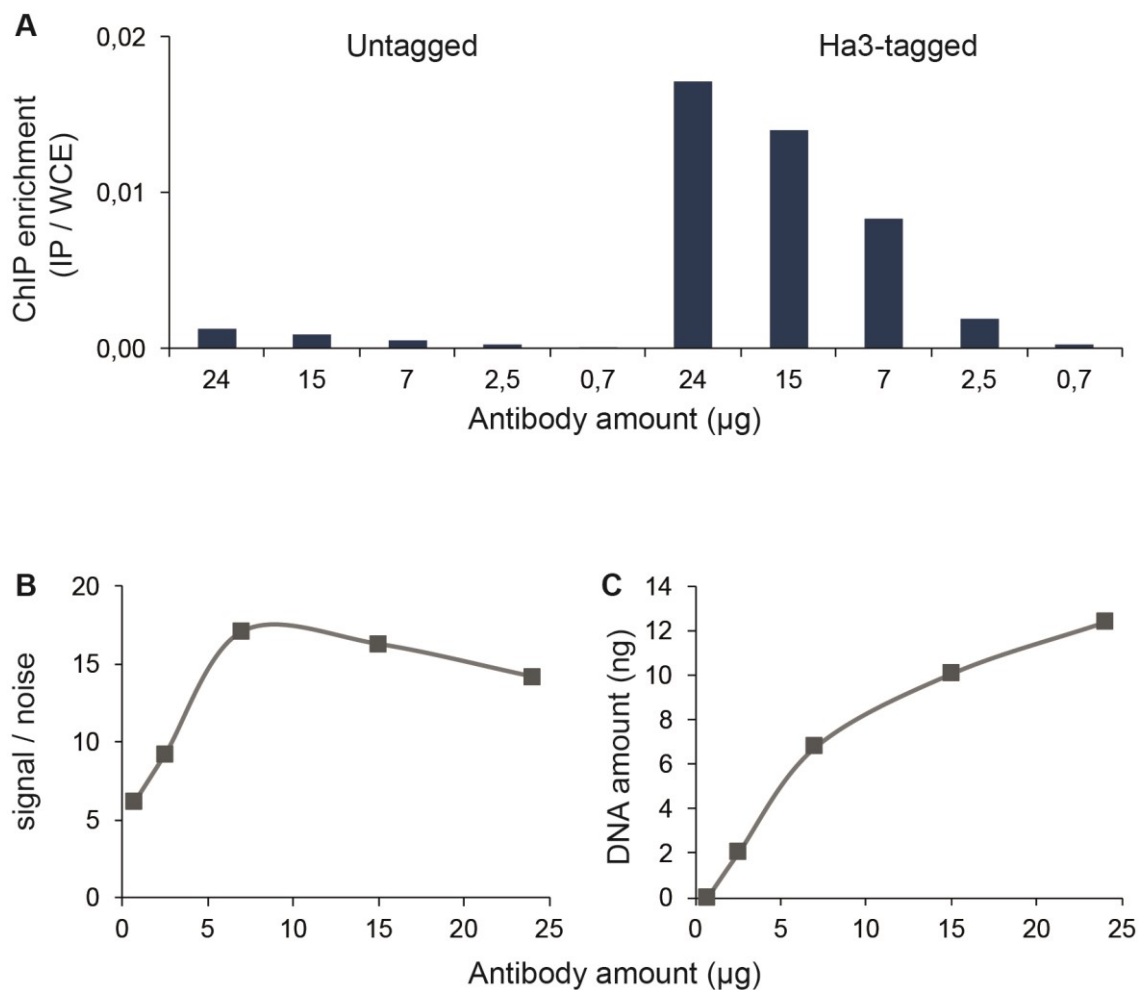


Figure 18: *Anti-ha antibody titration series.* (A) Enrichment of signal measured by ChIP-qPCR in the tagged and untagged samples. (B) The signal / noise ratio, calculated by dividing the ChIP-qPCR signal of the tagged sample by the corresponding value of the untagged sample. (C) DNA amount in the tagged samples.

signal in the tagged samples. Thus, the 3F10 antibody generates extremely clean, background-free ChIP samples and is by more than two orders of magnitude superior over the widely used 12CA5 antibody. Consequently, we established the 3F10 antibody as our standard ChIP antibody.

### Input DNA

To increase the DNA amount in the ChIP samples, we increased the amount of input material and measured how the ChIP signal reacts to this change. We found that the calChIP-qPCR signal is almost invariant towards different amounts of DNA in the

samples (Figure 19 A). This insensitivity towards the input DNA concentration makes it possible to increase the amount of input material, without biasing the calChIP-qPCR results, but allowing for a more efficient sequencing library preparation, due to higher amounts of DNA in the samples. The technical problem is that measuring the DNA concentration of the samples is only possible at the end of the ChIP workflow, when the

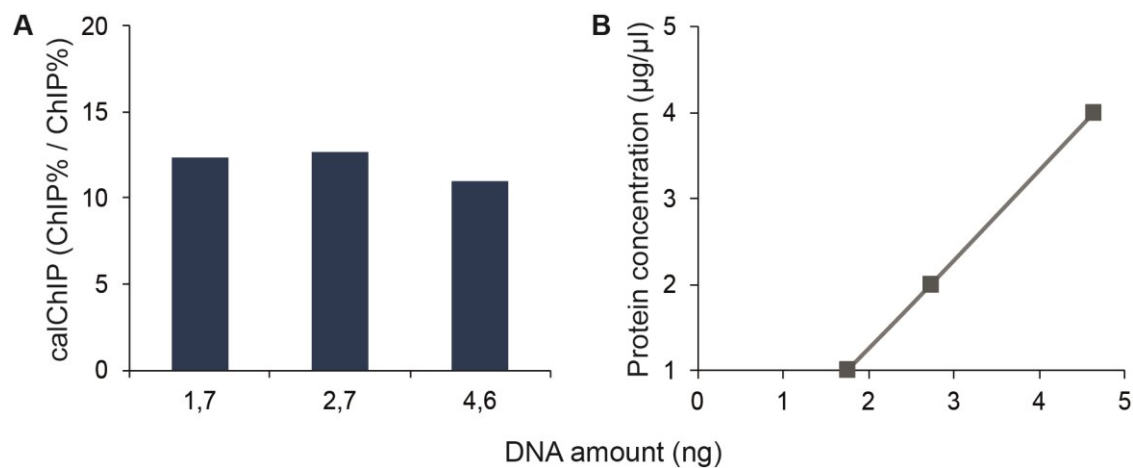


Figure 19: *Titration of the input material in a calChIP-qPCR experiment.* The horizontal axis in both diagrams denotes the amount of DNA in the samples. On the left side the calChIP-qPCR signal for three different DNA concentrations is shown. On the right side the DNA amount in the samples was correlated to the protein concentration in the whole cell extract before purification of the DNA.

samples underwent the final purification, making it difficult to directly use the DNA concentration as a measure for the correct amount of input material in the samples. The protein concentration in the samples, on the other hand, can easily be measured in the crude extract after sonication, by using, for example, a colorimetric Bio-Rad Protein Assay. Correlating the protein concentration of the samples with their DNA content after purification revealed an almost exact linear relationship between those parameters (Figure 19 B), establishing the protein concentration as a reasonable estimate for the final DNA concentration. Consequently, from this time one, we measured the protein concentration during every ChIP experiment, to ensure sufficiently high amounts of input material in the ChIP samples.

### Fragment size

One problem arising from increasing the amount of input material was that the size distribution of chromatin fragments shifted to the right, indicating a less intense

fragmentation under identical sonication conditions (Figure 20 A). Increasing the sonication intensity, while leaving the amount of input material at the highest tested

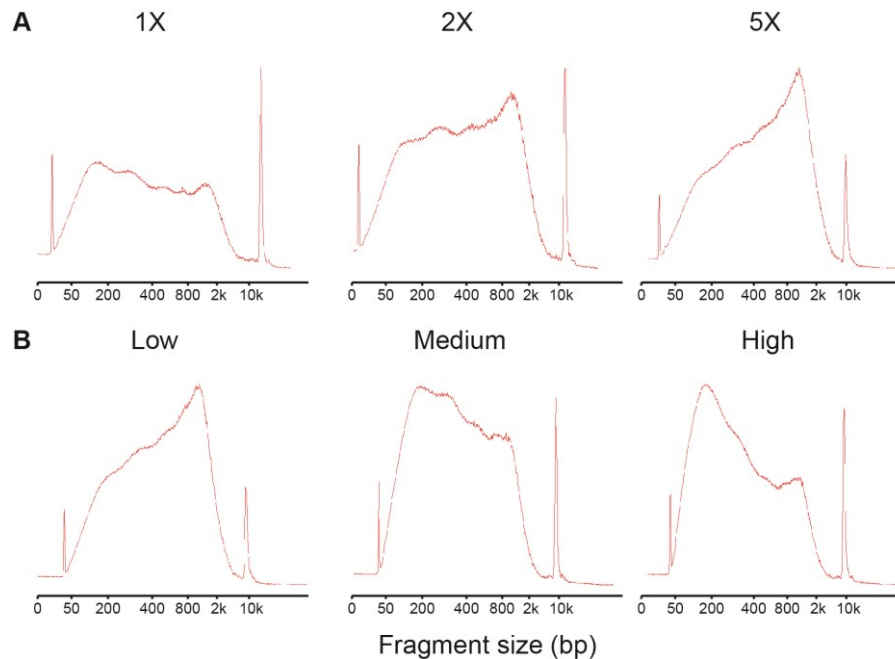


*Figure 20: Bioanalyzer profiles of an input titration series show the chromatin fragment size distributions after shearing on a Covaris water bath sonicator. The horizontal axis on the small diagrams denotes the fragment size in base pairs after shearing. (A) Profiles of three different amounts of input material, fragmented under identical conditions. (B) Fragmentation of 5X input samples with increasing sonication intensities.*

amount, corrected for this effect and shifted the profiles back towards smaller chromatin fragments (Figure 20 B).

Thus, we established a five-fold higher amount of input material, compared to our initial ChIP-qPCR protocol, sonicated with maximal intensity, as the best condition for ChIP-Seq samples.

### **Calibrated ChIP-Seq of a meiotic arrest/release time course**

Having established a calibrated ChIP-Seq protocol for meiosis, we next aimed to analyze samples from a meiotic arrest/release experiment. To this end, we induced a *CDC20-mAR* strain, containing *REC8-ha3* to enter meiosis and after eight hours, the cells arrested in metaphase I. Then, we released this strain from the arrest, and the cells synchronously underwent the two meiotic divisions. Starting from the release, we took samples every 20 minutes. To exclude that the derived cohesin pattern is affected by the synchronization

procedure we kept the cells in a prolonged metaphase I arrest in another experiment and assessed whether the cohesin pattern changed under these conditions. To achieve this, we again used *CDC20-mAR REC8-ha3* cells, in which the cells arrested in metaphase I, but contrary to the first experiments, we never released them into anaphase I. Immunofluorescence analysis revealed that both cultures stably arrested in metaphase I with the majority of cells displaying a metaphase I spindle after 8 hours (Figure 21). The released culture reached the peak of anaphase I spindles after 40 minutes, proceeded through the second meiotic division and showed four equal masses of DNA in most of the cells at the end of the time course, indicating completion of meiosis. These immunofluorescence kinetics were comparable to previously established kinetics (Figure 13 A). The arrested culture, by contrast, displayed metaphase I spindles throughout the whole time course.

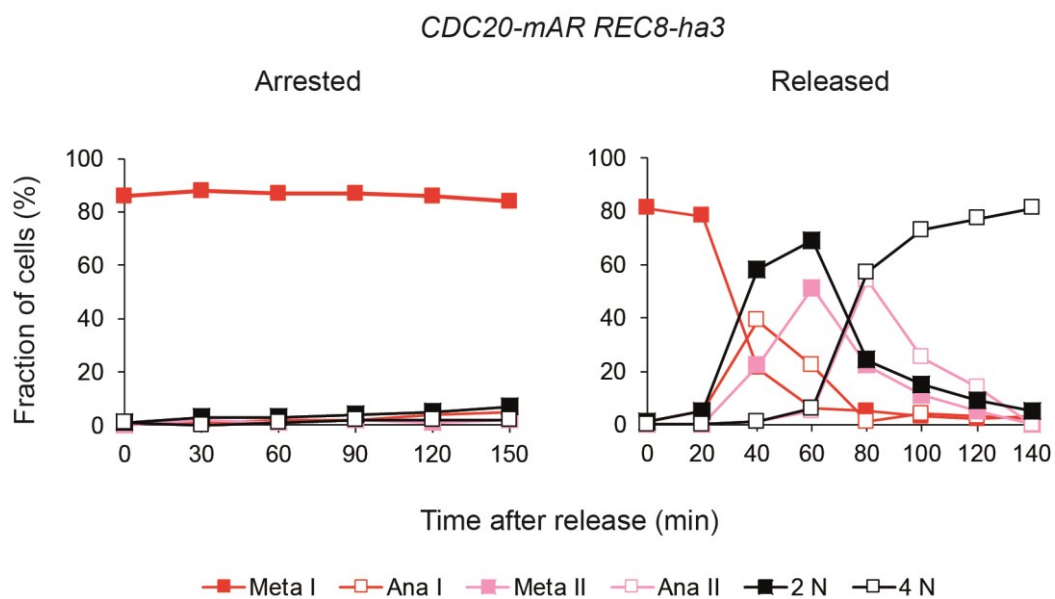


*Figure 21: Immunofluorescence countings of meiotic spindles and nuclear division of meiotic time course samples of *CDC20-mAR REC8-ha3* strains. Spindles were visualized by staining of tubulin with a specific antibody. Nuclei were visualized by DAPI staining of DNA.*

We continued by subjecting these samples to library preparation, NGS, mapping and calibration to generate calChIP-Seq profiles for a genome-wide data analysis. We started by comparing the metaphase I Rec8 profiles of all 16 chromosomes. Projecting all profiles on the same scale visualized the different sizes of the chromosomes comprising the *S. cerevisiae* genome, ranging from 230 kb to 1,5 Mb (Figure 22). Similar to previous results

(Kiburz et al., 2005), independently of their size, all chromosomes displayed an almost

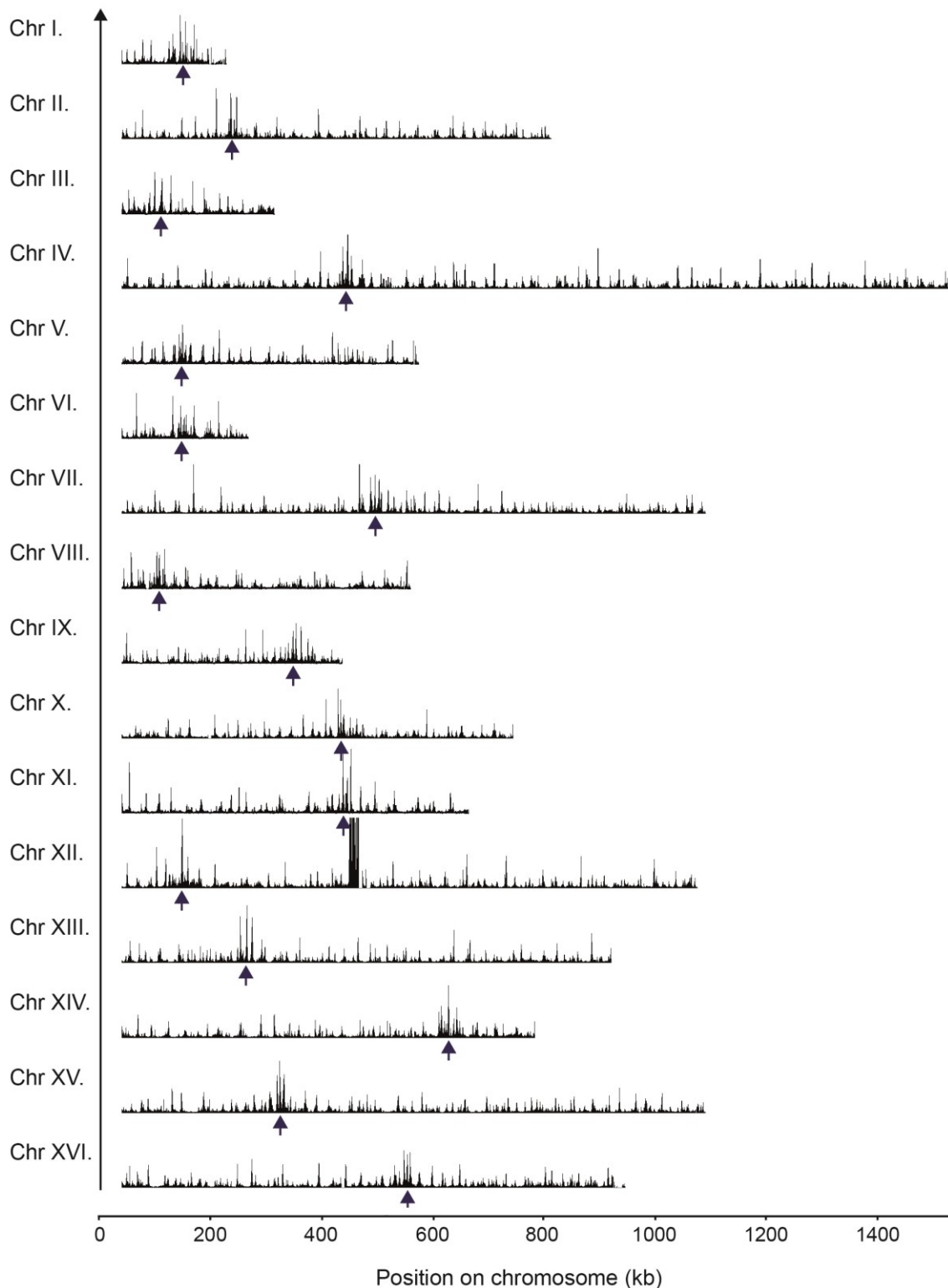


*Figure 22: Calibrated ChIP-Seq profiles of Rec8 in metaphase I of all 16 chromosomes of S. cerevisiae. The horizontal axis denotes the chromosomal position in base pairs, on the same scale for all chromosomes. The quantitative calChIP signal makes the intensities of individual chromosomes directly comparable to each other. The dark blue arrow indicates the position of the centromere. The signal accumulation near the center of chr XII. is an artefact from repetitive rDNA loci.*

equal accumulation of cohesin in the pericentromeric region and showed unevenly spaced cohesin peaks on the chromosomes arms in metaphase I. We observed a high degree of variation concerning the position of the centromere. Whereas the centromere was localized almost in the center for some of the chromosomes, it was localized acrocentrically for others.

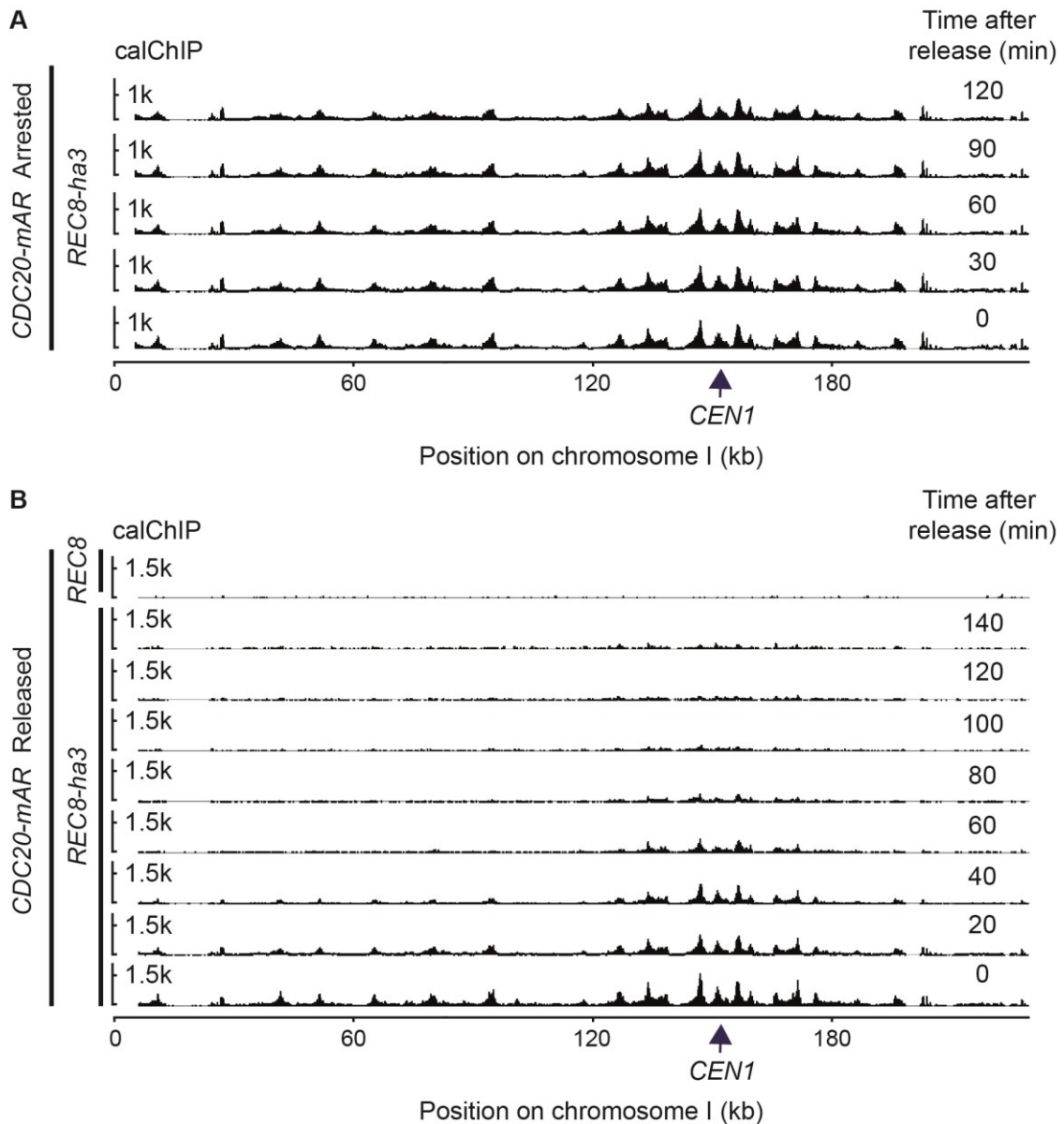


Figure 23: Calibrated ChIP-Seq profiles of chromosome I of CDC20-mAR REC8-ha3 strains. The vertical axis measures the calibrated signal intensity of Rec8-ha3. The time scale denotes minutes after the release from the metaphase I arrest. Upper profile: The culture was kept in a prolonged arrest. Lower profile: The cells were released from the arrest 8 hours after transfer to SPO.

Next, we analyzed individual time points of the arrest/release experiment, displayed as time series of calChIP-Seq profiles (Figure 23). These profiles showed that 40 minutes after the release, the peaks on the chromosome arms were almost entirely reduced (Figure 23 B). At this time point, the released culture reached the peak of anaphase I (Figure 21). Thus, the calChIP-Seq histogram at 40 minutes visualized the state of cohesin at the time of the first meiotic division: Arm cohesin is cleaved, allowing the spindle microtubules to pull to opposite spindle poles the maternal and paternal sister chromatid pairs, which are still held together by the fraction of protected pericentromeric cohesin. Interestingly, the cohesin peaks in the pericentromeric region also became smaller after 40 minutes, confirming the previous qPCR results that pericentromeric cohesin is already cleaved in meiosis I (Figure 14) and only a small fraction of the initial metaphase I cohesin is protected. After 80 minutes, also the peaks in the pericentromeric region are almost undetectable, indicating completion of the second meiotic division. Cleaving the pericentromeric cohesin enables the meiosis II spindle to pull the two sister chromatids to opposite poles, resulting in four equal masses of DNA. In the arrested culture, the Rec8-ha3 peaks became slightly broader in this time frame (Figure 23 A). However, no drastic changes could be observed, demonstrating that cohesin is stably bound to chromosomes over a long time in a metaphase I arrest. Hence, by arresting the cells in metaphase I, we did not generate unphysiological loading or loss of cohesin over time. The total amount of cohesin was constant for more than 9,5 hours, and the localization of the cohesin peaks did not change.

Taken together these results demonstrate that the obtained profiles reflect very well the physiological situation in wild-type cells and our synchronization system does not interfere with the physiological cohesin pattern. Moreover, these results demonstrate that it is possible to increase the temporal and spatial resolution of cohesin dynamics by combining a biochemical calibrated ChIP-Seq assay with the novel *CDC20-mAR* synchronization system.

### **Two-step cohesin cleavage in meiosis**

Having demonstrated that our experimental set-up is working and that the cohesin fraction, which is localized around at the centromere in metaphase I, is not identical to the protected cohesin fraction, we now aimed to analyze and characterize the protected

cohesin fraction with high spatial resolution on all chromosomes. Previously, our lab showed that the casein kinase 1 $\delta$  from budding yeast (called Hrr25) is involved in regulating the stepwise loss of cohesin during the two meiotic divisions (Arguello et al., 2017). By inactivating the analog-sensitive mutant of Hrr25 (called hrr25-as1) after the

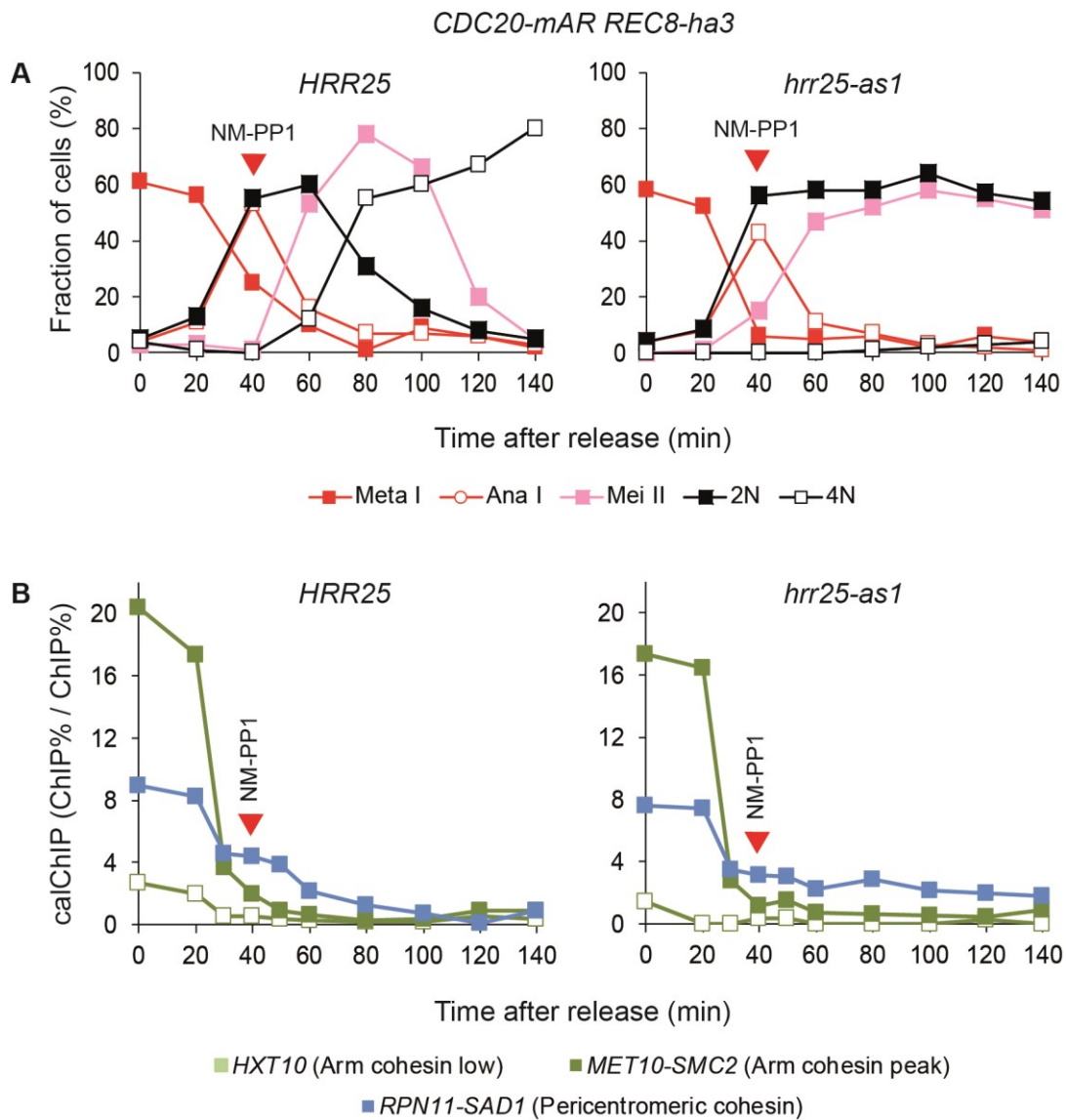


**Figure 24: Meiotic time course samples of *CDC20-mAR REC8-ha3 HRR25* (control) and *CDC20-mAR REC8-ha3 hrr25-as1* (experimental) strains.** The cells were released from the metaphase I arrest at 0 minutes. After 40 minutes, the *hrr25-as1* inhibitor NM-PP1 was added. (A) Immunofluorescence counting of meiotic spindles and nuclear division to assess the meiotic stage of individual time point samples. Spindles were visualized by staining of tubulin with a specific antibody. Nuclei were visualized by DAPI staining of DNA. (B) Calibrated ChIP-qPCR of the same meiotic samples. Three different loci on chromosome VI. were analyzed.

cells underwent the metaphase I-to-anaphase I transition, it is possible to arrest the cells in a meiosis II-like state. This arrest makes it feasible to preserve the protected centromeric cohesin fraction, as it physiologically occurs during the short phase of

metaphase II, for a prolonged time. For this experiment, we used *CDC20-mAR REC8-ha3 hrr25-as1* experimental strains and *CDC20-mAR REC8-ha3 HRR25* control strains. Both strains were induced to undergo meiosis and arrested in metaphase I, followed by a synchronous release into anaphase I. Starting from the release, we took samples in 10 or 20 minutes intervals, respectively. 40 minutes after the release, we inhibited the activity of the *hrr25-as1* protein. Immunofluorescence analysis revealed that both cultures stably arrested in metaphase I with the majority of cells displaying a metaphase I spindle after 8 hours (Figure 24 A). After the release, both cultures underwent the metaphase-to-anaphase transition with comparable synchrony. 40 minutes after the release both cultures reached the peak of anaphase I spindles. The control strain proceeded through the second meiotic division, completed meiosis and showed four equal masses of DNA in most of the cells at the end of the time course. The experimental strain, on the other hand, formed meiosis II spindles but failed to undergo the second nuclear division and was unable to disassemble meiosis II spindles during the time course, as shown previously (Arguello et al., 2017). Analyzing those samples using calChIP-qPCR (Figure 24 B), revealed an abrupt loss of arm cohesin in both strains, once we released the cells from the metaphase I arrest. Also, pericentromeric cohesin was lost in both strains, starting from the release, but at a lower rate. Whereas the arm cohesin signal collapsed with the “arm cohesin low” signal approximately 50 minutes after the induction of *Cdc20* in both strains, the pericentromeric curve was still above the other two curves at this time point, reflecting partial protection of the initial pericentromeric cohesin. 80 minutes after the release all three cohesin signals collapsed to the same low level in the *HRR25* strain. In the *hrr25-as1* samples, by contrast, a small pericentromeric qPCR signal was retained and reproducibly detectable in all consecutive time points, giving the first insight into the amount of the protected meiosis II-specific cohesin fraction. Because the cells of the experimental strain failed to divide their nuclei a second time, but instead mostly remained with two equal masses of DNA, one could conclude that the remaining cohesin provides enough cohesion to resist the pulling spindle forces.

We continued by subjecting these samples to library preparation, NGS, mapping and calibration to generate calChIP-Seq profiles for a genome-wide data analysis (Figure 25). These profiles showed that consistent with the qPCR measurement, 30 minutes after the release, the peaks on the chromosome arms were almost entirely reduced in both strains. The peaks in the pericentromeric region, by contrast, became smaller after 30 minutes,

again confirming previous results that pericentromeric cohesin is already cleaved in meiosis I. In the *HRR25* strain, after 80 minutes, the curves of all three qPCR loci

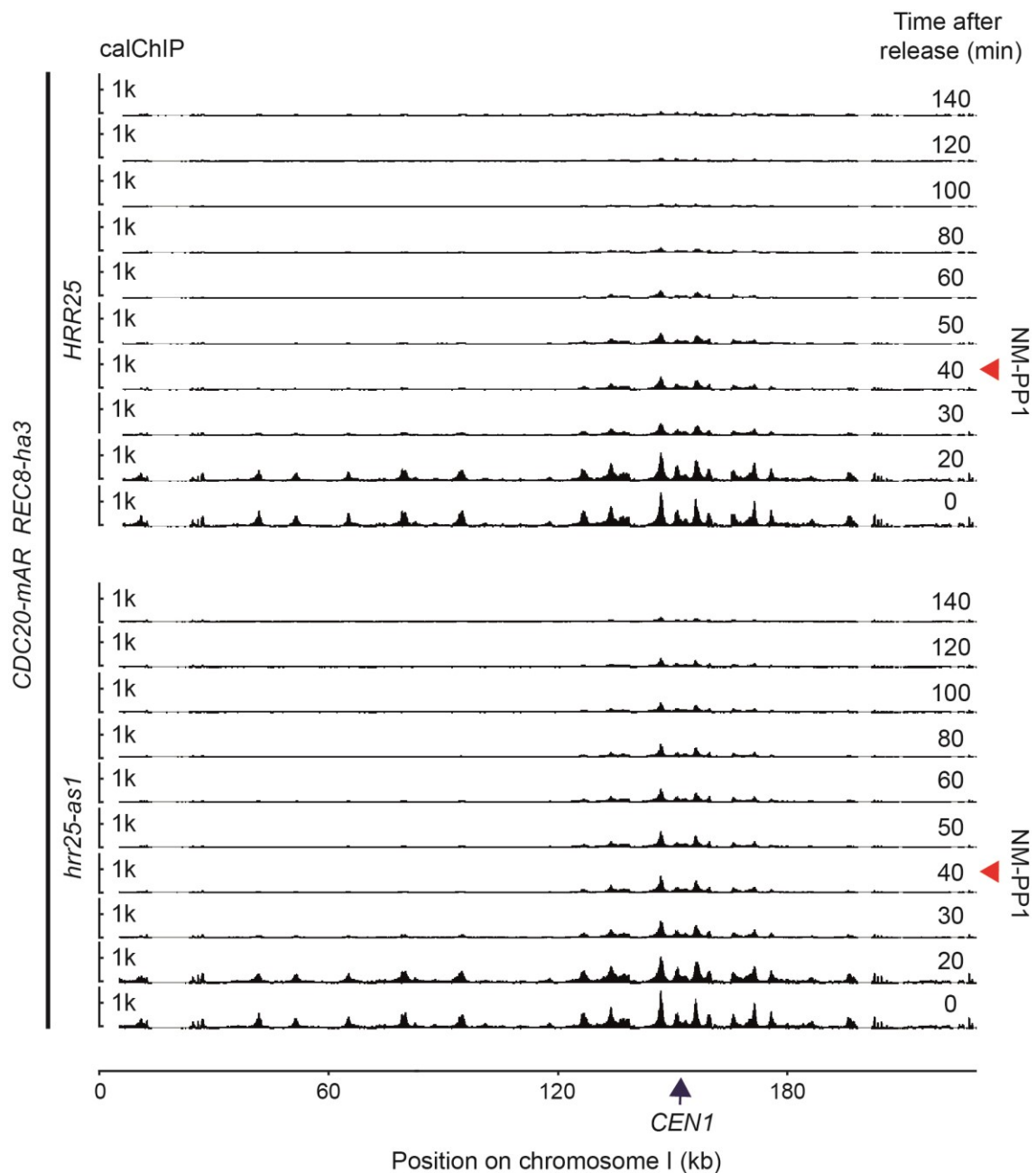


**Figure 25: Calibrated ChIP-Seq profiles of *Rec8-ha3* on chromosome I, from samples of *CDC20-mAR REC8-ha3 HRR25* and *CDC20-mAR REC8-ha3 hrr25-as1* strains. The vertical axis measures the calibrated signal intensity of *Rec8-ha3*. The time scale denotes minutes after the release from the metaphase I arrest. 40 minutes after the release the *hrr25-as1* inhibitor *NM-PP1* was added to inactivate the enzyme.**

collapsed to the same low level, which is consistent with the calChIP-Seq profile, in which the peaks are almost utterly absent after 80 minutes. Thus, the cohesin dynamics we measure by using calChIP-qPCR match the calChIP-Seq results. In the *hrr25-as1*

strain, on the other hand, a small pericentromeric cohesin fraction was preserved until the end of the time course. We observed an identical pattern on other chromosomes. Hence, these results confirm that the low amount of cohesin we observe in the vicinity of the centromere in the wild-type after 30 minutes, indeed represents the meiosis II cohesin pattern. Moreover, these findings are consistent with our qPCR measurements and

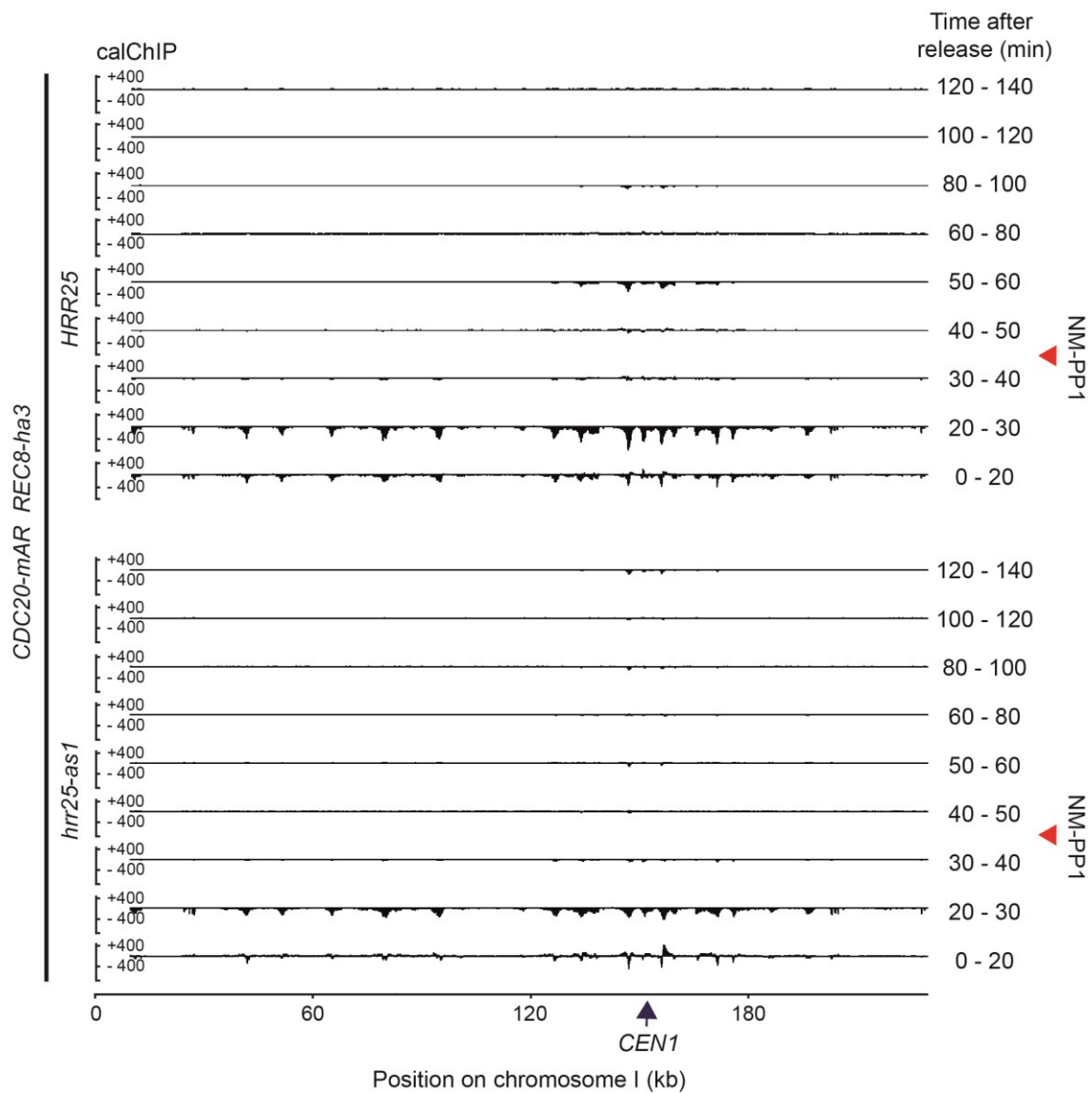
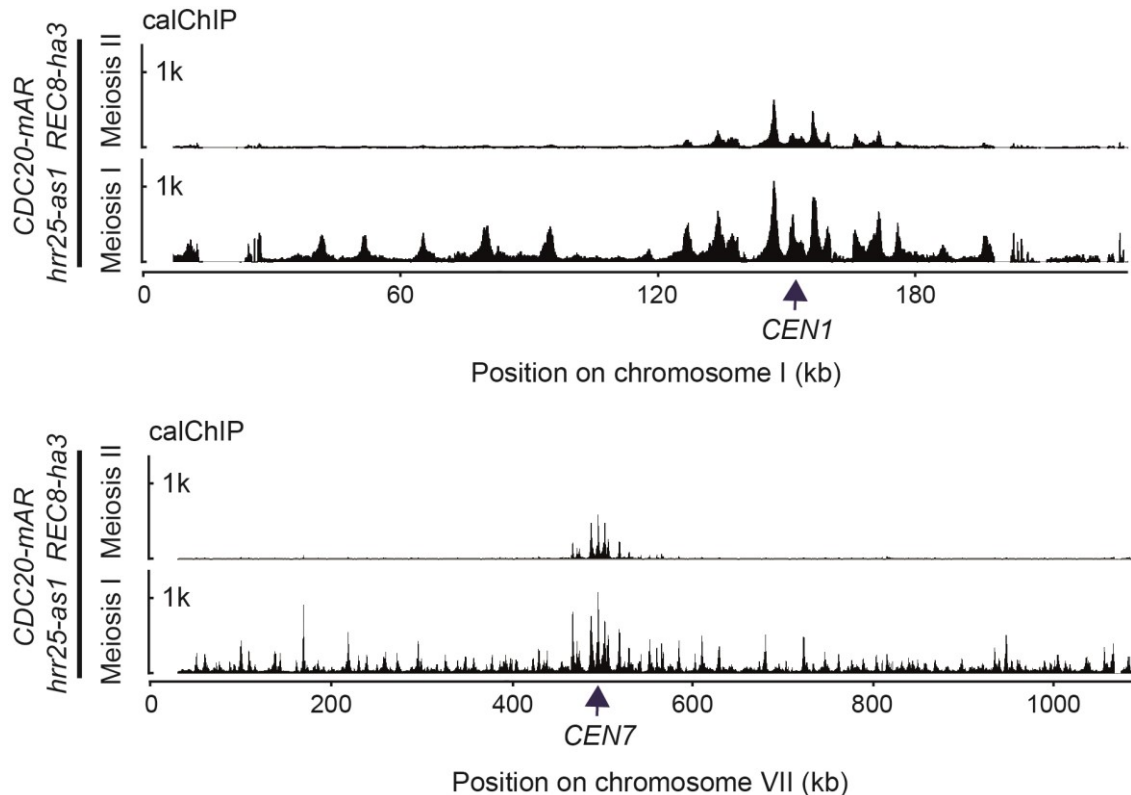


Figure 26: **Differential calibrated ChIP-Seq profiles of Rec8-ha3.** The profiles depict the difference between two conventional calibrated ChIP-Seq profiles. The vertical axis measures the differential calibrated signal intensity of Rec8-ha3. Negative values indicate a loss of Rec8-ha3 between two time points. The time scale denotes minutes after the release from the metaphase I arrest. 40 minutes after the release the *hrr25-as1* inhibitor NM-PP1 was added to inactivate the enzymatic activity.

confirm that the amount of pericentromeric cohesin, which provides cohesion in meiosis II is very little.

Having available quantitative calibrated ChIP-Seq profiles with a very reduced noise level allowed generating differential calChIP-Seq profiles (Figure 26). These differential profiles were generated by subtraction of one profile from the profile of the previous time point, visualizing the dynamic changes during the time course. Consequently, these profiles did not show protein occupancy at a specific time point, but the difference in occupancy between two time points, resulting in negative values. This approach allowed visualizing the meiotic two-step cohesin cleavage with very high resolution in the *HRR25* control strain. In this strain, most of the cohesin is cleaved from chromosomes between 20 and 30 minutes after the release. The second wave of cleavage occurs between 50 and 60 minutes and removes the protected pericentromeric cohesin in meiosis II. In the *hrr25-as1* experimental strain, by contrast, only the first wave of cleavage between 20 and 30 minutes could be detected, whereas no second wave of cleavage occurred.

Previous work estimated the size of the protected pericentromeric region indirectly by correlating metaphase I Rec8 and Sgo1 profiles (Kiburz et al., 2005). Arresting the cells in a meiosis II-like state using the *hrr25-as1* allele, allowed us for the first time to directly



**Figure 27: Calibrated ChIP-Seq profiles of Rec8-ha3 on chromosome I (upper profiles) and chromosome VII (lower profiles) of *S. cerevisiae*.** The vertical axis denotes the quantitative calChIP signal. The size of the protected region is approximately 50.000 bp and this size is very similar between chromosomes, regardless of the total chromosome length.

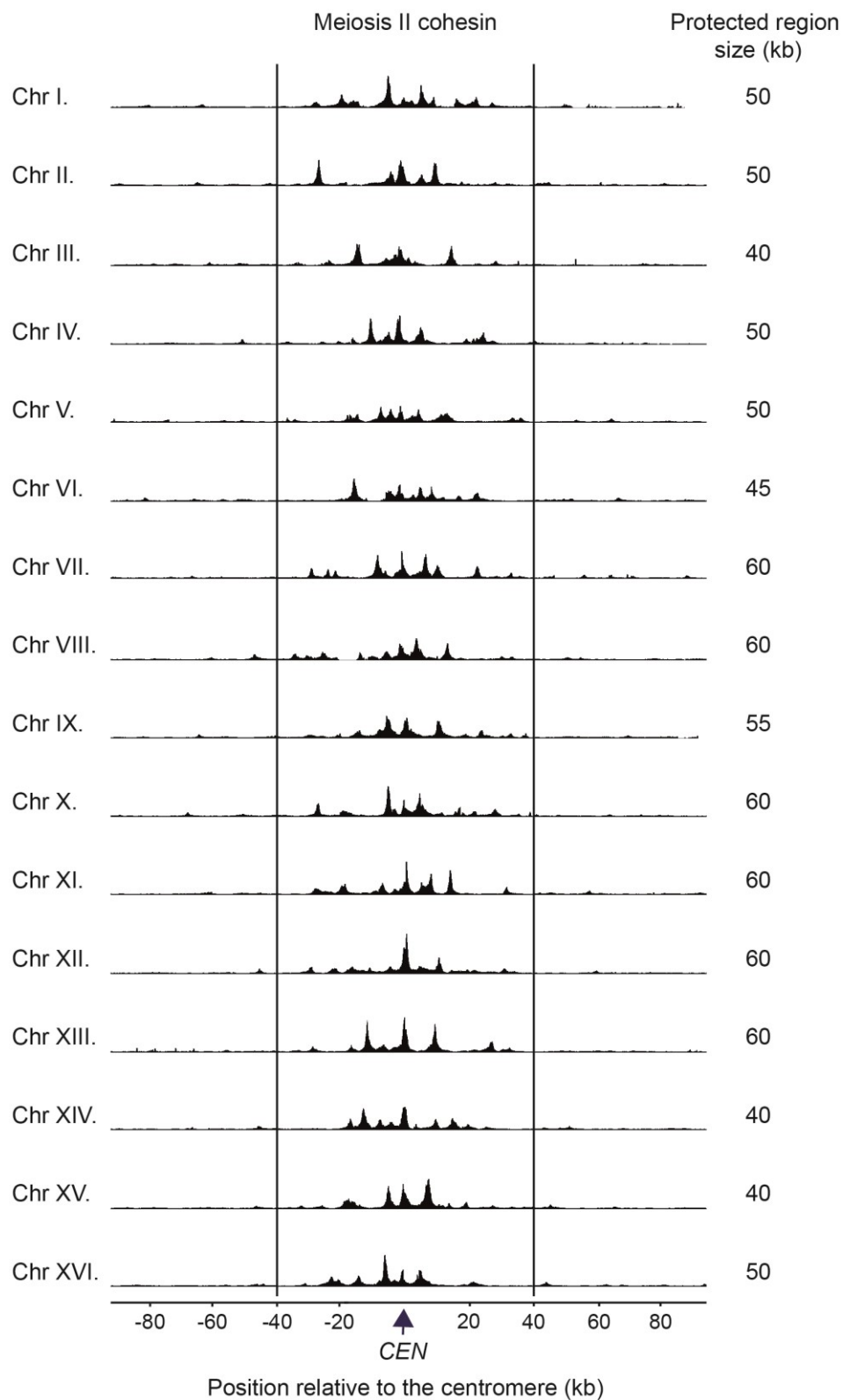


Figure 28: *Profiles of the meiosis-specific cohesin subunit Rec8-ha3 in meiosis II.* CDC20-mAR REC8-ha3 hrr25-as1 strains were induced to enter meiosis and arrested in metaphase I. 40 minutes after the release from the arrest, hrr25-as1 was inhibited, keeping the cells in a meiosis II-like state. The profiles of all chromosomes were aligned at the position of the centromere. The size of the region with Rec8-ha3 occupancy was measured graphically.

visualize the meiosis II cohesin in *S. cerevisiae* (Figure 27). We used this approach to

measure the size of the protected pericentromeric region by measuring the size of the region of meiosis II cohesin occupancy individually for each chromosome (Figure 28). On average of all 16 chromosomes, Rec8-ha3 is localized to a region of 51 kb around the centromere in meiosis II. However, we observed differences in the size of this between chromosomes. Interestingly, the size of this protected pericentromeric region does not statistically correlate with the total length of the chromosome.

### Quantification of calibrated ChIP-Seq data

Having established that the qualitative description of the cohesin dynamics during the two meiotic divisions is the same using qPCR data or calibrated sequencing data, we wanted to know whether this holds true for the quantitative analysis. For this purpose, we composed a time course series of calibrated ChIP-Seq profiles of chromosome VI., which harbored the binding sites of the qPCR primers (Figure 29). We now quantified the calibrated ChIP-Seq profiles by correcting the signal for each base pair with the respective signal from the untagged control, followed by summing-up the corrected signals for all base pairs between the qPCR primer binding sites. To make the data comparable, we normalized the qPCR and ChIP-Seq data to the highest signal in the respective data set, which is the metaphase I signal of the *MET10-SMC2* “arm cohesin peak” site (Figure 30). Both quantification methods measured a residual amount of 16 % and 18 %, respectively, for the “arm cohesin peak” region 30 minutes after the release, followed by 7 % for both methods, 40 minutes after the release. These almost identical numbers demonstrated that both approaches measured very similar changes in occupancy for the chromosome arm site. The initial amount at the *RPN11-SADI* “pericentromeric cohesin” site was at 44 %, when measured with calChIP-qPCR, compared to 38 %, when measured with calChIP-Seq. 40 minutes after the release the pericentromeric signal was at 18 % and 16 %, respectively. These percentages again demonstrated that both methods lead to very similar results, with slightly lower values for the calChIP-Seq quantification. Collectively, this shows that it is possible to quantify dynamics of protein occupancy over time, using calibrated ChIP-Seq data, yielding results which are comparable to quantification by qPCR. The advantage of quantification by calibrated ChIP-Seq data is that it is possible now to quantify chromosomal regions of any size, up to the whole chromosome. This quantification of any chromosomal locus, regardless of its length,

would not be possible using qPCR because here the length of the loci is limited by the distance of the two qPCR primer binding sites, which are typically around 200 bp apart.

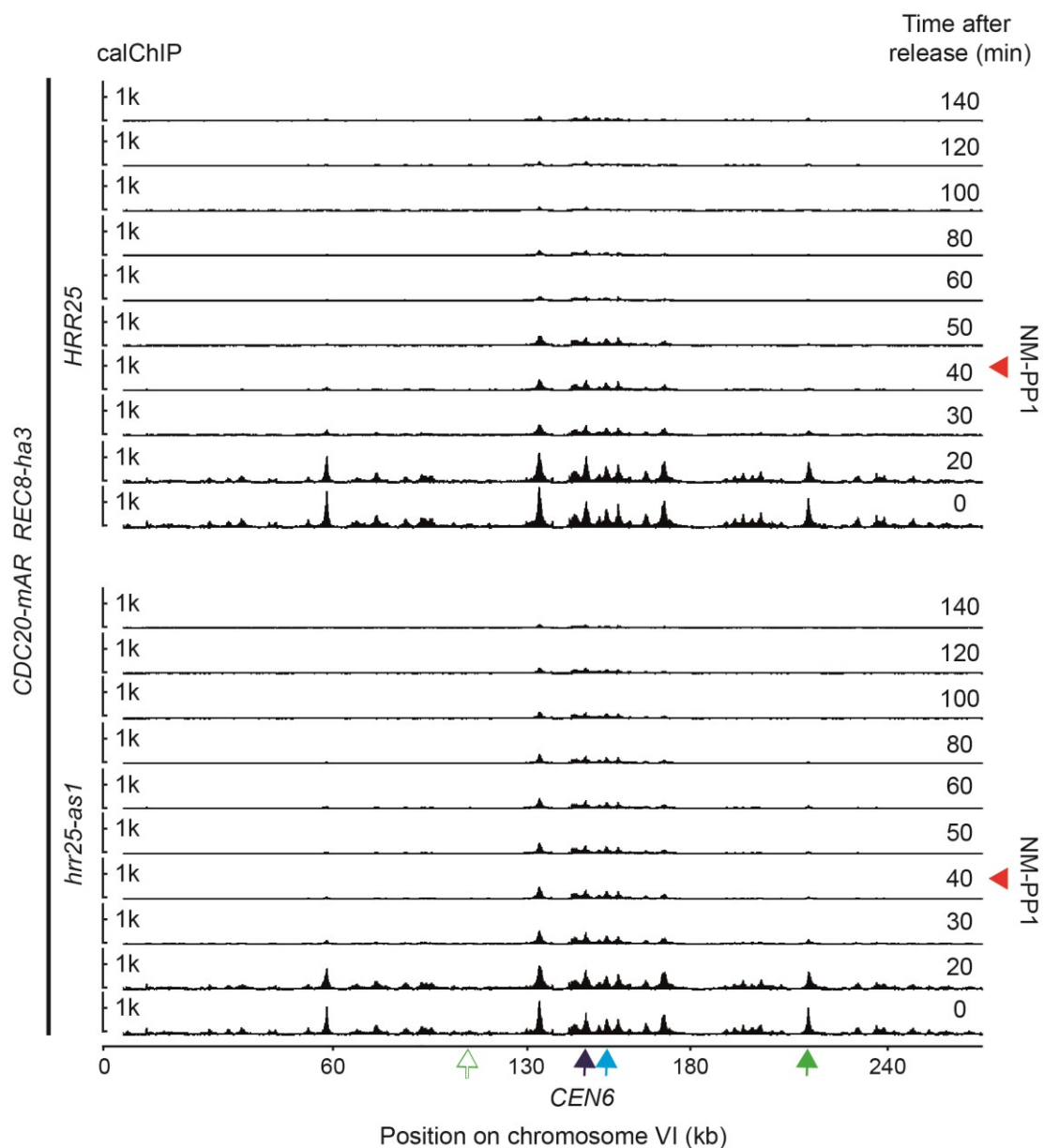


**Figure 29: Calibrated ChIP-Seq profiles of Rec8-ha3 on chromosome VI. from samples of CDC20-mAR REC8-ha3 HRR25 and CDC20-mAR REC8-ha3 hrr25-as1 strains.** The vertical axis measures the calibrated signal intensity of Rec8-ha3. The time scale denotes minutes after the release from the metaphase I arrest. 40 minutes after the release the hrr25-as1 inhibitor NM-PP1 was added to inactivate the enzyme. The light blue arrow indicates the binding site of the “pericentromeric” RPN11-SAD1 qPCR primers. The green arrows indicate the binding site of the “arm cohesin peak” MET10-SMC2 qPCR primers. The white arrows indicate the binding site of the “arm cohesin low” HXT10 qPCR primers.

Concerning meiosis, the protected pericentromeric region is of particular interest. This region is approximately 51 kb large (Figure 28). Hence, for the first time, it is now possible to accurately quantify the cohesin amount in this protected region during the two

meiotic divisions. Therefore, we quantified the amount of cohesin in the protected region in metaphase I and meiosis II, individually for each chromosome (Table 4). We found that on average of all chromosomes 41 % of the metaphase I cohesin in the

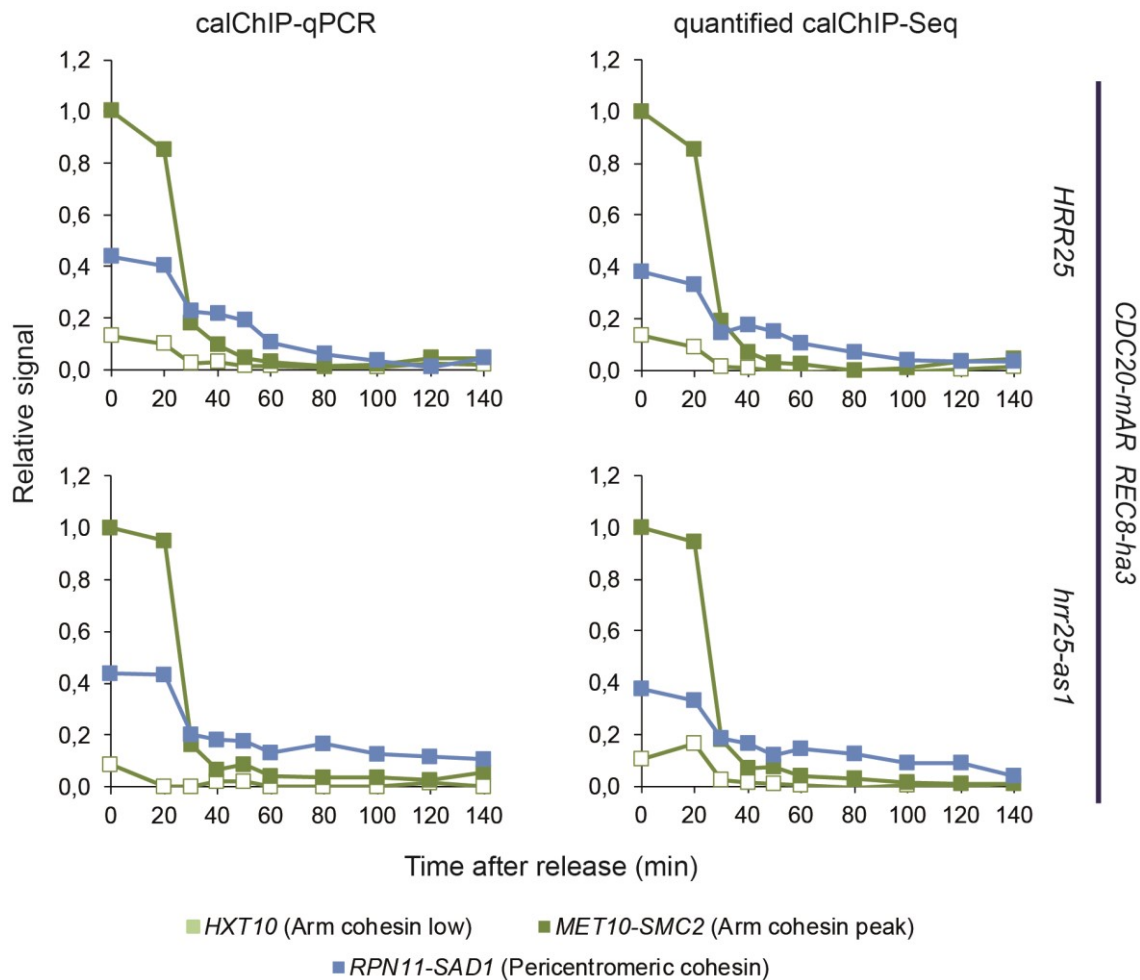


**Figure 30: Quantification of Rec8 cohesin at three different loci on chromosome VI., using either calChIP-qPCR or calibrated ChIP-Seq data.** Quantification is relative to the initial Rec8 level at the “arm cohesin peak” site, to make both methods comparable. The time scale denotes minutes after the release from the metaphase I arrest. Both quantification methods yield comparable results.

pericentromeric region was protected from cleavage in meiosis I and preserved until meiosis II. This number implied that on average 59 % of the metaphase I cohesin in the pericentromeric region was cleaved already in meiosis I. Interestingly, we found substantial differences between chromosomes. Some chromosomes protected a higher percentage of their metaphase I cohesin, some a lower percentage. Strikingly, we found that this fraction of protected cohesin correlated very well with the length of the chromosome (Figure 31 B). This correlation with the chromosome length suggests that

longer chromosomes protect a larger fraction of pericentromeric cohesin than shorter chromosomes. However, the size of the protected region (Figure 28) did not correlate with the protected cohesin fraction, excluding that the higher amount of protected meiosis II-cohesin is an effect from a larger protected region. Moreover, correlating the size of

*Table 4: Quantification of the cohesin amount in the protected pericentromeric region in metaphase I and metaphase II, individually for each chromosome.*

Chromosome	Chromosome size (bp)	Cohesin metaphase I (calChIP)	Cohesin metaphase II (calChIP)	Protected fraction
1	230218	11066758	3952720	0,36
2	813184	8426001	3757940	0,45
3	316620	8032269	3255900	0,41
4	1531933	9510907	3867793	0,41
5	576874	7648140	3015031	0,39
6	270161	8952693	3078295	0,34
7	1090940	8945500	4090199	0,46
8	562643	8746125	3360222	0,38
9	439888	8476428	3628525	0,43
10	745751	8651539	3522278	0,41
11	666816	9714057	3902170	0,40
12	1078177	8929499	3578986	0,40
13	924431	9090941	4112192	0,45
14	784333	9657326	3769817	0,39
15	1091291	9124848	4156501	0,46
16	948066	8136880	3563424	0,44

the protected region to the total length of the chromosome did not yield a significant correlation. Also, we could not find a correlation between the absolute amount of metaphase I cohesin with chromosome size (Figure 31 A), excluding that the stronger protection of pericentromeric cohesin of larger chromosomes was a side effect from a higher amount of initial cohesin loading.

Taken together, for the first time we provide data on the precise direct quantification of the protected meiosis II-specific cohesin fraction, individually for each chromosome. We conclude and thereby confirm our previous results that the cells cleave a substantial amount of pericentromeric cohesin already in meiosis I, and hence, do not protect all pericentromeric cohesin from cleavage in meiosis I. Thus, a protected and an unprotected

cohesin fraction is present in the region around the centromere, indicating that the distinction between arm cohesin and pericentromeric cohesin is not identical to the classification into unprotected cohesin and protected cohesin. This suggests that the mechanism of protection not be only determined by localization of the cohesin protein

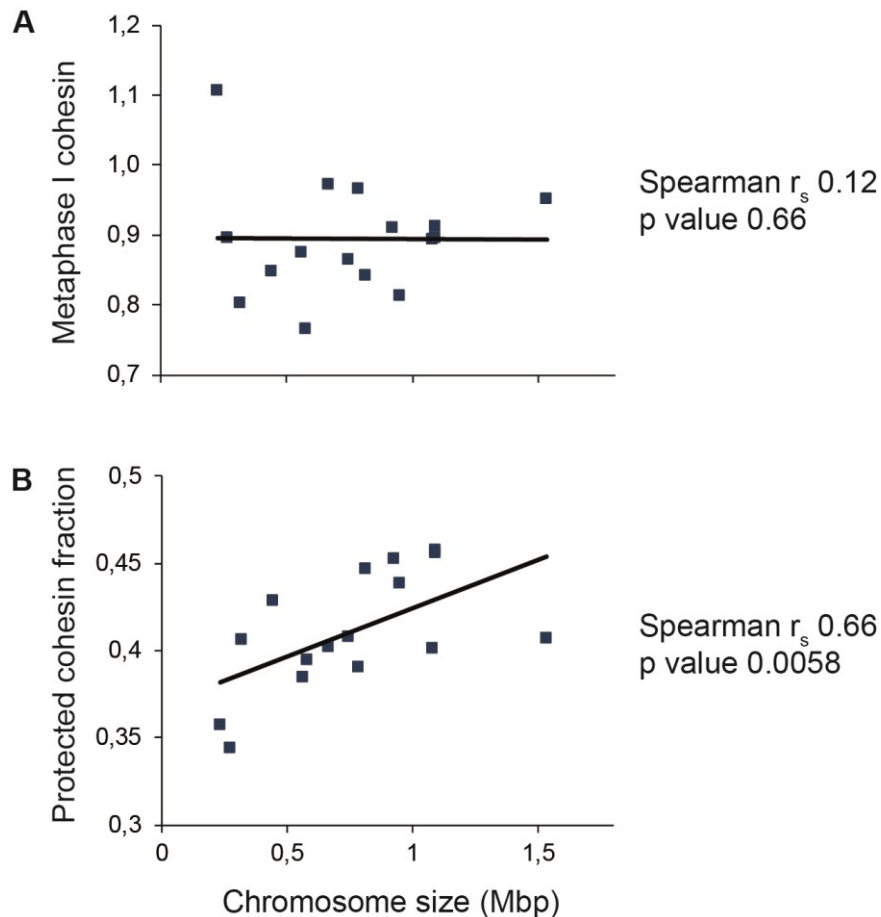


**Figure 31: Statistical analysis.** (A) Relationship between the amount of metaphase I cohesin in the protected region and the chromosome size. The vertical axis denotes the amount of metaphase I cohesin in the protected region, quantified using calibrated ChIP-Seq data. Each data point represents one chromosome. No statistically significant relationship can be established between the chromosome size and the amount of metaphase I cohesin. (B) Relationship between the fraction of protected pericentromeric cohesin and the chromosome size. The Spearman's rank correlation coefficient is 0.66, with a p value of 0.005, indicating a statistically highly significant relationship ( $\alpha = 0.05$ ).

complex. Consequently, the amount of cohesin that is left in meiosis II and that is sufficient to link sister chromatids in meiosis II, is very small, compared to initial cohesin levels. Strikingly, we found that the fraction of protected cohesin correlates with chromosome size, suggesting that a stronger protection mechanism is working for larger chromosomes.

## Quantification of samples from a prolonged metaphase I arrest

In previous experiments, we found that the ChIP-qPCR signal of Rec8 was continuously dropping at all loci, if we did not release the cells from the metaphase I arrest but kept the cells in a prolonged arrest (Figure 13 B). Quantification of the calChIP-Seq data in the binding regions of the qPCR primers of the experiment presented in Figure 21 to Figure 23, confirmed that the signals continuously dropped over the duration of the time course in a prolonged metaphase I arrest. The “arm cohesin peak” signal, for example, fell to a level of less than 50 % after two hours (Figure 32).

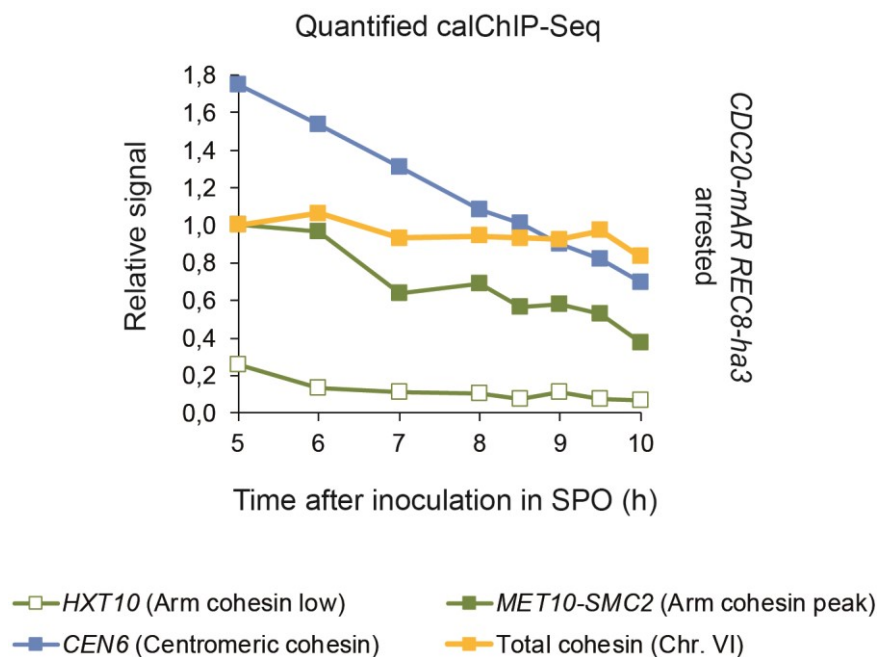


*Figure 32: Quantification of Rec8 cohesin at the three qPCR loci on chromosome VI, and along the total length of chromosome VI, using calChIP-Seq data of CDC20-arrest REC8-ha3 strains, which were kept in a prolonged metaphase I arrest. Quantification is relative to the Rec8 level at the MET10-SMC2 locus. The signal at all three loci steadily declines over time, whereas the total cohesin amount stays almost constant, indicating distal spreading of cohesin.*

The corresponding calChIP-Seq profiles of the metaphase I arrested culture, by contrast, did not display substantial changes in protein occupancy (Figure 23 A). Quantifying the total amount of cohesin over the full length of chromosome VI. in those samples confirmed that the amount of total cohesin was almost constant and no loss of signal could be detected (Figure 32). The same was valid for the average of all 16 chromosomes. Total cohesin only started to decrease at the last time point of a prolonged metaphase I arrest. These two, at first glance contradictory results, could be reconciled by a close inspection

of the ChIP-Seq profiles (Figure 23 A). In the first samples, cohesin formed sharp and high peaks at distinct chromosomal loci. Over time, the cohesin peaks became broader, while their height was reduced, indicating spreading of cohesin into the formerly distal regions of the peaks. Analyzing only a small region, like it is done using qPCR, lead to the notion that the cohesin signal was decreasing, suggesting a loss of cohesin. However, evaluating the ChIP-Seq profiles and quantifying the cohesin occupancy along the full length of the chromosomes, revealed that cohesin was not lost from chromosomes, but moved out of the analyzed region, thereby reducing the measured qPCR signal. Taken together, this example clearly demonstrates the advantage of the quantification using calibrated ChIP-Seq data, compared to the conventional method of using qPCR data for quantification. In this particular case, the quantification by qPCR data generates misleading results, resulting in an incorrect biological interpretation of the experimental data.

### **Centromeric protection**

Next, we used our calibrated ChIP-Seq workflow to analyze the cohesin protector Shugoshin in meiotic samples of *S. cerevisiae*. For this purpose, we used the same experimental setup we used for the analysis of Rec8, with the only difference that the strains harbored an Ha3-tagged version of Sgo1, instead of Rec8.

### **Establishment of centromeric protection**

We started by analyzing the metaphase I occupancy of Sgo1-ha3 and compared the obtained profile (Figure 33 A) to the previously generated Rec8-ha3 profiles (Figure 33 B). Strikingly, we found a precise co-localization in metaphase I between Sgo1 and Rec8 in the protected, pericentromeric region. On arm sites, by contrast, no Sgo1 peaks were detected, even though Rec8 peaks were present there. Comparing the metaphase II profile of Rec8 with the Sgo1 profile revealed that in metaphase II, Rec8 could only be found at loci, at which Sgo1 was already bound in metaphase I, consistent with Sgo1's function as protector of meiosis I cohesin.

As we were struck by the precise colocalization of Rec8 and Sgo1, we inspected the binding profiles of both proteins in more detail. Therefore, we zoomed-in to the protected

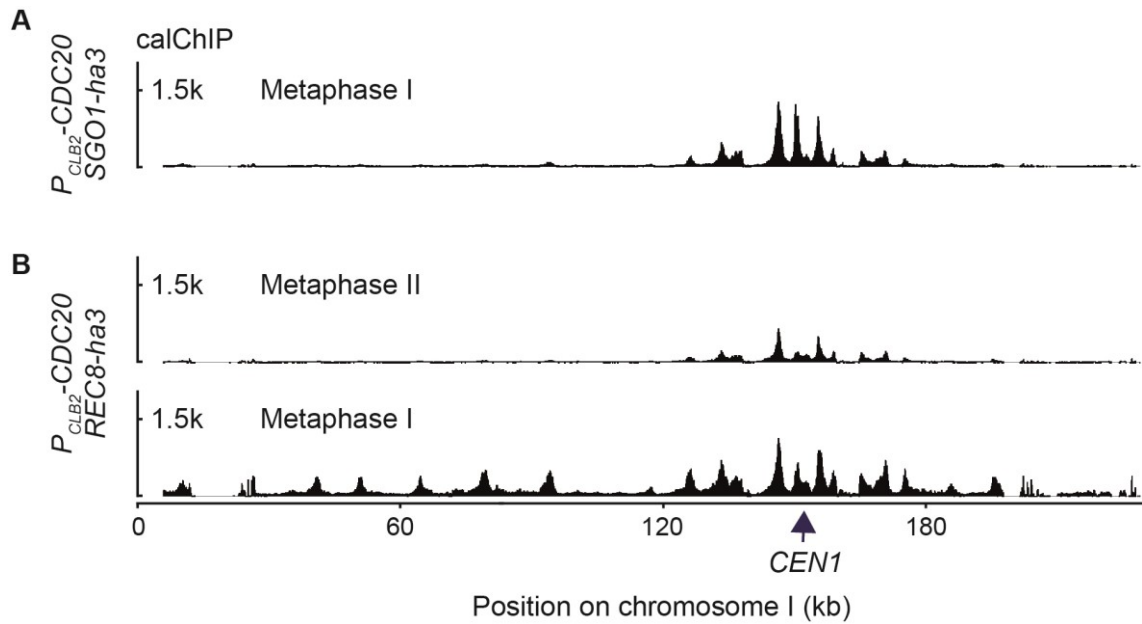


Figure 33: *Calibrated ChIP-Seq profiles of Rec8-ha3 and Sgo1-ha3 on chromosome I of S. cerevisiae. The vertical axis denotes the quantitative calChIP signal. Rec8 and Sgo1 co-localize in the protected pericentromeric region, whereas Sgo1 is absent on chromosome arms.*

pericentromeric region and generated an overlay of the Rec8 and Sgo1 profiles (Figure 34).

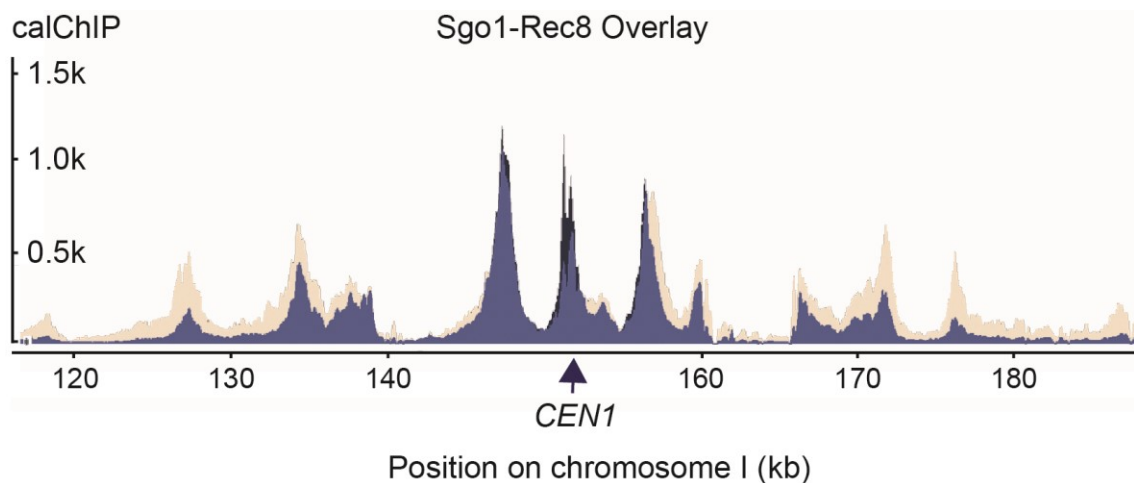


Figure 34: *Overlay of calChIP-Seq profiles of Rec8 and Sgo1 in the protected pericentromeric region of chromosome I. The protected region spans approximately 25 kb in each direction, starting from the centromere. The light blue areas in the histogram depict regions in which the Sgo1 and Rec8 signals overlap. The yellow areas represent regions, which are generated only by Rec8, but not Sgo1. The dark blue areas close to the centromere are regions, in which only a Sgo1 signal is present. The vertical axis denotes the calibrated ChIP-Seq signal. Sgo1 and Rec8 sharply co-localize, but both proteins deviate with respect to signal intensity.*

This overlay confirmed the first impression of an exact co-localization of both proteins, giving rise to the possibility of direct physical interaction. Moreover, this overlay revealed

that even though we detected both proteins at the same chromosomal positions, the two proteins deviated concerning their signal intensities. At the centromere, the Sgo1 signal was higher than the Rec8 signal, indicating an excess of Sgo1. At positions approximately 10 kb left and right of the centromere, where the next peaks were located, both proteins displayed the same signal height. Distal to those two peaks, the Sgo1 signal became lower than the Rec8 signal. At the outer end of the protected pericentromeric region, we found only Rec8 peaks, whereas the Sgo1 signal was reduced to a basal level. Thus, Sgo1 seemed to follow a gradient, with its highest point directly at the centromere. To assess the possibility of a direct physical interaction between Rec8 and Sgo1, we aimed to immunoprecipitated (IP) Rec8 from a native cell extract and checked whether Sgo1 coprecipitated with it. In the IP fraction, we observed strong bands for Rec8-ha3 and Sgo1-myc9, demonstrating that Sgo1-myc9 coprecipitated with Rec8-ha3 (Dr. Wei Ma, Zachariae Lab, unpublished).

Collectively, these results demonstrate that Sgo1 and Rec8 bind to the same chromosomal loci and both proteins directly physically interact with each other.

Next, we wanted to know if the localization of Rec8 in meiosis depends on Sgo1. Therefore, we aimed to generate calibrated ChIP-Seq profiles of Rec8-ha3 in the absence of Sgo1. Thus, we constructed *CDC20-mAR REC8-ha3 sgo1*-depletion experimental strains and *CDC20-mAR REC8-ha3 SGO1* control strains. Both strains were induced to enter meiosis and arrested in metaphase I, as was assessed by immunofluorescence counting (Figure 35 A). Eight hours after transfer into SPO medium, in the control and the experimental strain, more than 60 % of all cells displayed metaphase I spindles, indicating an entry into metaphase I. Subsequently, both strains were synchronously released into anaphase I. Thereupon, the *SGO1* strain progressed normally through both meiotic divisions and accumulated anaphase I spindles, followed by metaphase II spindles and finally, anaphase II spindles. The *sgo1*-depletion strain, by contrast, accumulated anaphase I spindles, followed by anaphase II spindles, whereas hardly any metaphase II spindles could be observed. This phenotype is consistent with a failure in the protection of centromeric cohesin. Without the protection machinery, which is recruited to chromosomes via Sgo1, all cohesin is cleaved in anaphase I and the spindles are not able to generate stable attachments to kinetochores in meiosis II, immediately resulting in elongated anaphase II-like spindles. Thus, the immunofluorescence analysis confirms the successful depletion of *SGO1* in the experimental strain. Next, we subjected the samples

to our calibrated ChIP-Seq protocol. The calChIP-qPCR profile revealed that the *SGO1* strain displayed cohesin dynamics, comparable to previous experiments. In the *sgo1*-depletion strain, by contrast, the pericentromeric signal was lost prematurely, again indicating impaired centromeric protection (Figure 35 B). Analyzing the Rec8-ha3

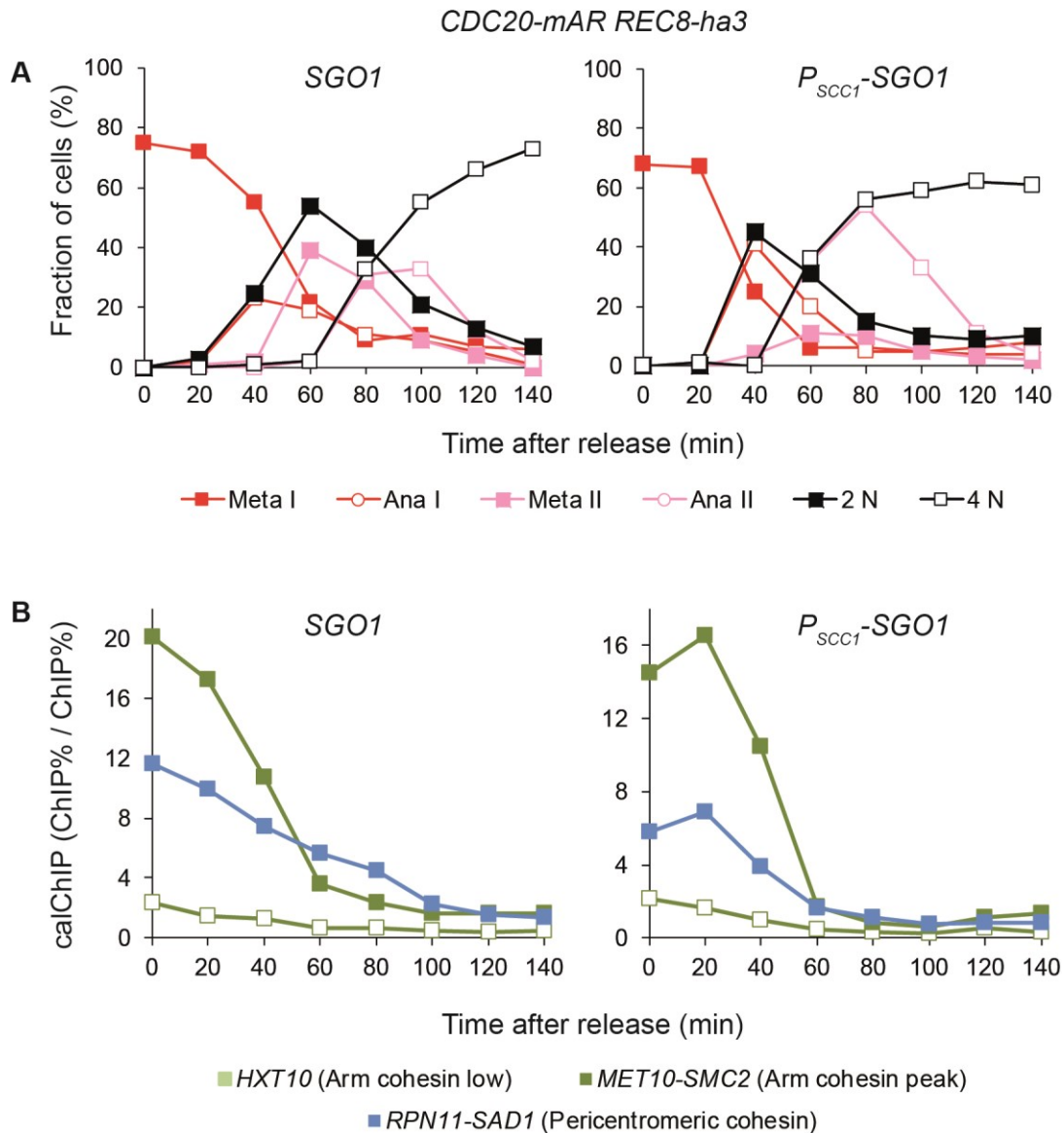


*Figure 35: Meiotic time course samples of CDC20-mAR REC8-ha3 SGO1 (control) and CDC20-mAR REC8-ha3 sgo1-depletion strains. (A) Immunofluorescence counting of meiotic spindles and nuclear division to assess the meiotic stage of individual time point samples. Spindles were visualized by staining of tubulin with a specific antibody. Nuclei were visualized by DAPI staining of DNA. (B) calChIP-qPCR of the same meiotic samples. Three different loci on chromosome VI. were analyzed.*

calChIP-Seq metaphase I profiles (Figure 36) revealed that Rec8-ha3 recruited normally to chromosomes in both strains, excluding the possibility that Sgo1 is required for recruitment of Rec8.

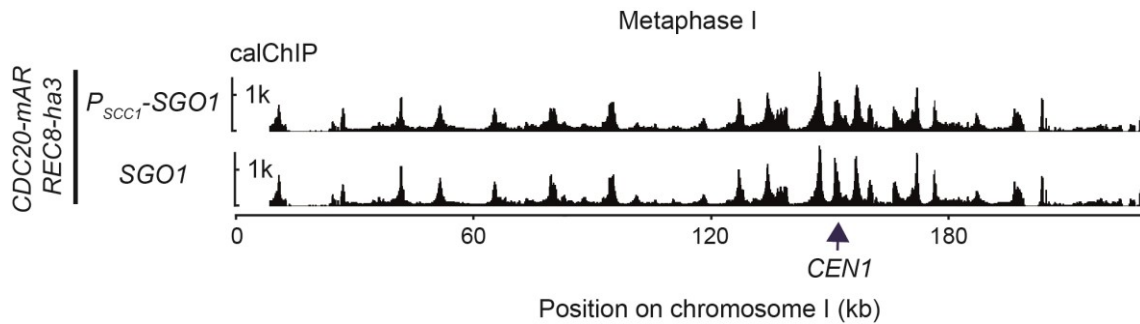
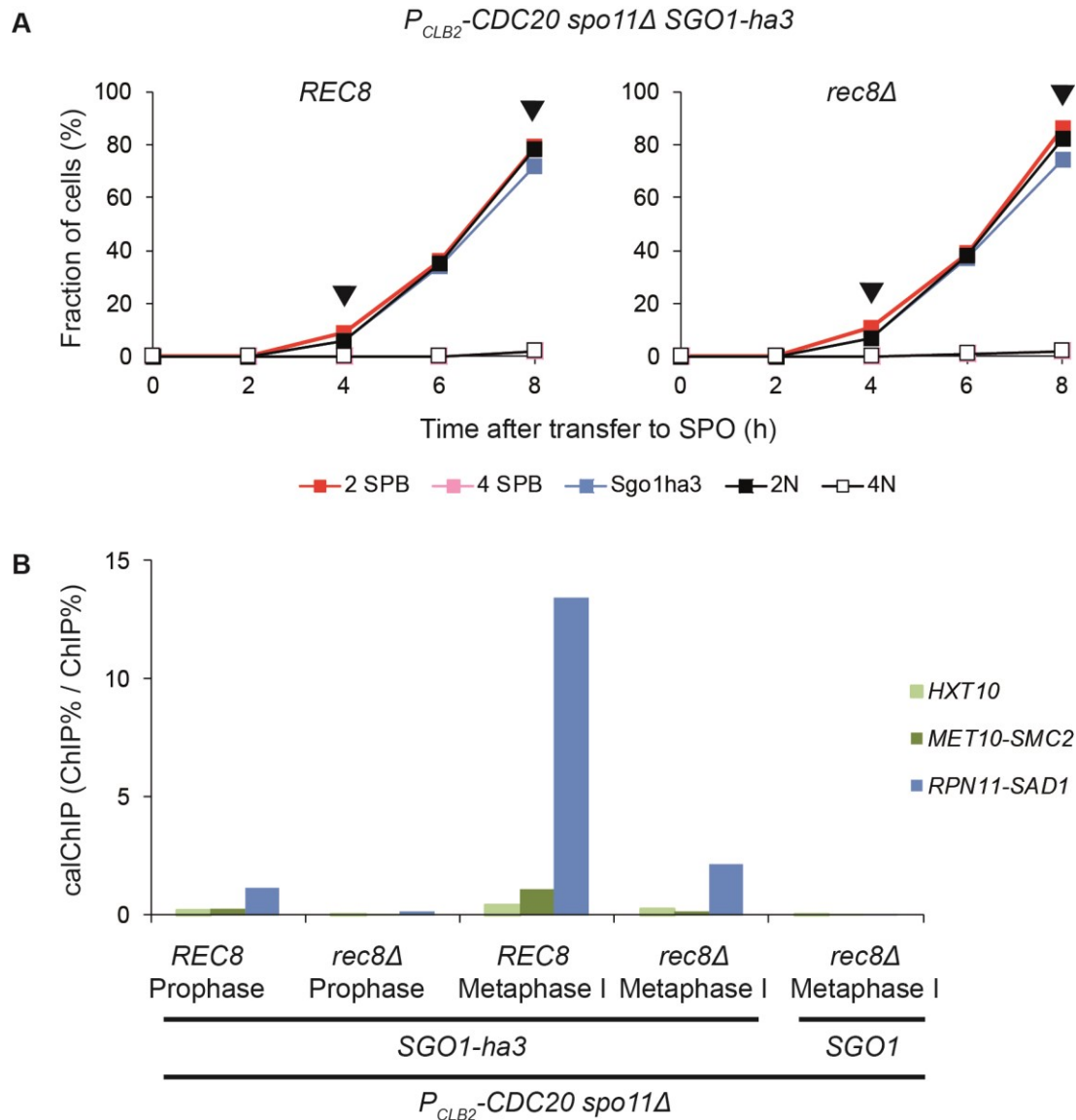


Figure 36: Calibrated ChIP-Seq profiles of *Rec8-ha3* on chromosome I of samples from *CDC20-mAR REC8-ha3 SGO1* (control) and *CDC20-mAR REC8-ha3 sgo1*-depletion strains. Samples were taken 8 hours after inoculation in SPO, before the cells were released from the metaphase I arrest. The vertical axis measures the calibrated signal intensity of *Rec8*. The localization of *Rec8* does not depend on *Sgo1*.

Next, we wanted to know if the localization of *Sgo1* in meiosis depends on *Rec8*. Therefore, we aimed to generate calibrated ChIP-Seq profiles of *Sgo1-ha3* in the absence of *Rec8*. Strains in which *REC8* was deleted are fully viable, as the cells express *REC8* only in meiosis and the mitotic proliferation is not affected. However, for meiosis, deletion of *REC8* has severe consequences, as the cells arrest in prophase due to the recombination checkpoint, because *Rec8* is required for completion of meiotic recombination (Klein et al., 1999). This problem can be circumvented, by the additional deletion of the *SPO11* gene. *Spo11* is a topoisomerase-like enzyme, which initiates meiotic recombination by the formation of double-strand breaks in DNA (Bergerat et al., 1997; Keeney et al., 1997). Thus, we constructed *CDC20-arrest SGO1-ha3 spo11Δ rec8Δ* experimental strains and *CDC20-arrest SGO1-ha3 spo11Δ REC8* control strains. A *CDC20-arrest SGO1 spo11Δ REC8* strain served as untagged control. The *CDC20-arrest spo11Δ rec8Δ* double mutant enters meiosis, skips meiotic recombination and arrests in metaphase I, as was assessed by immunofluorescence counting (Figure 37 A). Eight hours after transfer into SPO medium, in the control and the experimental strain, nearly 80 % of all cells display two spindle pole bodies, indicating an entry into metaphase I and in both strains the cells accumulated *Sgo1-ha3* in the nucleus. After four and eight hours, samples from all strains were taken and subjected to our calibrated ChIP protocol (Figure 37 B). Analyzing the obtained calChIP-Seq profiles, we found that four hours after transfer to SPO medium, when the general *Sgo1* protein levels are still low in the cells (Figure 42 A), only very little *Sgo1* was recruited to chromosomes (Figure 38, lower two profiles). After eight hours, by contrast, a high occupancy of *Sgo1-ha3* was measured in the metaphase control sample (Figure 38, second profile from the top). Strikingly, in the

metaphase sample of the *rec8Δ* strain, the Sgo1-ha3 pattern was drastically altered. We observed a sharp peak at the centromere, but it lacked all pericentromeric Sgo1 peaks.



**Figure 37: Meiotic time course samples of CDC20-arrest *spo11Δ* SGO1-ha3 strains containing REC8 or *rec8Δ*.** (A) Immunofluorescence counting of spindle pole bodies, nuclear accumulation of Sgo1-ha3 and nuclear division to assess the meiotic stage of individual samples. Spindle pole bodies were visualized by staining of Tub4 with a specific antibody. Nuclei were visualized by DAPI staining of DNA. The black arrows indicate the time of sampling. (B) Calibrated ChIP-qPCR of the samples taken at 4 hours (prophase) or 8 hours (metaphase I). The bar graphs show Sgo1-ha3 enrichment. Three different loci on chromosome VI. were analyzed. The vertical axis displays the calibrated ChIP signal. The localization of Sgo1 does depend on Rec8.

This result shows that Rec8 is required for the pericentromeric localization of Sgo1, but not for its centromeric recruitment.

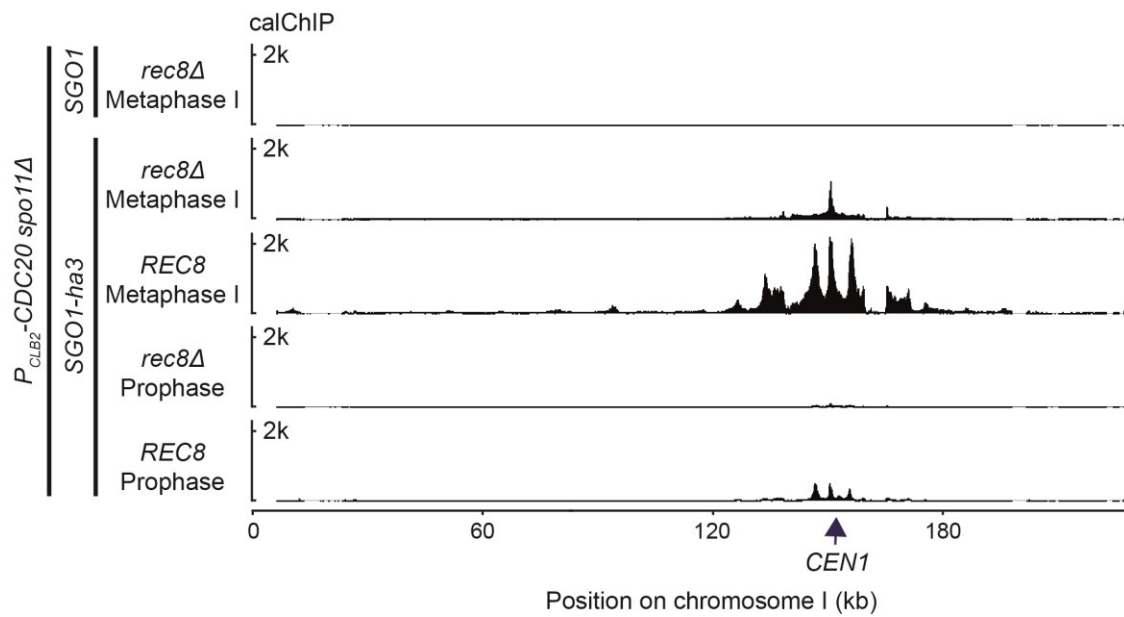


Figure 38: *Calibrated ChIP-Seq profiles of Sgo1-ha3 on chromosome I in samples from a meiotic time course of CDC20-arrest spo11Δ SGO1-ha3 strains containing REC8 or rec8Δ. The vertical axis measures the calibrated signal intensity of Sgo1-ha3. Prophase samples were taken 4 hours after inoculation in SPO medium, metaphase I samples were taken 8 hours after inoculation in SPO medium. Rec8 is required for pericentromeric localization of Sgo1, but not for centromeric localization.*

Having demonstrated that Rec8 is required for the recruitment of Sgo1 to chromosomes, we wanted to know if the amount of chromosome-bound Rec8 is correlated with the amount of chromosome-bound Sgo1. To address this question, we quantified the amount of Rec8 and Sgo1 in the protected region, individually for each chromosome, as described

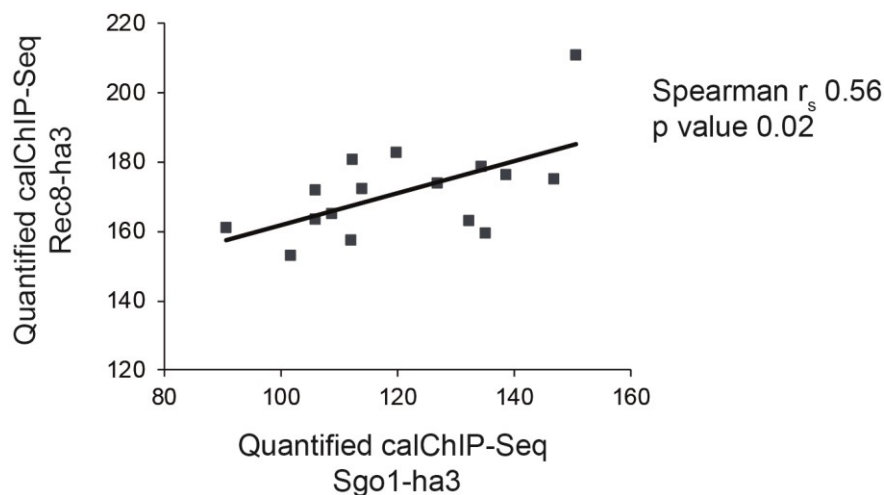
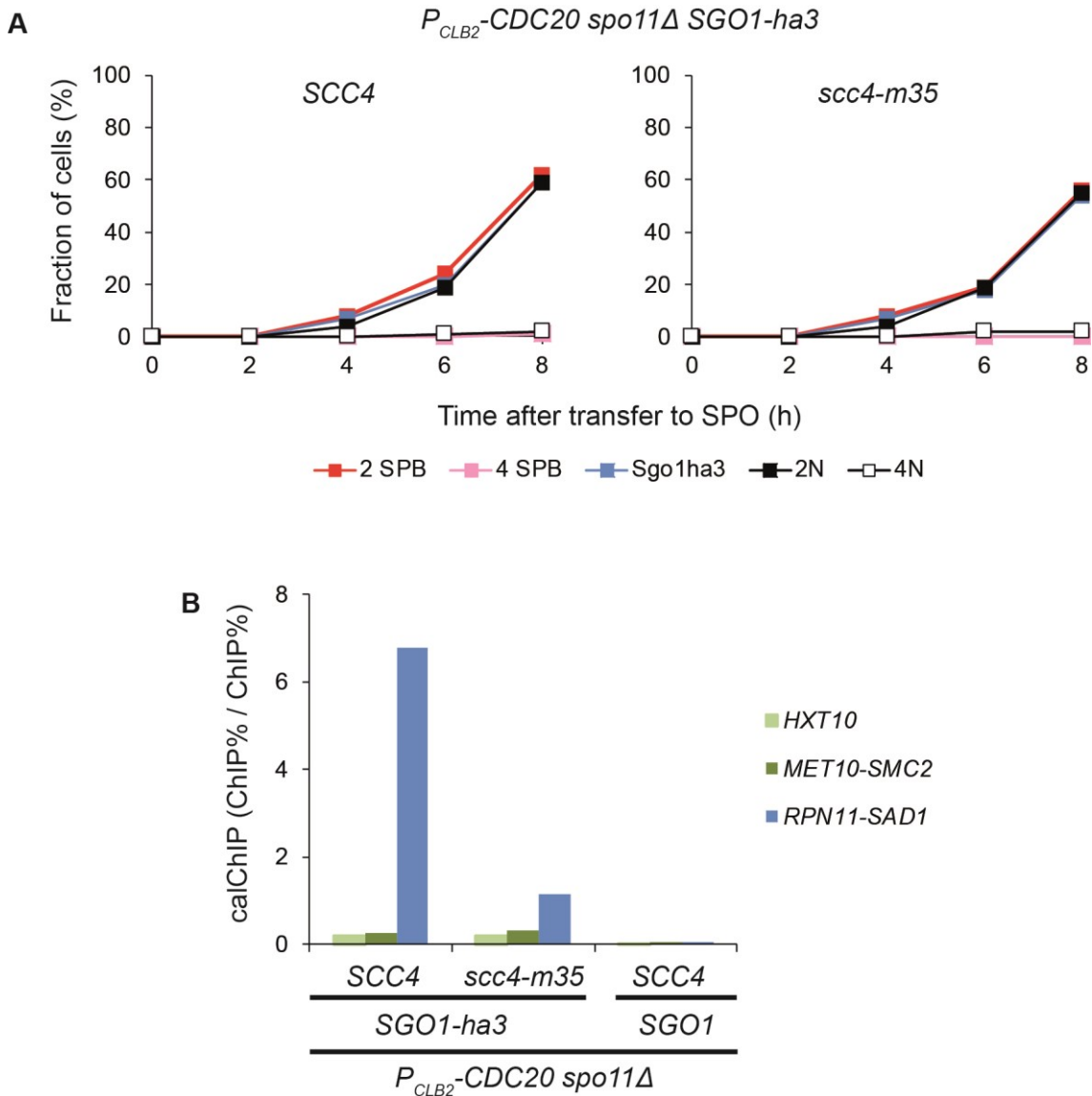


Figure 39: *Relationship between the amount of metaphase I cohesin in the protected region and metaphase I Sgo1 in the protected region. The amount of both proteins was measured by quantification of the respective calibrated ChIP-Seq data. Each data point represents one chromosome. The Spearman's rank correlation coefficient is 0.56, with a p value of 0.02, indicating a statistically significant relationship ( $\alpha = 0.05$ ).*

in previous chapters (Table 4). Subsequently, we tested if those two variables are correlated and found a statistically significant relationship (Figure 39). This result further strengthens the notion of a function of Rec8 in the recruitment of Sgo1.



**Figure 40: Meiotic time course samples from CDC20-arrest *spo11Δ* SGO1-ha3 strains containing SCC4 or *scc4-m35*.** (A) Immunofluorescence counting of spindle pole bodies, nuclear accumulation of Sgo1-ha3 and nuclear division to assess the meiotic stage of individual samples. Spindle pole bodies were visualized by staining of Tub4 with a specific antibody. Nuclei were visualized by DAPI staining of DNA. The horizontal axis shows hours after transfer into SPO medium. (B) Calibrated ChIP-qPCR of the samples taken at 8 hours (metaphase I). The bar graphs show Sgo1-ha3 enrichment. Three different loci on chromosome VI. were analyzed. The vertical axis displays the calibrated ChIP signal. (C) Western-blot of the corresponding samples to demonstrate depletion of Cdc5.

During meiosis, only Rec8-containing cohesin complexes provide cohesion (Rankin, 2015). Thus, by deleting the cohesin subunit Rec8, the chromatin structure is severely

altered. Therefore, it is conceivable that the partial loss of Sgo1 signal in a *rec8Δ* strain is an unspecific effect of a perturbed chromatin structure. To address this issue, we went on to analyze the Sgo1 binding to chromatin in a strain harboring a mutant allele of the cohesin loader subunit *SCC4*, while expressing wildtype levels of *REC8*. It was shown that by inserting mutations into a conserved patch of Scc4 (*scc4-m35*), the cohesin loader is not recruited anymore to chromatin, thus, drastically reducing the levels of topologically loaded cohesin (Hinshaw et al., 2015). However, cohesin is not entirely absent from chromosomes in these strains, thus, preserving a basic level of cohesion. To this end, we constructed *CDC20-arrest spo11Δ SGO1-ha3* strains containing either *SCC4* or *scc4-m35*. These strains, together with an untagged control, were induced to enter meiosis. Eight hours after transfer to SPO medium, approximately 60 % of the cells in each strain displayed two spindle pole bodies, indicating an arrest in metaphase I (Figure 40 A). At this time, we took samples, which were fixed in formaldehyde and subjected to our ChIP protocol (Figure 40 B). The calibrated ChIP-Seq profile of the *SCC4* control

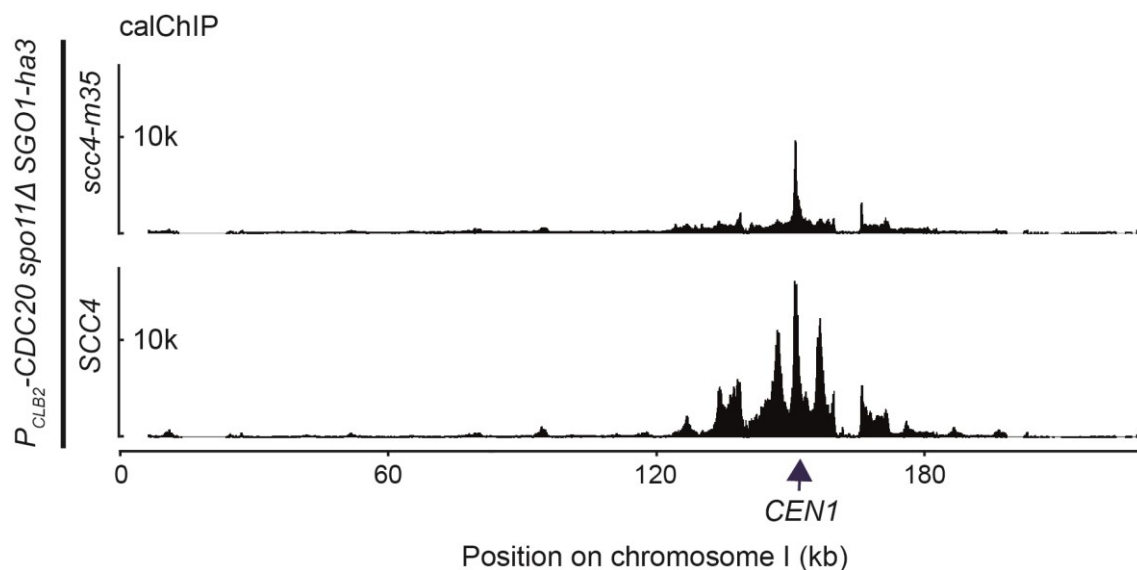


*Figure 41: Calibrated ChIP-Seq profiles of Sgo1-ha3 on chromosome I in samples from a meiotic time course of CDC20-arrest spo11Δ SGO1-ha3 strains containing SCC4 or scc4-m35. The vertical axis measures the calibrated signal intensity of Sgo1. Samples were taken 8 hours after inoculation in SPO medium. A functional Scc2/Scc4 cohesin loader complex is required for pericentromeric localization of Sgo1.*

strain exhibited an accumulation of Sgo1 in the pericentromeric region, consistently with the previous experiments. The *scc4-m35* experimental strain, on the other hand, displayed one single Sgo1 peak right at the centromere proper, whereas no pericentromeric accumulation of Sgo1 could be detected (Figure 41).

These profiles demonstrate that Rec8-containing cohesin, which is topologically loaded

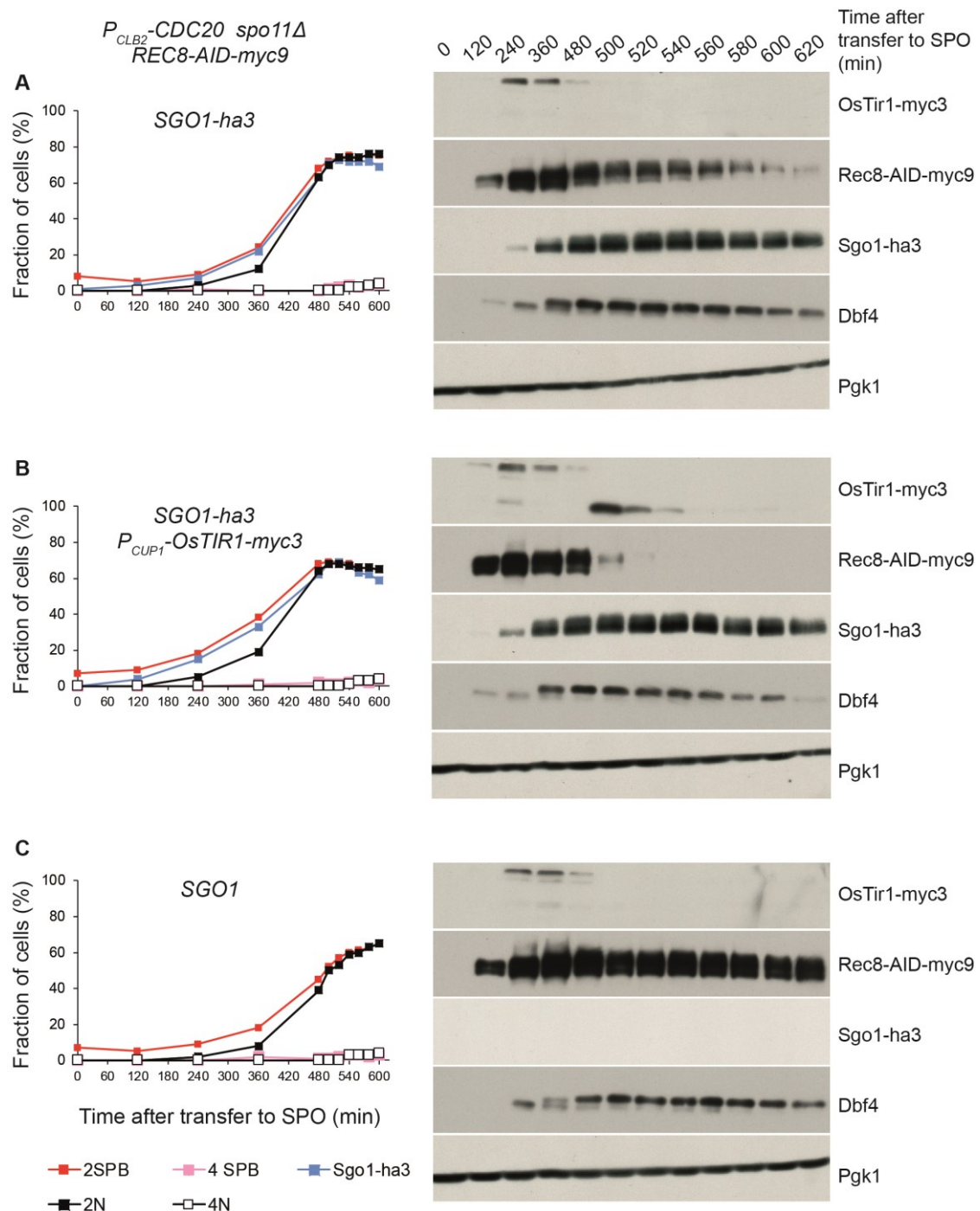


Figure 42: **Auxin-induced degradation of Rec8 in meiosis.** Meiotic time course samples of CDC20-arrest *spo11Δ* REC8-AID-myc9 SGO1-ha3 strains. The experimental strain, additionally harbors a copper-inducible OsTIR1 allele for induction of the AID-mediated Rec8 degradation. All cultures entered meiosis and arrested at metaphase I after 480 min (8 hours). Subsequently, copper and auxin were added to induce degradation of Rec8. Left side: Immunofluorescence counting of spindle pole bodies, nuclear accumulation of Sgo1-ha3 and nuclear division to assess the meiotic stage of individual samples. Spindle pole bodies were visualized by staining of Tub4 with a specific antibody. Nuclei were visualized by DAPI staining of DNA. The horizontal axis shows minutes after transfer into SPO medium. Right side: Immunoblot analysis of the same samples. Dbf4 is a meiosis I marker. Pgk1 serves as loading control. (A) Control strain. (B) Experimental strain. (C) Untagged control strain.

onto chromosomes by the cohesin loader complex, is required for the pericentromeric localization of Sgo1. Without topologically loaded cohesin, Sgo1 is recruited only at the centromere.

By using a *rec8Δ* mutant and a *scc4-m35* cohesin loader mutant, we have demonstrated that cohesin is required for recruiting Sgo1 to chromatin. However, we do not know if cohesin is only required for the loading of Sgo1 onto chromatin or if it is permanently anchoring it at chromosomes.

We, therefore, asked what happens to Sgo1, if we allow the cells to establish Sgo1 on chromosomes, and only subsequently, after Sgo1 is loaded onto chromosomes, artificially remove cohesin. To this end, we used the auxin-inducible degron (AID) system. This system was initially described by Nishimura et al. (2009) and has been used successfully in various organisms since then (Holland et al., 2012; Kanke et al., 2011; Zhang et al., 2015). It uses genes of the auxin response pathway of plants to conditionally inactivate proteins. To use this system in yeast, the target protein has to be tagged with an AID recognition sequence, and the strain needs to express the plant ubiquitin-ligase subunit *TIR1*, which mediates the response to auxin. The so transformed yeast strain can then be grown under standard conditions, but once auxin is added to the culture medium, the target protein is degraded within 30 minutes. We constructed strains harboring a *REC8-AID-myc9* allele in the previously used *CDC20-arrest spo11Δ SGO1-ha3* background. The experimental strain, additionally, harbored the Myc-tagged *TIR1* allele from rice (*O. sativa*), named *OsTIR1*, under a copper-inducible promoter.

Like in previous experiments, we induced meiosis in the control, experimental and untagged strains. All strains successfully entered meiosis and arrested in meiosis I, as can be judged by expression of the meiosis I marker gene *DBF4* on a western-blot (Figure 42). Moreover, the AID-myc9-tagged version of *REC8* was successfully expressed in all strains. Eight hours (480 minutes) after transfer to SPO medium, in the control and experimental culture, more than 60 % of all cells displayed two spindle pole bodies, indicating an arrest in metaphase I (Figure 42). At this time, we added copper sulfate to induce the *OsTIR1* allele, followed by addition of auxin to trigger degradation of the Rec8-AID-myc9 protein. 20 minutes later, at time point 500 minutes, a distinct band could be observed for the *OsTir1-myc9* protein in the experimental strain. Concomitant, the western-blot signal for the Rec8-AID-myc9 protein was drastically reduced, indicating successful degradation. Additionally, we took samples for ChIP in 60 minutes

intervals, starting at the time of induction of the AID system at eight hours (480 minutes). We subjected these samples to our calibrated ChIP-Seq protocol, but this time we split the samples and enriched for Rec8-AID-myc in one batch and Sgo1-ha3 in the other.

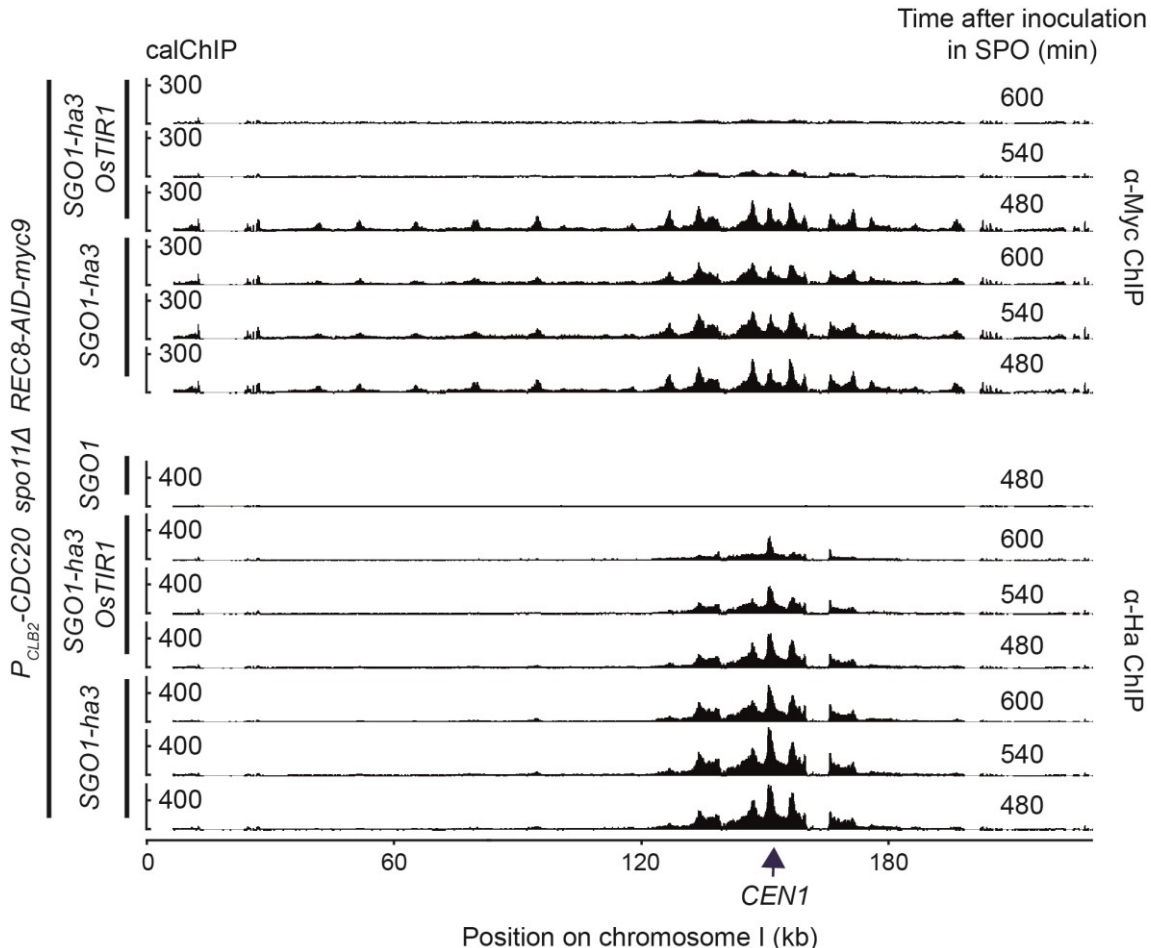


**Figure 43: Auxin-induced degradation of Rec8 in meiosis.** Calibrated ChIP-Seq profiles of Rec8 and Sgo1 on chromosome I from CDC20-arrest spo11Δ REC8-AID-myc9 SGO1-ha3 strains. The experimental strain, additionally harbors an copper-inducible OsTIR1 allele for induction of the AID-mediated Rec8 degradation. All cultures entered meiosis and arrested at metaphase I after 480 min (8 hours). Subsequently, copper and auxin were added to induce degradation of Rec8. At this time the first ChIP samples were taken. The upper profiles show the occupancy of Rec8. The lower profiles show the occupancy of Sgo1 in the same samples. The vertical axis in all profiles denotes the quantitative calibrated ChIP signal. The pericentromeric localization of Sgo1 is lost upon degradation of Rec8.

Thus, we could compare the ChIP signal of both proteins in the same samples.

The calChIP-Seq profiles for Rec8-AID-myc9 revealed that the control and experimental strains successfully loaded cohesin to comparable levels at 480 minutes (Figure 43). At 540 minutes, the control strain still displayed an identical profile for Rec8, whereas in the experimental strain, the ChIP signals were almost absent. Thus, the calChIP-Seq profiles confirmed the western-blot results and demonstrated successful degradation of Rec8. The

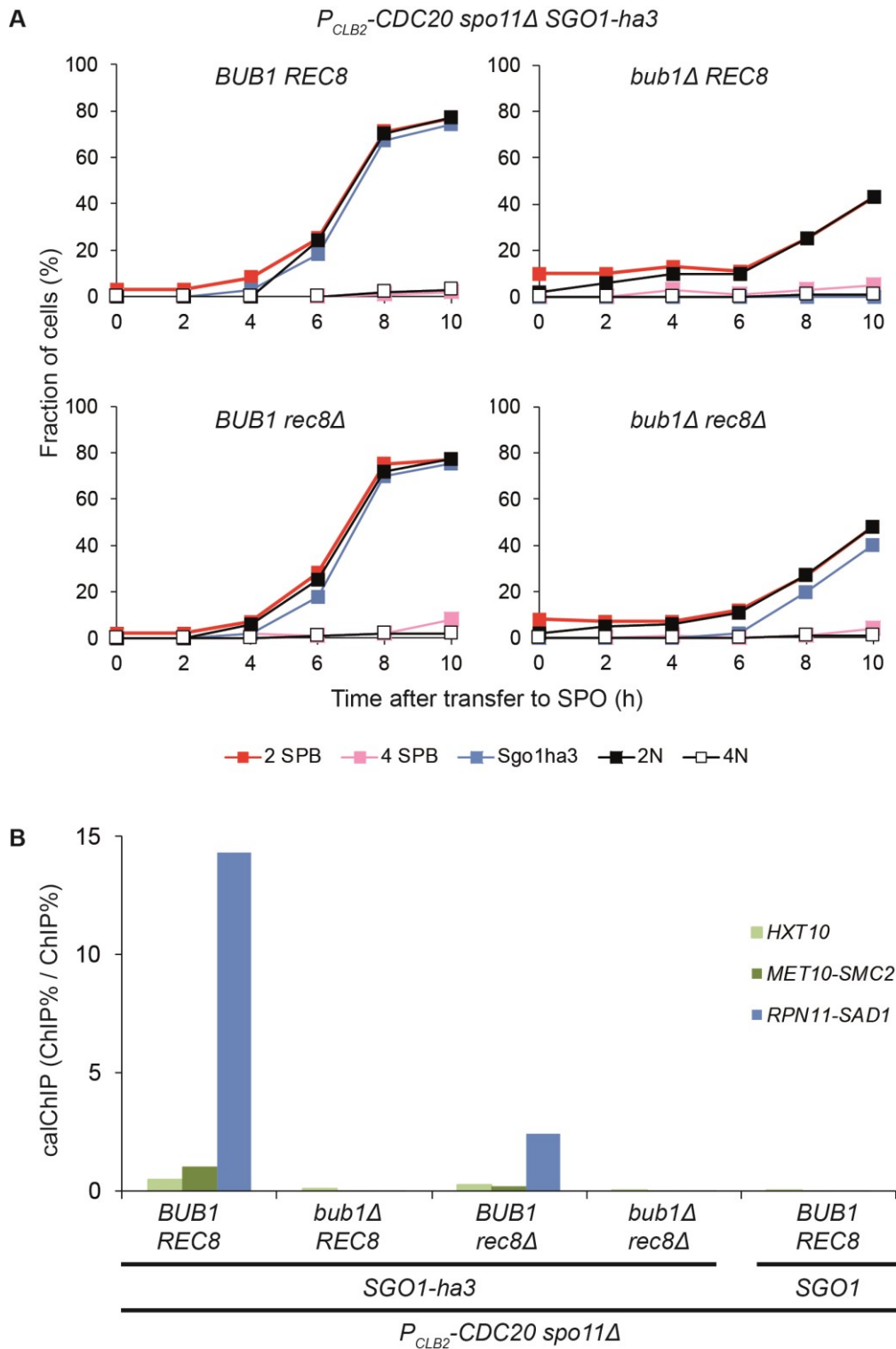


**Figure 44: Meiotic time course samples from CDC20-arrest *spo11Δ* SGO1-*ha3* strains containing either REC8 BUB1 (control), REC8 *bub1Δ*, *rec8Δ* BUB1 or *rec8Δ* *bub1Δ*.** (A) Immunofluorescence counting of spindle pole bodies, nuclear accumulation of Sgo1-*ha3* and nuclear division to assess the meiotic stage of individual samples. Spindle pole bodies were visualized by staining of Tub4 with a specific antibody. Nuclei were visualized by DAPI staining of DNA. (B) Calibrated ChIP-qPCR of the samples taken at 10 hours (metaphase I arrest). The bar graphs show Sgo1-*ha3* enrichment. Three different loci on chromosome VI. were analyzed. The vertical axis displays the calibrated ChIP signal.

calChIP-Seq profile for Sgo1-ha3 revealed that both strains also loaded Sgo1-ha3 to comparable levels at 480 minutes. The control strain kept a similar profile for Sgo1-ha3 in the consecutive time points, indicating stable recruitment of Sgo1. The experimental strain, by contrast, lost the pericentromeric signal of Sgo1-ha3 in the consecutive time points and only retained a sharp peak at the centromere.

This pattern confirms our previous results that cohesin is required for pericentromeric localization of Sgo1, but not its centromeric binding. Moreover, this result demonstrates that cohesin is not only required for the pericentromeric loading of Sgo1, but also for its persistence in the pericentromeric region.

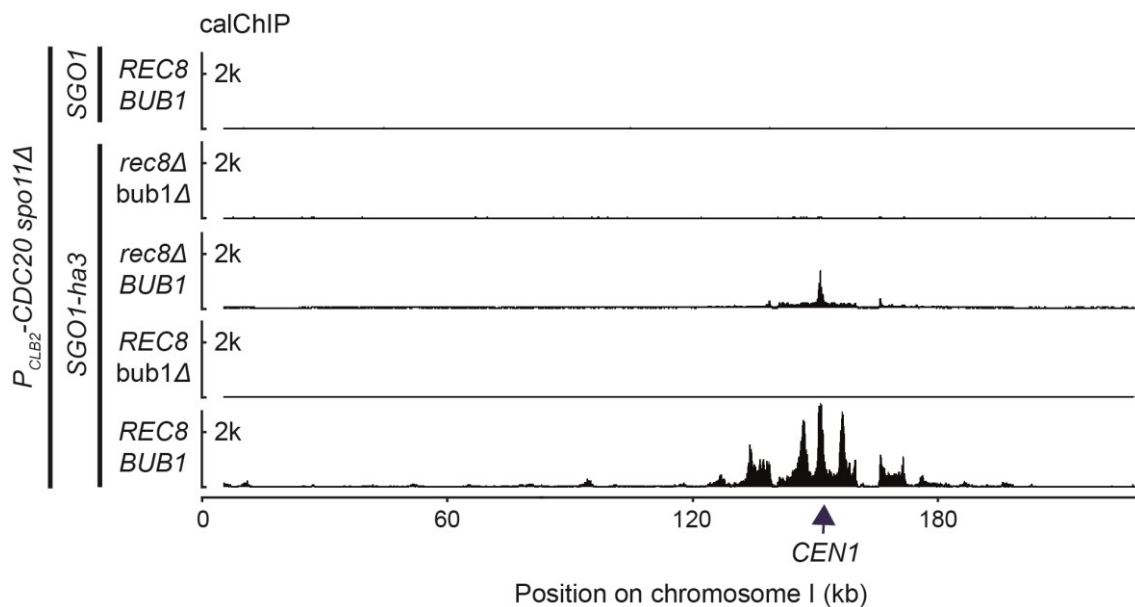


*Figure 45: Calibrated ChIP-Seq profiles of Sgo1-ha3 on chromosome I in samples from a meiotic time course of CDC20-arrest spo11Δ SGO1-ha3 strains containing either REC8 BUB1 (control), REC8 bub1Δ, rec8Δ BUB1 or rec8Δ bub1Δ. The vertical axis measures the calibrated signal intensity of Sgo1. Samples were taken 10 hours after inoculation in SPO medium. Bub1 is required for the chromosomal localization of Sgo1. Rec8 is required for the pericentromeric localization of Sgo1.*

Having established that the cells require cohesin for loading and permanent localization of Sgo1 in the pericentromeric region, we next asked how cohesin relates to the Bub1-dependent loading mechanism of Sgo1 that has been extensively described in the literature. Therefore, we aimed to analyze the binding of Sgo1 in strains, which do not express *BUB1* or do not express *BUB1* and the cohesin subunit *REC8*. Like in all previous experiments, we induced the strains to undergo meiosis and assessed the meiotic progression, using immunofluorescence counting (Figure 44 A). All strains entered

meiosis and separated their spindle pole bodies, indicating entry into metaphase I. Consistent with previous experiments, in the control and *rec8Δ* strain, more than 60 % of all cells displayed two spindle pole bodies after eight hours in SPO medium. Due to a reduced vitality of *bub1Δ* cells, the *bub1Δ*-containing strains progressed more slowly. However, after ten hours in SPO medium, also in these strains, approximately 40 % of all cells displayed two spindle pole bodies, making it possible to harvest enough material for ChIP analysis. Ten hours after transfer to SPO medium, we took samples from all strains and subjected them to our calibrated ChIP protocol (Figure 44 B).

The obtained profiles confirmed our previous results that in *rec8Δ* strains, Sgo1 cannot recruit to the pericentromeric region, but binds to a small region right at the centromere proper, giving rise to profiles with one single large peak (Figure 45). Interestingly, neither for the *bub1Δ* single mutant nor the *bub1Δ rec8Δ* double-mutant, any Sgo1-ha3 signal could be detected at all.

Taken together, these findings confirm previous reports about the requirement of Bub1 for the recruitment of Sgo1 to chromosomes. Without Bub1, Sgo1 does not recruit to chromosomes at all. Moreover, these findings demonstrate that the single large peak, we observe in profiles of cohesin mutants is Bub1-dependent.

### **Regulation of centromeric protection**

For mice, it was reported that deprotection of centromeric cohesin in meiosis II occurs via the conserved histone chaperone SET/TAF-1b, which acts as an inhibitor of PP2A's enzymatic function (Chambon et al., 2013). To test whether the same mechanism is working in *S. cerevisiae*, we deleted both yeast homologs of SET, called *NAP1* and *VPS75*, and thus, generate a *nap1Δ vps75Δ* double deletion mutant. If any of the two SET homologs acts as an inhibitor of centromeric deprotection in budding yeast, the double deletion strain should not be able to deprotect pericentromeric cohesin in meiosis II. Without deprotection in meiosis II, the cells would not be able to segregate sister chromatids in meiosis II. We decided to use live-cell imaging to analyze the behavior of sister chromatids in the course of the two meiotic divisions. To this end, we generated strains harboring a GFP-tagged version of tubulin to visualize the spindles, which allows the staging of individual cells. The sister chromatids of chromosome V were labelled by a system comprising the tet repressor (TetR) protein, labeled with a red fluorescent

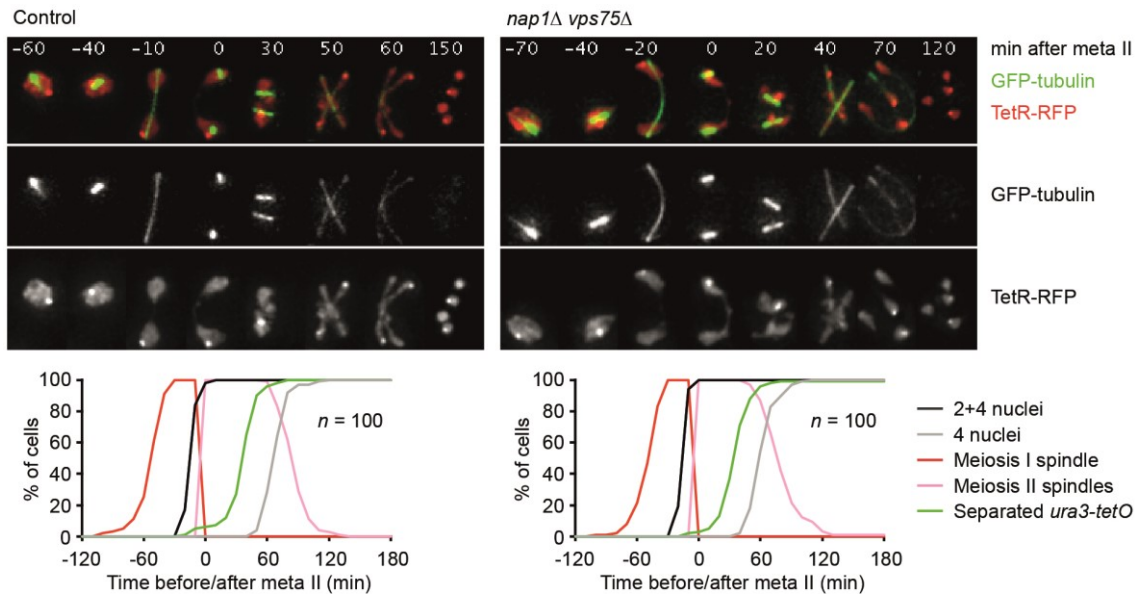


**Figure 46 Live-cell imaging of a I2PP2A-homolog deletion strain.** Control (left side) and *nap1Δvps75Δ* strain (right side) were induced to enter meiosis and imaged every 10 minutes. Spindles were visualized by a GFP-tubulin fusion-protein. Segregation of sister chromatids was assessed by imaging of chromosome V, labelled with the tet repressor (TetR) fused to the RFP tdTomato. Top: Representative time-lapse series. In both strains, sister chromatids of chromosome V appear as one dot in meiosis I, indicating intact cohesion, whereas in meiosis II, two RFP dots are visible, indicating separation of sister chromatids. Bottom: Scoring of 100 cells per strain. Number of visible nuclei, spindles and sister chromatid separation was counted. Time point 0 was defined as the time of meiosis II spindle formation. No failure in chromosome segregation could be observed in the mutant strain. This figure was published in: Jonak, K., Zagoriy, I., Oz, T., Graf, P., Rojas, J., Mengoli, V., and Zachariae, W. (2017). APC/C-Cdc20 mediates deprotection of centromeric cohesin at meiosis II in yeast. *Cell Cycle* 16, 1145–1152.

protein (RFP) and a repetitive array of tet operator (tetO) sequences, integrated close to the centromere (Matos et al., 2008). Expressed TetR binds to the tetO sequences and thus, labels the two sister chromatids, which can be observed as one dot, if the two chromatids are in close proximity or two dots if the sister chromatids have been split. We induced meiosis in the control and experimental strain and filmed both strains in the course of the meiotic division. In both strains, we scored 100 cells to determine their meiotic stage and status of sister chromatid cohesion (Figure 46). In the control strain, the cells displayed two RFP dots, as soon as the cells entered anaphase II, consistent with segregation of sister chromatids in anaphase II. The same temporal pattern of events was observed in the double deletion mutant, indicating an unperturbed centromeric deprotection.

Taken together, this result demonstrates that deprotection of centromeric cohesin does not depend on any of the of SET-homologs in *S. cerevisiae*.

Next, we asked if any of the other reported effectors of Sgo1, like PP2A-B' or Cdc5, are involved in regulation of Sgo1 in *S. cerevisiae*. To assess the effect of PP2A-B' on the regulation of Sgo1 binding, we used a *rts1Δ* strain. Rts1 is the B-type regulatory subunit

of PP2A in *S. cerevisiae*. To analyze the effect of Cdc5, we used a previously described *cdc5*-depletion allele (Matos et al., 2008). Both alleles were crossed into the previously

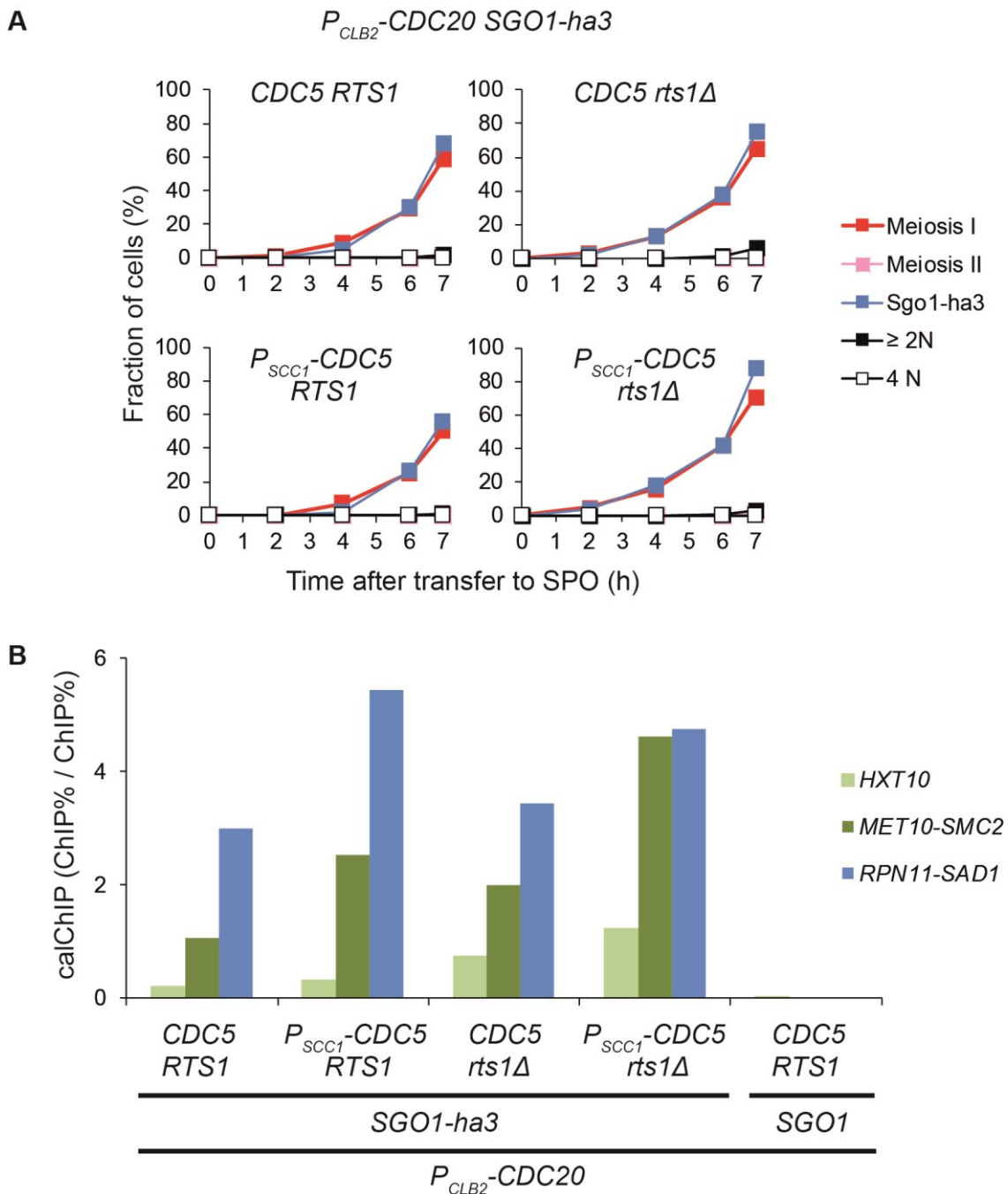


Figure 47: Meiotic time course samples from CDC20-arrest SGO1-ha3 strains containing either CDC5 RTS1 (control), *cdc5*-depletion RTS1, CDC5 *rts1*Δ or *cdc5*-depletion *rts1*Δ. (A) Immunofluorescence counting of spindles, nuclear accumulation of Sgo1-ha3 and nuclear division to assess the meiotic stage of individual samples. Spindles were visualized by staining of Tub1 with a specific antibody. Nuclei were visualized by DAPI staining of DNA. (B) Calibrated ChIP-qPCR of the samples taken at 7 hours. The bar graphs show Sgo1-ha3 enrichment. Three different loci on chromosome VI. were analyzed. The vertical axis displays the calibrated ChIP signal. The amount of chromosome-bound Sgo1 increases upon depletion of Cdc5.

used *CDC20-arrest SGO1-ha3* background. The control strain was wildtype for *RTS1* and *CDC5*. We induced all strains to undergo meiosis and assessed their meiotic

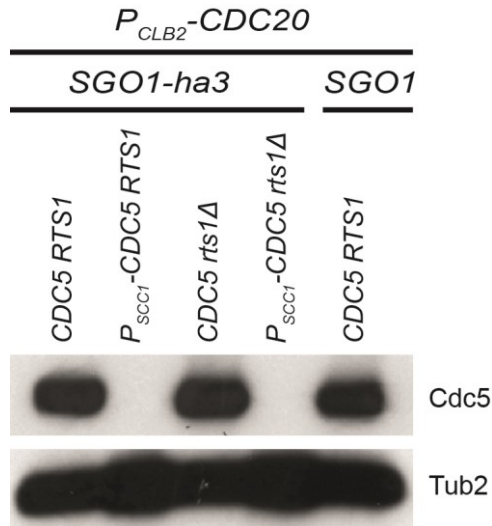


Figure 48: **Immunoblot analysis of cell extracts from meiotic cells, used for ChIP analysis.** *Cdc5* and *Tub2* were stained, using specific antibodies. *Cdc5* was efficiently depleted in *RTS1* and *rts1*Δ strains.

progression by immunofluorescence counting. All strains entered meiosis and accumulated meiosis I spindles and *Sgo1-ha3* to sufficiently high levels for a ChIP

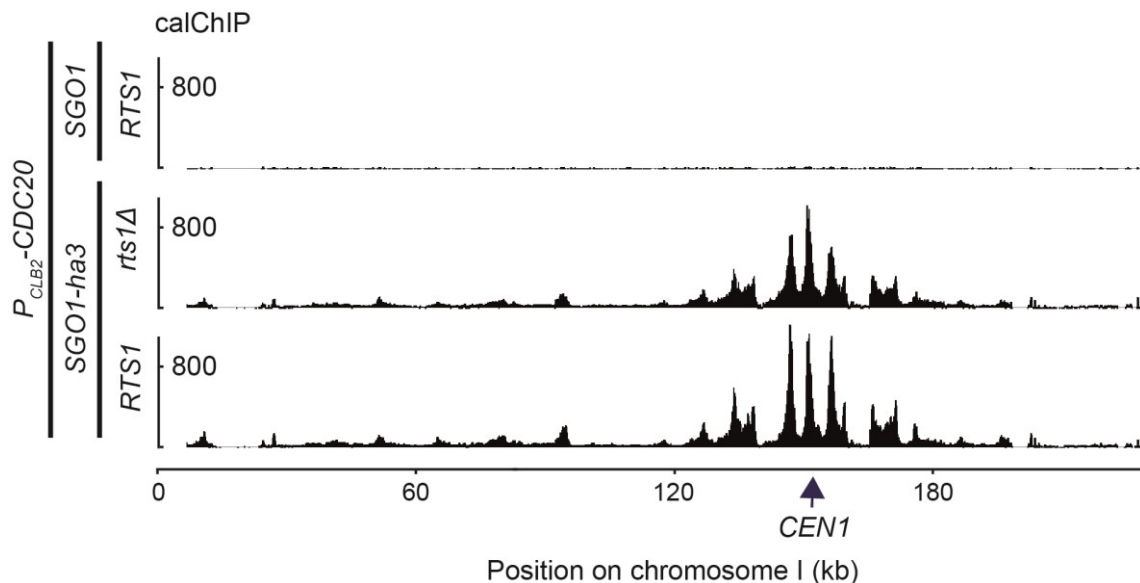
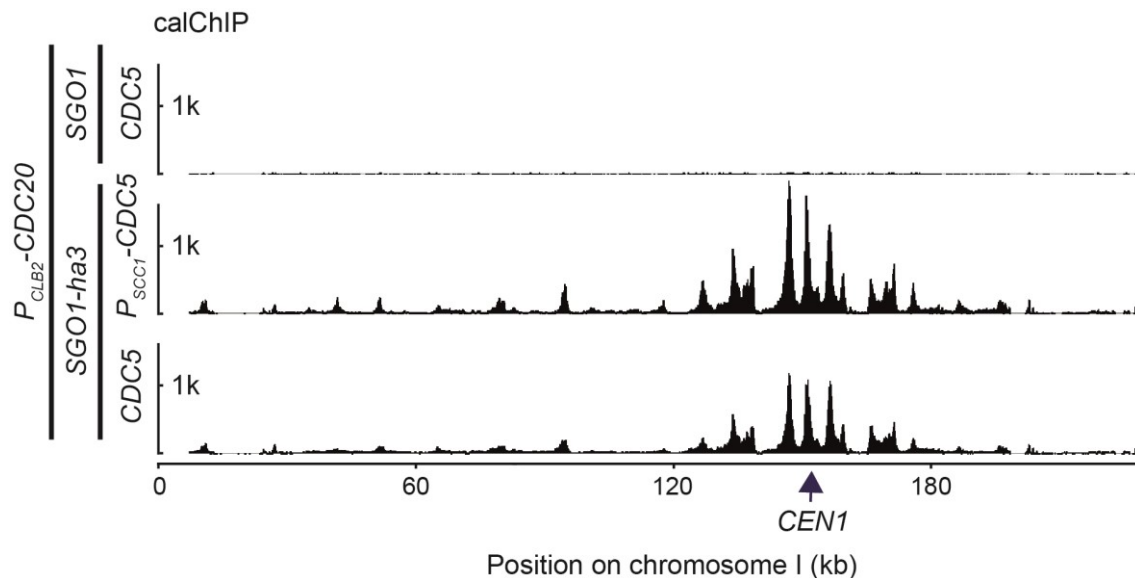


Figure 49: **Calibrated ChIP-Seq profiles of *Sgo1-ha3* on chromosome I in samples from a meiotic time course of *CDC20-arrest SGO1-ha3* strains, containing either *RTS1* or *rts1*Δ.** The vertical axis measures the calibrated signal intensity of *Sgo1*. Samples were taken 7 hours after inoculation in SPO medium. Deletion of *RTS1* has no effect on the *Sgo1* levels on chromatin.

analysis, seven hours after transfer to SPO medium (Figure 47 A). At this time, we took samples of all cultures and subjected them to our calibrated ChIP protocol (Figure 47 B).



**Figure 50: Calibrated ChIP-Seq profiles of *Sgo1-ha3* on chromosome I in samples from a meiotic time course of *CDC20*-arrest *SGO1-ha3* strains, containing either *CDC5* or a *cdc5*-depletion allele. The vertical axis measures the calibrated signal intensity of *Sgo1*. Samples were taken 7 hours after inoculation in SPO medium. Depletion of *Cdc5* increases the *Sgo1* levels on chromatin, around the centromere as well as on the chromosome arm.**

In parallel, we took samples for immunoblot analysis and thus confirmed the efficient depletion of *Cdc5* in the respective experimental strains (Figure 48). Comparing the calChIP-Seq profile of *rts1Δ* with the control revealed that *Sgo1* was recruited to comparable levels in both strains (Figure 49). The *Sgo1* peaks of the *rts1Δ* strain were slightly broader than that of the control strain, indicating some minor effect of PP2A-Rts1 on *Sgo1* localization. However, the overall *Sgo1* levels were comparable. Contrasting the calChIP-Seq profiles of the *cdc5*-depletion with the control, interestingly showed that the *Sgo1-ha3* levels were much higher in the *cdc5*-depletion than in the control strain. Inactivation of *Cdc5* caused more *Sgo1* loading in the pericentromeric region, but also on the chromosome arms. Whereas on the chromosome arms only a weak accumulation of *Sgo1* could be observed in the control strain, distinct peaks emerged on the chromosome arms in the *cdc5*-depletion (Figure 47 B, Figure 50). Subsequently, we compared the *Sgo1* level in the *rts1Δ* strain relative to a *rts1Δ cdc5*-depletion double mutant. Also, in the *rts1Δ* background, we observed a substantial increase of *Sgo1* on chromosomes, if *Cdc5*

was inactivated by depletion, confirming the previous observation (Figure 47 B, Figure 51).

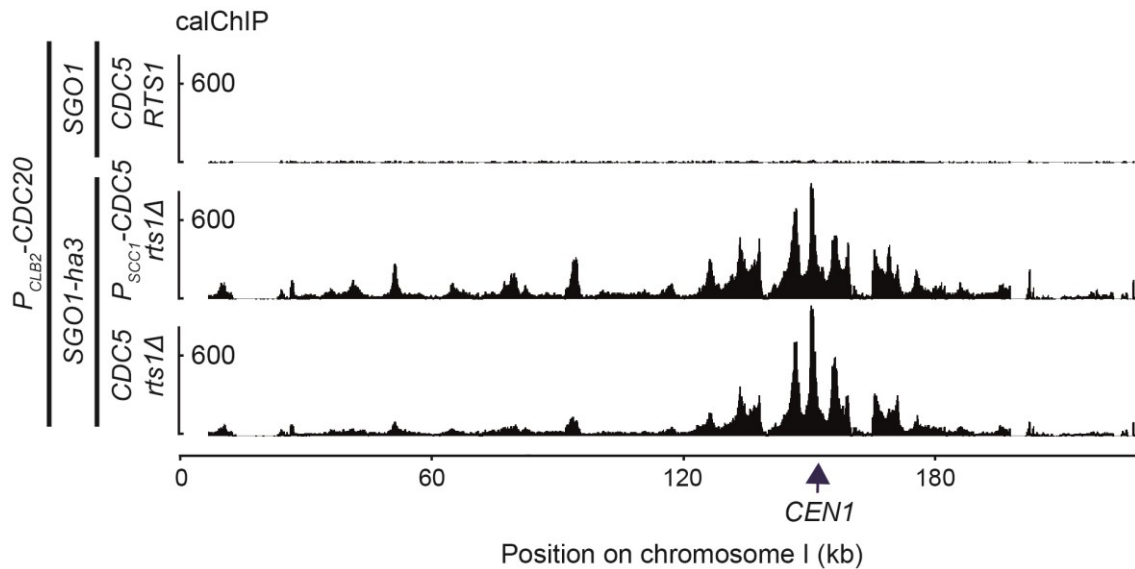


*Figure 51: Calibrated ChIP-Seq profiles of Sgo1-ha3 on chromosome I in samples from a meiotic time course of CDC20-arrest SGO1-ha3 strains, containing either CDC5 rts1A or cdc5-depletion rts1A. The vertical axis measures the calibrated signal intensity of Sgo1. Samples were taken 7 hours after inoculation in SPO medium. Depletion of Cdc5 increases the Sgo1 levels on chromatin in a rts1A background, especially on the chromosome arm.*

Taken together, Cdc5 is involved in regulating the binding of Sgo1 to chromosomes in *S. cerevisiae*. Active Cdc5 substantially reduces the Sgo1 levels in the pericentromeric region, but more importantly, also in on the chromosome arms. Thus, Cdc5 antagonizes the Sgo1 recruitment and keeps the chromosome arm regions free of Sgo1.

Having demonstrated previously that it is possible to accurately quantify the amount of chromosome-bound protein using calibrated ChIP-Seq data (Figure 30), we aimed to quantify the effect of Cdc5 on Sgo1 recruitment. To this end, we quantified the amount of chromosome-associated Sgo1 by correcting the signal for each base pair with the respective signal in the untagged control, followed by summing-up the untagged-corrected signals for all base pairs over the full length of all chromosomes. Subsequently, we calculated the average of all 16 chromosomes (Figure 52). Thus, we could show that by inactivating Cdc5, the chromosome-bound Sgo1 levels on average increased by more than 50 %. This result was precisely reproduced, quantifying the amount of chromosome-bound Sgo1 in the rts1Δ background.

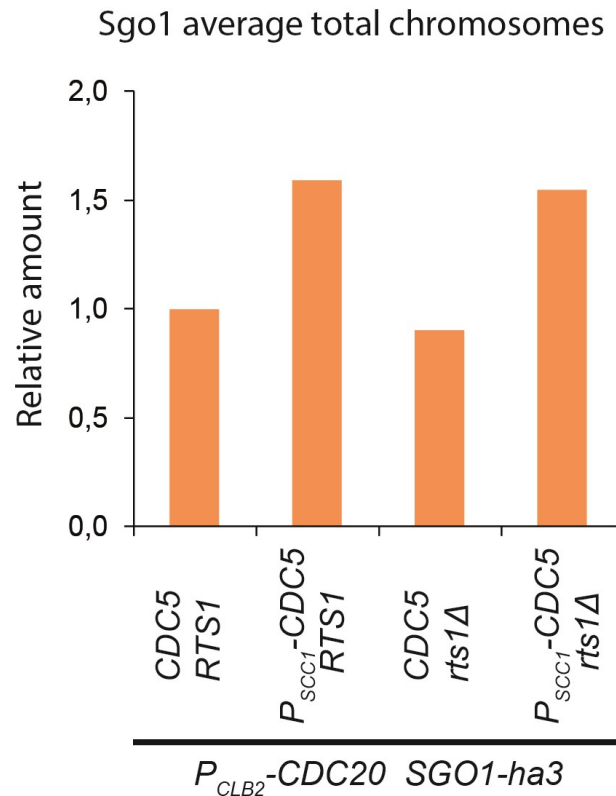
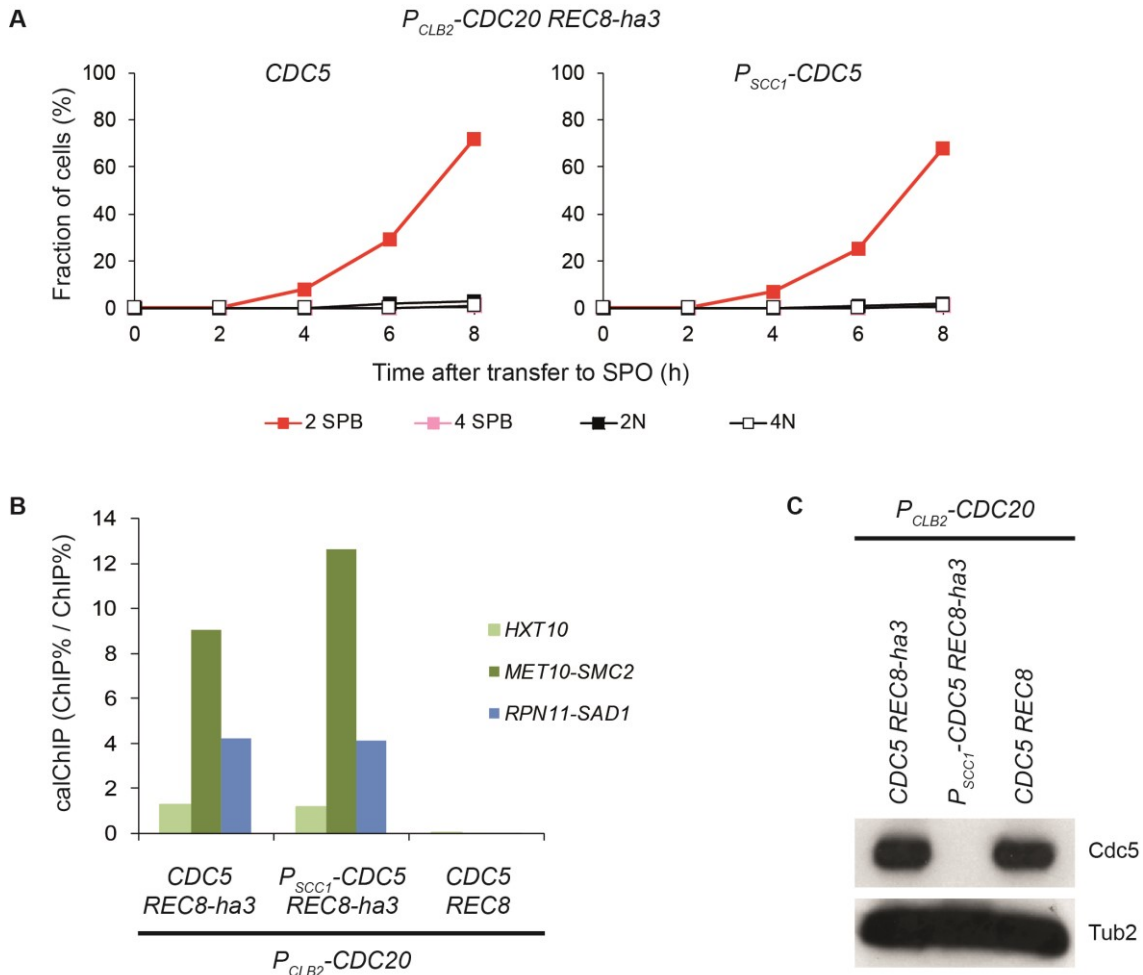


Figure 52: **Quantification of calibrated ChIP-Seq data.** The amount of Sgo1 along the whole chromosome axis was quantified in different genetic backgrounds, individually for each chromosome. The bar graphs represent the average of all 16 chromosomes. The values are relative to the Sgo1 amount in the CDC5 RTS1 control strain. Depletion of Cdc5 increases the amount of chromatin-bound Sgo1 by approximately 50 % in RTS1 and *rts1*Δ cells.

Having demonstrated that one function of Cdc5 is to regulate the Sgo1 levels in metaphase I of budding yeast meiosis, we next asked if we could see a similar effect, measuring cohesin levels in a *cdc5*-depletion. As we have shown previously that Sgo1 is loaded onto chromosomes via a cohesin-dependent mechanism, it seemed conceivable that the altered Sgo1 levels could be explained by an altered cohesin regulation. Therefore, we constructed *CDC20-arrest REC8-ha3* strains, harboring either a *cdc5*-depletion or *CDC5* allele. Together with an untagged control, all strains were induced to enter meiosis. The control and experimental strain arrested in metaphase I, as was assessed by immunofluorescence counting (Figure 53 A). Cdc5 was efficiently depleted, as was determined by immunoblotting (Figure 53 C). Eight hours after transfer into SPO medium, we took samples from all three strains and subjected them to our ChIP protocol and analyzed those samples using qPCR (Figure 53 B) and NGS. The calChIP-Seq profiles revealed that inactivation of Cdc5 causes a substantial increase of Rec8-ha3 levels (Figure 54). Interestingly, this increase of Rec8 occurred only at chromosome arm

sites. In the pericentromeric region, by contrast, the Rec8 levels were very comparable in the control and experimental strain.



**Figure 53: Meiotic time course samples from CDC20-arrest REC8-ha3 (control) and CDC20-arrest REC8-ha3 cdc5-depletion strains.** (A) Immunofluorescence counting of spindle pole bodies and nuclear division to assess the meiotic stage of individual samples. Spindles were visualized by staining of Tub1 with a specific antibody. Nuclei were visualized by DAPI staining of DNA. (B) Calibrated ChIP-qPCR of the samples taken at 8 hours. The bar graphs shows Rec8-ha3 enrichment. Three different loci on chromosome VI. were analyzed. The vertical axis displays the calibrated ChIP signal. (C) Immunoblotting of Cdc5 and Tub2 to demonstrate effective depletion of Cdc5 in the strains used in this time course.

Collectively, this shows that Cdc5 selectively controls the cohesin levels on chromosome arms in budding yeast meiosis and confirms our previous finding of a cohesin-dependent loading mechanism for Sgo1.

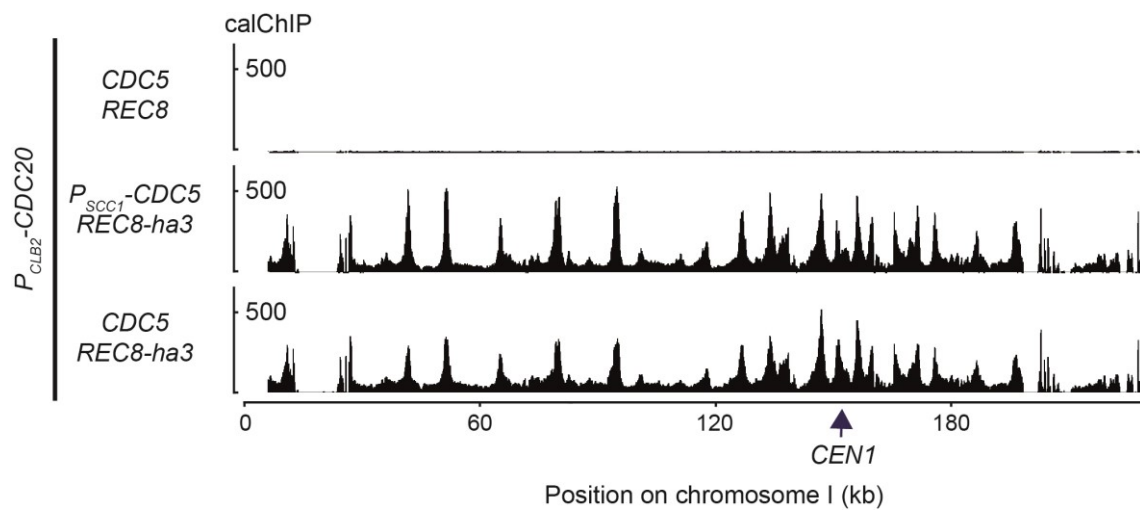


Figure 54: Calibrated ChIP-Seq profiles of *Rec8-ha3* on chromosome I in samples from *CDC20*-arrest *REC8-ha3* strains, containing either *CDC5* or a *cdc5*-depletion allele. The vertical axis measures the calibrated signal intensity of *Sgo1*. Samples were taken 8 hours after inoculation in SPO medium. Depletion of *Cdc5* increases the *Rec8* levels on chromatin, especially on the chromosome arm.

### 3. Discussion

#### Experimental workflow

To enhance the resolution of cohesin dynamics in meiosis, we established a novel experimental workflow by combining a calibrated and optimized ChIP-Seq assay with a new synchronization system for budding yeast meiosis. Some methods, like for example live-cell imaging, provide an excellent temporal resolution of cellular events. Other methods, like conventional ChIP-Seq, provide an excellent spatial resolution. But currently no method offers at the same time such a high temporal-spatial resolution like our novel experimental workflow. Collectively, our successfully established experimental workflow combines four key advantages. First, our synchronization system generates highly synchronous meiotic cultures. Second, due to the calibration, the technical noise in the data is very low. Third, quantitative ChIP-Seq data allow the temporal resolution of biological processes. Fourth, quantitative genome-wide data allow the quantification of protein-DNA interactions in large genomic regions, compared to small regions, using only ChIP-qPCR.

To establish this experimental workflow, we first optimized a standard ChIP-Seq protocol, specifically for the conditions of a meiotic time course experiment. We optimized the protocol by employing DOE, a method which is typically used for industrial processes planning (Tanco et al., 2007). Using DOE, we demonstrate that the composition of the shearing buffer is the most crucial single factor for the outcome of a ChIP experiment and particular care should be taken to first optimize its chemical composition, before testing other experimental settings. The relevance of the buffer composition is an important finding, as usually physical or technical parameters, like incubation times or treatment intensities, are optimized first when a new method is established. The second most essential parameters for the outcome of a ChIP experiment are the physical parameters of time of fixation and time of shearing. However, no statistically detectable two-factor interaction exists between these factors, making it possible to optimize those two factors independently.

Having optimized the ChIP-Seq protocol, we continued by combining this protocol with a recently published, novel calibration system for ChIP-Seq (Hu et al., 2015). It is important to note that this method is not based on spiking-in the same amount of DNA into all the

experimental samples and then using the signal from the spiked-in DNA to normalize the signal of the experimental samples. Instead, this calibration method is much more powerful and would also work if different amounts of calibration material had been added to the experimental samples. This calibration method uses the ChIP enrichment of the calibration genome (IP/WCE) to normalize the experimental signal. It is, therefore, crucial to measure the calibration signal in both, the IP samples and the WCE samples. This method is based on the assumption that samples from the same cell population generate identical ChIP enrichment signals. If the ChIP enrichment of samples from the same cell population deviate, it must be due to technical variation. The calibration strain population is the same in all aliquots, thus, the ChIP enrichment of the calibration strain should be the same in all samples and can be used to calibrate the experimental signal.

The calibrated ChIP method was described as a method to estimate changes of protein occupancy between samples, using ChIP-Seq. By using this system in our lab extensively, we realized that this system has two additional major advantages over conventional ChIP workflows that were not yet described explicitly in the literature. First, apart from making ChIP-Seq profiles quantitative, this system reduces most of the technical variation between samples, making it a potent tool, also for ChIP-qPCR experiments, because it increases the sensitivity of qPCR measurements. Second, by eliminating most of the technical noise, it allows for very intense shearing of the samples, which would otherwise reduce the signal-to-noise ratio to such an extent that it would not be possible anymore to detect biologically meaningful signals. Allowing for a very intense shearing of the chromatin enables to generate samples, in which the peak of the size distribution of chromatin fragments is close to the optimal length for sequencing library preparation at around 150 to 200 bp. This, in turn, makes the sequencing library preparation very efficient, which is advantageous, especially for low-abundant proteins.

### **Characterization of meiotic cohesin**

By using immunofluorescence assays, it was shown that cohesin around the centromere is protected from cleavage by separase in meiosis I and is only cleaved in meiosis II. (Klein et al., 1999; Watanabe and Nurse, 1999; Buonomo et al., 2000). From these observations, a model was conceptualized, in which chromosomal cohesin consists of two fractions. One fraction is located at the chromosome arms and is susceptible to cleavage

by separase in meiosis I. A second fraction is located around the centromere and is protected from cleavage by separase in meiosis I and only becomes susceptible to cleavage by separase in meiosis II. In this binary model, arm cohesin is completely removed from chromosomes in meiosis I and centromeric cohesin stays intact until meiosis II. Consequently, in this model, the localization of a cohesin complex defines to which fractions it belongs and what properties it has.

Contrary to this model, we demonstrate that once APC<sup>Cdc20</sup> is activated and hence, the cells start to undergo the metaphase-to-anaphase transition, cohesin is removed from all chromosomal loci, the arm region as well as the pericentromeric region. The difference between the arm region and the pericentromeric region is that in the pericentromeric region, additionally a small cohesin pool exists, which persists until meiosis II (Figure 14, Figure 23 B). Consequently, in the pericentromeric region two different cohesin fractions exist next to each other, a protected and an unprotected fraction. The consequence is that it is not sufficient for a particular cohesin complex to localize to the pericentromeric region to become protected in meiosis I and hence, the localization of a cohesin complex is not sufficient to define to which fraction it belongs and whether it becomes protected.

Cohesin has many physiological functions. One function is to provide cohesion between sister chromatids. The cohesion between sister chromatids in meiosis II is provided solely by the protected cohesin fraction, as the unprotected fraction is removed in meiosis I. Because the protected fraction is much smaller than the total amount of pericentromeric cohesin at the beginning of meiosis, the question arises what the function of the unprotected cohesin around the centromere is. For fission yeast, it was shown that cohesin is involved in the termination of transcription (Gullerova and Proudfoot, 2008). For metazoans, it was demonstrated that cohesin is involved in the genome-wide regulation of transcription, with significant alterations in gene expression upon cohesin impairment (Horsfield et al., 2007; Pauli et al., 2010). Moreover, cohesin was shown to be required for DNA repair (Sjögren and Nasmyth 2001) and chromosome condensation (Guacci et al., 1997). Consequently, the additional cohesin in the pericentromeric region in meiosis I might serve regulatory functions concerning transcriptional regulation, DNA repair or chromosome condensation, instead of providing cohesion.

Kiburz et al. (2005) quantified the size of the region in which cohesin is protected in meiosis I indirectly, by correlating the position of Rec8 in metaphase I with ChIP-Chip

data of the protection machinery and estimated its size to be 50 kb. Stabilizing Rec8 in meiosis II, using the *hrr25-as1* mutant, we were able to directly visualize the meiosis II-Rec8 fraction in a calChIP-Seq profile (Figure 28), thereby confirming that the size of the protected region on average of all chromosomes is 51 kb in *S. cerevisiae*. However, we observe differences in the size of this protected pericentromeric region between chromosomes, which do not correlate to the total length of the chromosome. Interestingly, the meiosis II cohesin pattern displays strong variation between chromosomes. This variation raises the question how the protection machinery is recruited reliably and robustly, to provide sufficient protection to cohesin which is distributed in such diverse spatial patterns. One mechanistic solution could be to recruit the protection machinery in a cohesin-dependent manner. A mechanism, which is in fact in place, as we found and will show in the chapter about the recruitment of the protection machinery.

Furthermore, we demonstrate that larger chromosomes preserve a higher percentage of their pericentromeric cohesin in meiosis II than smaller ones (Figure 31 B). Moreover, we show that this is not an effect from different sizes of the protected region, or different amounts of initial metaphase I cohesin (Figure 31 A). Thus, our data suggest that the activity of the protection machinery depends on the size of the chromosome and a more active protection machinery seems to be in place at larger chromosomes. This finding provides a possible explanation why the frequencies with which each chromosome is found in aneuploidy events are different. In human cells, significantly fewer of the large chromosomes and significantly more of the small chromosomes are lost in aneuploidy events (Martin and Rademaker 1990). Our data provide a possible mechanistic explanation for this observation, as we show that larger chromosomes preserve a higher percentage of their pericentromeric cohesin in meiosis II than smaller ones, presumably resulting in stronger cohesion. The quantitative difference of the protected cohesin fraction between the chromosomes is not exceptionally large, but the difference is nevertheless statistically significant, and it matches the cytological observation of a more stable propagation of larger chromosomes from the mother cell to the daughter cells.

This finding might also be relevant concerning reproduction-related disabilities in humans. Here, the risk for infertility and congenital disabilities is correlated with age. Moreover, often these problems result from chromosome missegregation defects in oocytes, which underlying molecular mechanisms are not yet understood. Kuliev et al. (2005) found that “more than half of the human oocytes obtained from IVF patients of

advanced reproductive age are aneuploid, due to meiosis I and meiosis II errors". Cohesin might be a key player in these kinds of defects, as it provides cohesion and is involved in the regulation of chromosome segregation (Herbert et al., 2015). For mice, it was shown that Rec8 levels on chromosomes are severely reduced in oocytes from old mice, and the resulting weakened centromere cohesion explains most MI chromosome segregation defects in those cells (Chiang et al., 2010). Hence, it is conceivable that in the future oocytes are assessed for the risk of reproduction-related disabilities by examining *in vivo* the cohesin concentration before fertilization, at least in clinical setups. For a medical risk assessment, it would be necessary to know what amount of cohesin is minimally required in oocytes for a faithful chromosome segregation. Our data might provide first useful insights into this question. One conclusion from our results is that the required amount of cohesin seems to be chromosome-specific. Consequently, for a reliable medical risk assessment, it would be necessary to quantify and assess all chromosomes individually and not only the total cohesin amount in the cell. Based on our data, no final answer can be given to the question what minimal cohesin amount provides sufficient cohesion for a faithful, error-free chromosome segregation. However, some helpful conclusions can be drawn from our data concerning this question: If larger chromosomes protect a higher fraction of their cohesin than smaller ones, there seems to be some evolutionary pressure on the cells to provide a more active centromeric protection for larger chromosomes. If the amount of cohesin on these large chromosomes would be more than sufficient to provide cohesion, in other words, if they did comprise a redundant backup, there would be no evolutionary pressure, because they would also segregate reliably with lower cohesin amounts. The fact that larger chromosomes protect more of their initial cohesin, in turn, means that it is likely that the cohesin amount we measure in meiosis II is in fact at the lower limit of what the cells need for a faithful segregation. Thus, our data provide the first insight, at least for *S. cerevisiae*, into how much cohesin is minimally required for providing sufficient cohesion to ensure faithful, error-free chromosome segregation.

Keeping the cells in a prolonged metaphase I arrest, we demonstrate that the arrest is reliable, robust and of high quality because no artificial accumulation of cohesin or premature loss of cohesin was detected (Figure 23 A). However, in the ChIP-Seq profiles of a prolonged metaphase I arrest, we observe that the cohesin peaks become slightly broader over time, while their height is reduced. The most likely mechanistic explanation for this is a distal diffusion of cohesin away from the original center of the peaks. This

distal diffusion could occur in all cells in a similar manner or to a different extent in different cells, resulting in an increase of heterogeneity in the culture. Using a gel-based assay, followed by western blotting and southern blotting it was shown that it is possible to generate stable, SDS-resistant cohesin-DNA complexes, just by cross-linking the cohesin subunit to each other, without cross-linking them to DNA or another chromatin subunit (Haering et al., 2008). This ability to generate stable cohesin-DNA complexes demonstrates the topological interaction between cohesin and chromatin. Our observations can be directly explained, using this topological model: A topological interaction would allow cohesin to move along the direction of the chromosome axis, resulting in potential distal diffusion over time, without dissociation of cohesin from chromosomes. Consistent with this notion, we observe an reduction of qPCR signals in a prolonged metaphase I arrest (Figure 13). This reduction can be explained by cohesin diffusing out of the analyzed small qPCR locus, spanning less than 200 bp. However, we did not measure a loss of total cohesin when we quantified the DNA-bound cohesin in a prolonged metaphase I arrest (Figure 32), confirming that cohesin is stably bound to DNA.

The alternative model of a direct interaction between cohesin and DNA via complementary interaction sites would lock individual cohesin molecules at their localization sites, making it difficult to explain our observations of a constant and slow peak broadening. An objection to this interpretation might be that proteins like transcription factors are also able to slide along DNA, without interacting topologically and that, consequently, a topological interaction is not a prerequisite for a movement along the direction of the chromosome axis. However, the sliding movement of non-topologically interacting proteins is a controlled, energy-dependent process. Without the actively controlled energy consumption, no sliding would occur. We observe a slow peak broadening over time, which is unlikely to be a controlled process, thus our observation supports the validity of the topological model.

Our results have another interesting implication. While it is widely accepted that cohesin interacts topologically with chromatin, two models have emerged to explain cohesin translocation on chromosomes. The sliding model proposes a movement of cohesin by transcriptional activity, while cohesin stays bound to chromatin. The relocation model, by contrast, proposes translocation by dissociation and association of cohesin at different sites (Ocampo-Hafalla and Uhlmann, 2011). We observe that cohesin peaks become

broader, once the majority of cells reach metaphase I and that this broadening increases in a prolonged arrest. According to the relocation model, the interaction of cohesin and chromatin is dynamic, with a constant dissociation and association of cohesin. In this model, to generate sharp cohesin peaks, the association event must occur at a specific site, which determines the center of the cohesin peak. If such a peak becomes broader over time, then the association region must expand, which would be an actively controlled process, whose function would be enigmatic. According to the sliding model, by contrast, our findings could be easily explained. In this model, cohesin is not dynamically associating and dissociating but stays bound to chromatin. The transcription machinery provides the translocation force, and peak formation occurs via an accumulation of cohesin molecules at this site. If the cells reach metaphase, the transcriptional activity decreases and hence, it is conceivable that without the pushing force of the transcription machinery the topologically bound cohesin would start to passively diffuse away from the peak site over time, resulting in a continuous broadening of the peak, as we observe it. Thus, our results strongly favor the sliding model over the relocation model.

### **Recruitment of the protection machinery**

While it is well established that Shugoshin is required for centromeric protection and that it fulfills this role by recruiting PP2A-B' to chromatin, it is much less clear how the binding of Shugoshin to chromatin is regulated and which are the relevant binding partners.

Using our novel experimental workflow, we demonstrate that in budding yeast, cohesin is involved in the recruitment of Sgo1 to chromosomes. Moreover, our data give the first insight into the specific mechanism of cohesin in Sgo1 localization, which is to translocate Sgo1 from its initial site of loading at the centromere to its site of permanent residence in the pericentromeric region. We will discuss a mechanistic model, for which we hypothesize that apart from being a recruitment platform for PP2A, an additional function of Sgo1 in centromeric protection might be to provide a physical link between PP2A and its substrate phospho-Rec8. Moreover, this model can explain how very diverse spatial patterns of cohesin can be robustly and reliably protected from cleavage in meiosis I. Finally, we provide the first evidence, suggesting that one function of the topologically bound cohesin might be to act as a transport factor along the chromosome axis.

Using calibrated ChIP-Seq of Rec8 and Sgo1, we detected a co-localization of Sgo1 and Rec8 in the region around the centromere (Figure 33). Our findings confirm previous results of Kiburz et al. (2005), who compared the ChIP-Chip profiles of WT Rec8 and Sgo1 and showed a co-localization of both proteins in this region. Due to the very low noise and the quantitative nature of our data, we were able to resolve additional characteristics of the relationship between these two proteins. We observe that Sgo1 follows a gradient relative to the Rec8 occupancy, which is highest at the centromere and steadily declines in the regions distal to the centromere (Figure 34). One possibility is that Sgo1 is loaded at the centromere and spreads from here into the pericentromeric region, raising the possibility that Sgo1 is not just recruited from the nucleoplasm to the chromosomes, but that this recruitment follows a specific path, which starts at the centromere.

Kiburz et al. (2005) further compared the ChIP-Chip profiles of Rec8 and Sgo1 in a *spo11Δ rec8Δ* strain and found that the Sgo1 signal is absent in this mutant. Our calibrated ChIP-Seq data also confirms this result (Figure 37, Figure 38). However, these experiments do not address the problem that by deleting the cohesin subunit *REC8*, the chromatin structure is severely altered because, during meiosis, only Rec8-containing cohesin complexes provide cohesion (Rankin, 2015). Moreover, some reports in the literature explicitly exclude the involvement of cohesin in Sgo1 localization in fission yeast and *Drosophila*, respectively (Kitajima et al., 2004; Lee et al., 2004). Due to these concerns, we also tested the Sgo1 localization in a *scc4-m35* cohesin loader mutant background, in which the cohesin levels on chromosomes are drastically reduced, but cohesin is not entirely absent from chromosomes (Hinshaw et al., 2015). Thus, the cells in the *scc4-m35* mutant deviate from the cells of the *rec8Δ* strain in two critical respects: First, in the *scc4-m35* mutant, wildtype-levels of *REC8* are expressed, restoring the presence of soluble Rec8-cohesin complexes in the nucleoplasm, excluding unintended side-effects from the lack of soluble cohesin complexes. Apart from providing cohesion, cohesin complexes have other regulatory functions, which might be re-established in this background. Second, low levels of functional cohesin are recruited to chromosomes, also in the absence of the cohesin loader, resulting in a low basal level of cohesion (Hinshaw et al., 2015). Consequently, the main difference between the *SCC4* control strain and the *scc4-m35* mutant strain is the amount of cohesin complexes, which are topologically loaded onto chromosomes, because this function is provided by the cohesin loader

complex. This specific difference between the strains demonstrates that not just the presence of cohesin complexes in the nucleoplasm, but the topological loading of Rec8-cohesin onto chromosomes is required for the pericentromeric recruitment of Sgo1, indicating a specific function of topologically loaded Rec8 for the pericentromeric localization of Sgo1 (Figure 40, Figure 41). In a third experiment, by using the AID system, we artificially removed Rec8 from chromosomes in metaphase I, after the cells have already fully established cohesion and after the cells finished loading of Sgo1 onto chromosomes. With this experiment, we confirm that after cohesion of sister chromatids has been established and after the cells have loaded Sgo1 onto chromosomes, Sgo1 is lost from chromosomes, if Rec8 is artificially removed (Figure 43). Furthermore, this experiment demonstrates that the kinetics with which Sgo1 and Rec8 are lost from chromosomes deviate from one another. Upon cleavage of Rec8 from chromosomes, the corresponding calChIP-Seq signal for Rec8 is lost within 60 minutes after induction of the AID system. The pericentromeric Sgo1 signal, by contrast, is still partially retained after 60 minutes and only lost after 120 minutes. The centromeric signal of Sgo1 is entirely unaffected by the removal of Rec8. This confirms that the pericentromeric localization of Sgo1 requires cohesin, but not the centromeric recruitment. The experiment further demonstrates that once Sgo1 is recruited to the pericentromeric region, it can reside there for a prolonged time, even in the absence of cohesin, suggesting the presence of another pericentromeric receptor for Sgo1. It is very likely that this heterochromatin receptor consists of the proteins Iml3 and Chl4, as it was demonstrated that the inactivation of those proteins results in reduced chromosomal Sgo1 levels (Kiburz et al., 2005). Thus, we demonstrate that cohesin acts as a transport and loading factor for Sgo1 into the protected pericentromeric region, where it is subsequently transferred to its heterochromatin receptor.

By using *bub1Δ* and *bub1Δ rec8Δ* strains, we demonstrate that additionally Bub1 is required for recruiting Sgo1 to chromosomes (Figure 44, Figure 45). This result confirms several reports in the literature about a Bub1-dependent Sgo1 loading mechanism (Kiburz et al., 2005; Kitajima et al., 2004; Kitajima et al., 2005; Tang et al., 2004). Moreover, our results give insights into the relationship between Bub1 and cohesin concerning the loading of Sgo1. Our findings suggest that Bub1 acts upstream of Rec8 in the recruitment of Sgo1 because without Bub1, Sgo1 cannot localize to chromosomes at all. Without Rec8, by contrast, Sgo1 cannot recruit to the pericentromeric region, but can still bind to

a small region at the centromere. This binding at the centromere, in turn, must be Bub1-dependent, as we observe it in strains expressing *BUB1*, but not the cohesin subunit *REC8*. Taken together, we have confirmed that Sgo1 and Rec8 precisely co-localize in the region surrounding the centromere (Figure 33). We have demonstrated that Sgo1 follows a gradient, which is highest at the centromere and declines continuously distal to the centromere (Figure 34). By using an IP-WB assay, we have shown that cohesin and Sgo1 physically interact (Dr. Wei Ma, Zachariae Lab, unpublished). We have demonstrated that the pericentromeric localization of Sgo1 depends on topologically loaded Rec8 (Figure 41), whereas the localization of Rec8 does not depend on Sgo1 (Figure 36). We have confirmed that additionally, Bub1 is required for loading of Sgo1 on chromatin and we have demonstrated that the Bub1-mediated loading results in a sharp peak right at the centromere in calibrated ChIP-Seq profiles, whereas Sgo1 is not recruited to the pericentromeric region without topologically-bound cohesin (Figure 45).

Therefore, we propose a new three-step loading model for Sgo1, in which cohesin acts as a transport factor for Sgo1 along the chromosome axis. According to this model, Sgo1 and cohesin are both loaded onto chromosomes at the centromere by independent mechanisms. The loading of Sgo1 is Bub1-dependent and involves phosphorylation of histone H2A (Kitajima et al., 2004; Kawashima et al., 2010; Tang et al., 2004). The loading of cohesin is *Scs2/Scs4*-dependent and involves phosphorylation of Ctf 19 by DDK (Ciosk et al., 2000; Hinshaw et al., 2017). As both proteins are loaded at the centromere, they come in close vicinity and interact physically. Subsequently, the topologically bound cohesin is transported away from its site of loading into the pericentromeric region by a sliding movement, triggered by the transcription machinery (Lengronne et al., 2004; Bausch et al., 2007; Stigler et al., 2016). Cohesin takes the physically bound Sgo1 away with it and transports it into the pericentromeric region, where it interacts with its heterochromatin receptor, which comprises the proteins *Iml3* and *Chl4* (Kiburz et al., 2005). Thus, cohesin acts as a transport factor for Sgo1 in the pericentromeric region and thereby ensures the correct localization of the protection machinery relative to its substrate cohesin.

An alternative model is that cohesin is loaded at the centromere, translocated to its sites of permanent residence in the pericentromeric region and soluble Sgo1 subsequently binds cohesin. However, we favor the first model because the second model cannot explain the requirement of Bub1 for Sgo1's recruitment to chromatin. Several groups

showed, and we have confirmed these results, that Bub1 is required for the recruitment of Sgo1 to chromatin. (Kiburz et al., 2005; Kitajima et al., 2004; Kitajima et al., 2005; Tang et al., 2004). Cells without functional Bub1 are not able to recruit Sgo1 at all. Furthermore, we have shown that in meiotic cells, which do not topologically load cohesin but have active Bub1, Sgo1 is still recruited at the centromere in a Bub1-dependent manner (Figure 38, Figure 41). Thus, the function of Bub1 is to recruit cohesin into the region close to the centromere. However, contrary to cells, which co-load cohesin at the centromere, the translocation of Sgo1 into the pericentromeric region distal to the centromere does not occur in those cells. These findings demonstrate that the function of Bub1 is to load Sgo1 at the centromere, but Bub1 is not sufficient for its pericentromeric spreading. Thus, we strongly favor a model in which cohesin is initially loaded at centromeres in a Bub1-dependent way and then translocated into the pericentromeric region in a cohesin-dependent way.

Additionally, according to our three-step loading model, Sgo1 fulfills a new, second function for centromeric protection of cohesin. It is well established that Sgo1 is required for centromeric protection and that its function is to recruit PP2A-B' to chromosomes (Katis et al., 2004; Kerrebrock et al., 1995; Kitajima et al., 2004; Kitajima et al., 2006; Marston et al., 2004; Rabitsch et al., 2004; Riedel et al., 2006). According to our model, Sgo1 additionally binds to cohesin and thus, links the phosphatase PP2A-B' physically to its substrate, which is the phosphorylated Rec8. Bringing an enzyme and its substrate into proximity increases the "effective concentration" of the substrate, thus, drastically increases the enzymatic activity. This high activity of the phosphatase, in turn, ensures a tight protection mechanism, which is necessary for an error-free and reliable meiotic division. Consequently, for the first time, we propose that Sgo1 might have a second function in centromeric protection, which is to link the phosphate PP2A-B' to its substrate phospho-Rec8.

Moreover, our new three-step loading model allows us to reconcile an apparent controversy in the literature, related to the function of cohesin in Sgo1 recruitment. If the cells load Sgo1 in a three-step process, inactivation of cohesin does not remove all Sgo1 from chromosomes, because of the first, Bub1-dependent step, which still recruits some Sgo1 at the centromere. If the used experimental method does not provide enough resolution to distinguish the centromeric from the pericentromeric region, like it is the case for many immuno-staining-based methods, the obtained data might be misleading.

One might get the impression that removal of cohesin only mildly reduces the Sgo1 levels, leading to the conclusion that cohesin is not crucial for the recruitment of Sgo1. However, we cannot exclude the possibility that cohesin might not be involved in the localization of Shugoshins in organisms other than budding yeast.

### **Regulation of centromeric protection**

If Sgo1 and with it PP2A were recruited to chromosome arm sites, it would have catastrophic consequences, as it would protect arm cohesin from cleavage in meiosis I, thus, preventing the first meiotic division (Kitajima et al., 2006; Riedel et al., 2006). Consequently, one important question concerning the regulation of the recruitment of the centromeric protection machinery is how to exclude Sgo1 from chromosome arms.

Tang et al. (2006) showed that in human cells, PP2A is required for the chromosomal localization of Sgo1 in mitosis. Even though Sgo2 is responsible for the protection of centromeric cohesin in human meiosis, and not Sgo1, this finding nevertheless raises the possibility that PP2A might also be involved in the recruitment of Sgo1 in budding yeast meiosis. We demonstrate that the Sgo1-ha3 levels are comparable in an *RTS1* and *rts1Δ* strain, excluding the possibility that PP2A-Rts1 controls its own recruitment to chromosomes in budding yeast meiosis (Figure 49). However, the Sgo1-ha3 calChIP-Seq pattern of the *rts1Δ* strain looks broader and more diffuse than that of the *RTS1* control strain. PP2A-Rts1 binds Sgo1 in a 1:2 stoichiometry, meaning that one PP2A-Rts1 complex binds two Sgo1 monomers (Xu et al., 2009). The binding site of PP2A-Rts1 is a coiled-coil domain, which is formed by homodimerization of two Sgo1 proteins. One could speculate that each Sgo1 monomer might bind to a different cohesin moiety, thus, physically linking two spatially distant cohesin complexes. Hence, it is conceivable that without the binding force of PP2A-Rts1 cohesin drags apart the dimerized Sgo1 monomers, resulting in a more spread-out Sgo1 pattern.

Using immunostaining of *Drosophila* cells, Clarke et al. (2005) showed that in mitosis, the POLO kinase is required for removing the Shugosin-homolog MEI-S332 from chromosomes at the metaphase-to-anaphase transition. Using immunostaining of chromosome spreads from human cells, Tang et al. (2006) demonstrated that depletion of Plk1, the human POLO kinase-homolog, restores the chromosomal localization of Sgo1 in cells, which were co-depleted of PP2A. These studies demonstrate that the POLO

kinase exhibits a Shugoshin-antagonizing function in mitosis of *Drosophila* and humans. It is unknown whether this Shughoshin antagonizing function is a conserved property of the POLO kinase or if it is specific to mitosis in the investigated organisms. Using our novel experimental workflow, we demonstrate that Cdc5 regulates the binding of Sgo1 to chromosomes also in meiosis of *S. cerevisiae* (Figure 47, Figure 50, Figure 51). Active Cdc5 substantially reduces the Sgo1 levels in the pericentromeric region, and also on the chromosome arms (Figure 50). Thus, Cdc5 antagonizes the Sgo1 recruitment and keeps the chromosome arm regions free of Sgo1. However, contrary to our results, Clarke et al. (2005) only reported about the persistence of MEI-S332 at the centromeres, but not about a change on chromosomes arm sites, possibly due to lack of spatial resolution and sensitivity of the used immuno-staining method. Therefore, for the first time, we demonstrate that the activity of Cdc5 is required for controlling Sgo1 levels on chromosomes in *S. cerevisiae* meiosis. Moreover, we show that without Cdc5, Sgo1 also recruits to chromosome arms sites.

One concern with respect to our findings might be that depletion of Cdc5 results in a very tight metaphase I arrest and thus, the calChIP-Seq pattern might reflect a tightly arrested culture, without any escaping cells, resulting in an apparently higher chromosomal loading of Sgo1. However, as we have demonstrated previously (Figure 23), the arrest by depletion of Cdc20 by expression of *CDC20* from the *CLB2* promoter is tight and robust, and no cohesin is removed from chromosomes over a time frame of almost two hours. Therefore, the pattern in the *CDC20*-arrested control strain shows a tightly arrested culture, excluding that the additional accumulation of Sgo1 in the *cdc5*-depletion is a side-effect of a tighter arrest in a *cdc20 cdc5* double depletion background.

Additionally, we demonstrate that Cdc5 also controls the levels of chromosome-bound cohesin in meiosis (Figure 54). Depletion of Cdc5 results in increased levels of Rec8 at chromosome arm sites. Previously it was shown that the overall cohesin level in meiotic prophase cells is higher than in meiotic metaphase I cells and that this reduction of cohesin from prophase to metaphase I is regulated by Cdc5 (Yu and Koshland, 2005). Our results confirm that cohesin is reduced by a Cdc5-dependent mechanism. Moreover, due to the high spatial resolution of our assay, we can contribute additional information and show that cohesin is specifically removed from chromosome arm sites in a Cdc5-dependent manner in budding yeast meiosis. Hence, for the first time, we provide robust evidence for a prophase-pathway-like removal of cohesin in budding yeast.

Furthermore, our finding that Cdc5 controls the levels of chromosome-bound cohesin in meiosis supports our model of a cohesin-dependent Sgo1 loading mechanism. If a cohesin-dependent mechanism loads Sgo1 onto chromosomes, one would expect that a higher amount of chromosome-bound cohesin recruits a higher amount of chromosome-bound Sgo1. We observe precisely this. Inactivation of Cdc5 causes an increase of chromosome-bound cohesin and consequently of Sgo1 (Figure 50, Figure 54). Inactivation of Cdc5 leads to an upregulation of cohesin, specifically on chromosome arms. Concomitant, we observe recruitment of Sgo1 to chromosome arms, which is something we never observed in any *CDC5* strain.

## 4. Material and Methods

### Yeast strains

All experiments were performed with the laboratory strain SK1 of *S. cerevisiae*. All strains were auxotrophic for histidine, leucine, tryptophan, and uracil, making it possible to use the respective auxotrophy-complementing genes as selective markers. The genotype of all strains was *ho::LYS2 his3::hisG leu2::hisG trp1::hisG ura3*. All diploid strains were homozygous for their respective alleles unless stated otherwise.

Construction of new strains was performed by the mating of the appropriate haploid strains, followed by sporulation, dissection of tetrads and selection on appropriate selection plates. Alternatively, new strains were obtained by transformation and selection for genomic integration of the transformed DNA.

The allele to deplete Cdc20 by expression of *CDC20* from the *CLB2* promoter was obtained from the Angelika Amon Lab, Massachusetts Institute of Technology, USA via the strain A5567. The allele to deplete Sgo1 by expression of *SGO1* from the *SCC1* promoter was obtained from the Kim Nasmyth Lab, Oxford University, UK via the strain K12298. The deletion allele of *RTS1* (*rts1Δ*) was obtained from the Kim Nasmyth Lab, Oxford University, UK via the strain K13088. The allele to deplete Cdc5 by expression of *CDC5* from the *SCC1* promoter was obtained from the Kim Nasmyth Lab, Oxford University, UK via the strain K10834 and it was previously described in Matos et al. (2008). The mutated allele of the *SCC4* cohesin loader subunit (*scc4-m35*) was obtained from the Kim Nasmyth Lab, Oxford University, UK via the strain K25036 and it was previously described in Hinshaw et al. (2015). The *REC8-AID* system was obtained from the Neil Hunter Lab, University of California, Davis, USA via the strains NHY6683 and NHY7649.

The *C. glabrata* wild-type strain was obtained from the National Collection of Yeast Cultures (NCYC), Norwich, UK, with the accession number NCYC 388, deposited by IFO, Japan, 1953.

## Plasmid construction

### *C. glabrata* tagging plasmid

We designed a series of tagging plasmids in silico, harboring the C-terminal part of the *C. glabrata* SCC1 gene, followed by a NheI-flanked epitope tag (Ha3, Myc9 or Pk9), a marker cassette conferring resistance to Nourseothricin (Goldstein and McCusker, 1999), and the terminator of the *CgSCC1* gene. The gene in the Nourseothricin resistance cassette is under control of the translation elongation factor 1 alpha (*TEF*) promoter, which is a constitutively active promoter, able to control gene expression in yeast. This whole tagging cassette is flanked by a XmnI site and MfeI site, respectively. Both restriction sites are unique in the tagging plasmid. As both restriction enzymes work well under identical reaction conditions, it is possible to separate the tagging construct from the vector backbone by a simple double digest reaction. Releasing the tagging construct from its vector backbone generates a linear fragment of 2949 bp, which is homologous to the C-terminal part of the *C. glabrata* SCC1 ORF and the SCC1 terminator, allowing for genomic integration at this specific locus. The construct was synthesized and ligated into a pMA-RQ vector backbone by Thermo Fisher Scientific GENEART, Regensburg, Germany.

## Yeast transformation

For transformation, approximately 2 µg transforming DNA, purified on a Qiagen PCR purification column or via sodium acetate/ethanol precipitation was used.

### *S. cerevisiae* transformation

The protocol was modified after the method by Ito et al. (1982). An overnight yeast culture was grown to OD 0.6-0.8. Cells were harvested by centrifugation at 4000 rpm for 5 min, washed twice with 0.5 volumes of 1 M LiAc-Sorbitol (D-Sorbitol, ≥ 98 %, Sigma-Aldrich, Merck, Darmstadt, Germany; Lithium acetate dihydrate 98 %, Sigma-Aldrich, Merck, Darmstadt, Germany) solution and resuspended in the rest of the LiAc-Sorbitol solution after discarding the supernatant. The transformation mixture comprises up to 20 µl of DNA, 15 µl of Salmon sperm DNA (Salmon Sperm DNA, sheared (Ambion, Thermofisher Scientific, Waltham, USA), which was heated to 95 °C and cooled in water-ice shortly before use, 100 µl of cell suspension and 280 µl of PEG 4000 solution (Carl

Roth GmbH, Karlsruhe, Germany). The transformation mixture was incubated at room temperature for 60 min, before addition of 40  $\mu$ L of DMSO (Sigma-Aldrich, Darmstadt, Germany) and another round of incubation for 15 min at 42 °C. After this, 1 ml of YPD was added. The cell suspension was spun down, the supernatant was discarded, and cells were plated on respective selection plates. For dominant markers, cells were incubated at 25 °C for 5 hours in YPD medium before plating on selection plates.

### ***C. glabrata* transformation**

A protocol modified after Gietz et al. (1992) was used. An overnight yeast culture was grown to OD 0.6-0.8. Cells were harvested by centrifugation at 4000 rpm for 5 min, washed once with an equal volume of sterile water. The cells were resuspended in 1/100 volume of 100 mM LiAc (pH 7.5). The transformation mixture comprises 50  $\mu$ L of cell suspension, 240  $\mu$ L of 50% PEG (3500), 36  $\mu$ L of 1 M LiAc, 50  $\mu$ g of heat-denatured salmon sperm DNA and transforming DNA. The transformation mixture was then incubated at 30 °C for 30 min, followed by addition of 45  $\mu$ L DMSO and incubation at 42 °C for 15 min. The cell suspension was spun down, the supernatant was discarded, and cells were plated on respective selection plates. For dominant markers, cells were incubated at 25 °C for 5 hours in YPD medium before plating on selection plates.

### **Culture media**

The basis of most culture media is a mixture of 1 % yeast extract and 2 % bacto peptone (YP), as described in Sherman (1991). For a mitotic yeast culture, YP medium containing 2 % D-Glucose and 0,005 % Adenine (YPD) was used. For induction of meiosis, YP medium containing 2 % potassium acetate (YEPA) was used. Sporulation medium (SPO) contains 100 mM sodium acetate, 25 mM potassium chloride, 3 mM magnesium sulfate and 20 mM sodium chloride (all from VWR Chemicals, Leuven, Belgium). For the corresponding culture plates, the media were additionally supplemented with 2 % bacto agar. For selection plates for dominant marker cassettes kanMX, natMX or hphMX (Goldstein and McCusker, 1999; Wach et al., 1994), YPD plates were supplemented with 100  $\mu$ g/ml G418 (Kan), 200  $\mu$ g/ml CLONAT (Nat) or 500  $\mu$ g/ml hygromycin B (Hph), respectively. Media and all described buffers were mixed, using purified water from a

Milli-Q Advantage A10 machine (Merck, Darmstadt, Germany). For all media and buffers, the pH was measured with a Mettler Toledo Seven Compact machine.

### **Induction of meiosis**

Meiosis was induced as described previously (Oelschlaegel et al., 2005). Briefly, haploid cells were grown on a YPG plate, to enrich for cells with functional mitochondria. On the second day, haploids were mated and grown o/n. On the third day, the mating mixture was streaked to single colonies on a YPG plate and grown for 48 h at 25 °C. On day five, single-colonies were picked and streaked into a patch on a YPD plate and grown for another 23 h. On day six, diploid cells were repeatedly spread to a YPD plate until the cells formed a cellular monolayer. Subsequently, the cells were grown for 23 h to produce an even lawn. This step results in a physiological synchronization of the cells. On day seven, cells were inoculated in liquid YPG medium at an OD of 0.3 and grown for 12 h at 30 °C. This leads to a transient G1 arrest. On day eight, the cells were washed with SPO medium and inoculated to liquid SPO medium at a final OD<sub>600</sub> of 6.0. The cell density was measured with a spectrophotometer, after sonication of the samples with a Sonoplus sonicator. For a metaphase arrest, samples were grown for 8 h after inoculation to liquid SPO (unless stated otherwise). For a synchronous meiotic time course, using the CDC20-mAR system, samples were taken every 20 minutes or every 10 minutes after the release into anaphase I. For expression of *CDC20* to release the cells into anaphase I in the *CDC20-mAR* system, 10 µM CuSO<sub>4</sub> (Merck, Darmstadt, Germany) were added.

For inhibition of analog-sensitive kinases, the PP1 analog NM-PP1 (Cayman Chemical, Michigan, USA) was used (Bishop et al., 2000) at a final concentration of 5 µM.

For targeted protein degradation by the auxin-inducible degron system (Nishimura et al., 2009), 10 µM CuSO<sub>4</sub> was used to induce the OsTir1 SCF ligase subunit, followed by addition of a final concentration of 2 mM indole acetic acid (IAA) (Tokio Chemical Industry, Tokyo, Japan) dissolved in DMSO 30 minutes later.

### **Fixed-cell immunofluorescence**

Microscopy samples were prepared as described in Salah and Nasmyth (2000). Briefly, cells were fixed in formaldehyde (final concentration 3 % (v/v)) overnight and washed three times with KPi buffer (0.1 M potassium phosphate [Potassium dihydrogen phosphate and dipotassium hydrogen phosphate, Carl Roth GmbH, Karlsruhe, Germany] pH 6.4) and once with spheroplasting buffer (0.1 M KPi pH 7.4, 1.2 M sorbitol, 0.5 mM MgCl<sub>2</sub> [Magnesium chloride hexahydrate, Merck, Darmstadt, Germany]) the next morning. The yeast cell wall was digested by addition of 6 µl 1 M DTT (Thermo Scientific, Waltham, USA) and 20 µl of Zymolyase (1 mg/ml) (Zymolyase T100, AMS Biotechnology, Abingdon, UK). Time of incubation was determined by regular visual inspection of the cells under a DIC light microscope. Spheroplasts were loaded on a microscope glass slide, which was pre-treated by 0.1 % Poly-L-Lysine solution (Merck, Darmstadt, Germany), to adhere them to the glass surface. Samples were then blocked by addition of 5 µl PBS-BSA (0.04 M K<sub>2</sub>HPO<sub>4</sub> (Carl Roth GmbH, Karlsruhe, Germany), 0.01 M KH<sub>2</sub>PO<sub>4</sub> (Carl Roth GmbH, Karlsruhe, Germany), 0.15 M NaCl, 0.1 % NaN<sub>3</sub>, 1 % BSA [Jackson ImmunoResearch, West Grove, USA]) per sample for 30 minutes. Following this, the samples were stained with the respective primary antibodies, which were incubated for 1 hour, followed by 3 washing steps with PBS-BSA and subsequent staining with the corresponding secondary antibody, followed by another four washing steps. Finally, the samples were submerged in a DAPI containing solution (100 mg p-phenylenediamine [Merck, Darmstadt, Germany] + 10 ml PBS, pH 8.0 were added to 90 ml of glycerol [VWR Chemicals, Leuven, Belgium] and DAPI [(Molecular Probes, Eugene, USA)] at 0.05 µg/ml) and slides were sealed by a coverslip and nail polish. Samples were analyzed on a fluorescence microscope Axioskop 2 (Carl Zeiss AG, Oberkochen, Germany).

### **Live-cell imaging**

Live-cell imaging of meiotic cells was performed as described previously (Okaz et al., 2012). Briefly, cells were induced to enter meiosis and diluted to OD<sub>600</sub> using SPO medium. Aliquots of 300 µl were loaded into 8-well Lab-Tek chamber slides (Nunc, 155409) coated with Concanavalin A (Sigma C5275, 0.5 mg/ml in PBS). The imaging system was a DeltaVision Elite system controlled by the SoftWoRx software, version 5.0

and equipped with an environmental chamber for temperature control. Optical components comprised a microscope (Olympus IX71), InsightSSI solid-state illumination system, objective (Olympus UPlanSApo 100X/1.4 NA), and a CCD camera (Photometrics CoolSnap HQ2). Imaging acquisition was performed every 10 minutes over a total time frame of 12 hours. The red and green channel was used for imaging. The filter was a 12 % neutral density filter (TrueLight Additional ND filter, ND090-37 12 %T, Lumencor). Exposure times were 50-300 ms, depending on the fluorescence intensity of the samples. For each time point, 8 optical sections in the z-direction with a distance of 1  $\mu\text{m}$  were acquired, deconvolved, and projected to a single 2D-image. Post-acquisition data processing was performed using the ImageJ software (Rasband, W.S., ImageJ, U.S. National Institutes of Health, Bethesda, MD, <http://imagej.nih.gov/ij/>). For quantification, 100 cells were followed individually through meiosis, and the optical markers were scored. Finally, representative cells were selected, and images were assembled by merging data from different optical channels, using the ImageJ Stack Combiner plugin.

### **Western blotting**

Proteins were analyzed by dissolving 5 to 10 ml of meiotic yeast culture at a final concentration of 10 % in trichloroacetic acid (TCA) (Merck, Darmstadt, Germany). The cell extracts were spun-down, resuspended again in 10 % TCA and broken, using glass beads on a vibrax machine. The cell extract was resuspended in 0.2 ml 1 X Laemmli sample buffer and 0.1 ml Tris (Merck, Darmstadt, Germany) was added. After boiling the samples for 10 min, the protein concentration was determined using a Bradford assay (Protein Assay Dye Reagent Concentrate, Bio-Rad, Munich, Germany) and 50-200  $\mu\text{g}$  protein were loaded on an 8 % SDS polyacrylamide gel and the gel was run o/n at a low voltage. For the preparation of the western blot, a PVDF membrane, which is very hydrophobic, was treated with methanol (Fisher Scientific, Leics, UK) for a few minutes. Subsequently, the membrane was washed with water and transferred to blotting buffer (3 g Tris base, 14,4 g glycine and 1 ml of 20 % SDS [Serva, Heidelberg, Germany] per 1 liter). The western-blot was assembled by putting the PAGE gel between 4 sheets of blotting paper on both sides. The blot was run for 2-3 hours at 0.8 mA per square cm. Subsequently, the blot was stained using appropriate antibodies.

## Chromatin immunoprecipitation

A standard meiotic time course was performed, as described under “Induction of meiosis”. Sampling volume was 10 ml to 60 ml, depending on the ChIP target. Samples were fixed in formaldehyde (formaldehyde 16 % (w/v), methanol-free, Thermo Scientific, Waltham, USA) at a final concentration of 3 % (v/v) for 22 minutes and washed twice, using ice-cold KPi buffer (0.1 M potassium phosphate pH 6.4), followed by a final wash in spheroplasting buffer (0.1 M KPi pH 7.4, 1.2 M sorbitol, 0.5 mM MgCl<sub>2</sub>). The supernatant was removed and samples stored at -80 °C. The sample was thawed on ice and resuspended in 1 ml spheroplasting buffer containing 1 mM PMSF (AppliChem, Darmstadt, Germany). Pre-fixed *C. glabrata* samples were added to the *S. cerevisiae* samples. 25 µl 1M DTT was added and samples were incubated for 15 min/25 °C, followed by addition of 90 µl zymolyase (1 mg/ml) and incubation for 10 min/35 °C. Samples were washed once in spheroplasting buffer containing 1 mM PMSF and 5 mM EDTA (Sigma-Aldrich, Merck, Darmstadt, Germany) to remove DTT and zymolyase and stored on ice. Subsequently, samples were washed once in rinsing buffer (10mM HEPES-KOH (pH 7.55) [Acros Organics, New Jersey, USA]) and resuspended in shearing buffer (10 mM HEPES-KOH pH 7.5, 1 mM EDTA, 1 % Triton X-100 [Serva, Heidelberg, Germany], 0.1 % Na Deoxycholate [Merck, Darmstadt, Germany]), containing 1X cOmplete Protease inhibitor cocktail tablets (Roche Diagnostics, Mannheim, Germany) and 1X Halt Protease Inhibitor Cocktail (Halt Thermofisher Scientific, Waltham, USA). Following this, samples were loaded into a Covaris Millitube (Millitube, 1 ml, Covaris, Woburn, USA) and sonicated on a Covaris E220 for 30 minutes/140 watts/17 % duty factor. Water temperature limits were set to 3 °C-8 °C; the water level was 5. 10X Shearing-to-IP buffer (410 mM HEPES-KOH pH 7.5, 1 mM EDTA, 1 % Triton X-100, 0.1 % Na Deoxycholate, 1.4 M NaCl) was added to the samples to a final concentration of 1X. Samples were cleaned from cell debris and emulsified components by spinning-down at 14000 rpm/5 min/4 °C and transfer of the clean middle part of the supernatant to a new tube. The protein concentration in the samples was determined by a Bradford assay, measured on a spectrophotometer. Samples were adjusted to the same protein concentration using IP buffer (50 mM HEPES-KOH pH 7.5, 1 mM EDTA, 1 % Triton X-100, 0.1 % Na Deoxycholate, 140 mM NaCl) containing 1X cOmplete Protease inhibitor cocktail tablets and 1X Halt Protease Inhibitor Cocktail. The samples were pre-cleared by incubation with 300 µl washed dynabeads Protein A (Novex, Life Technologies, Oslo,

Norway) for 1 h/4 °C. 50 µl of the pre-cleared samples were transferred to a fresh tube and stored as Whole cell extract sample at 4 °C. The respective amount of affinity purified antibody (7 µg 3F10) was added to the remaining samples for 2 h/4 °C. Immunoprecipitation was performed by addition of 100 µl dynabeads protein A, which were blocked for 30 minutes using IP buffer containing BSA (10 mg/ml), and incubation overnight at 4 °C. The next day, samples were washed once with a series of buffers: 1) IP buffer, 2) IP buffer containing 500 mM NaCl, 3) washing buffer (10 mM Tris-HCl pH 8.0, 0.5 % Na Deoxycholate, 1 mM EDTA, 250 mM LiCl [VWR Chemicals, Leuven, Belgium]), 4) TE buffer (10 mM Tris-HCl pH 8.0, 1 mM EDTA), 5) TES buffer (50 mM Tris-HCl pH 8.0, 10 mM EDTA, 1 % SDS) and incubated at 65 °C/8h-o/n to reverse the crosslinks. For purification, 6 µl of RNase A (RNase A from bovine pancreas, Merck, Darmstadt, Germany) (10 mg/ml) was added 1h/37 °C, followed by 15 µl of Proteinase K (Merck, Darmstadt, Germany) (20 mg/ml) 2 h/65 °C. After this, 10 µl Na Acetate (Merck, Darmstadt, Germany, 3M, pH 5.2) was added, and samples were loaded onto a PCR purification column (QIAquick PCR Purification Kit, Qiagen, Hilden, Germany). Samples were washed with the kit's washing buffer and eluted with the kit's elution buffer in a final volume of 50 µl. Samples were stored at -80 °C. Sample concentrations were determined fluorometrically (Qubit 3.0, Thermofisher Scientific, Waltham, USA).

## qPCR

IP samples were diluted 1:50 in sterile, PCR-grade water. WCE samples were diluted 1:250. For the primer-master mix, qPCR primers were added at a final concentration of 1.7 µM to the 2X SYBR green master mix (2X Power SYBR Green PCR Master Mix, Life Technologies, Warrington, UK), which was added at a final concentration of 1X. 15 µl of the primer-master mix was added to 10 µl of IP or WCE sample per well of a 96-well reaction plate (MicroAmp Fast Optical 96-Well Reaction Plate, Applied Biosystems, Thermofisher Scientific, Waltham, USA). A non-template control water sample was added to the plate. For each measurement a 1:4 dilution series was included as a standard for quantification of the result. Every measurement was carried out in duplicates, so each sample was loaded twice on the plate. For each sample, the mean of the two duplicates was calculated. All pipetting was performed using sterile tips. After loading of the samples, the reaction plate was sealed with an optical adhesive film, briefly spun-down

and mixed by using a plate mixer. The qPCR reaction was carried out on a StepOne Plus real-time PCR system (Applied Biosystems, ThermoFisher Scientific, Waltham, USA). For quality control of each run, a melt curve analysis was performed afterward. Additional quality control parameters were the coefficient of determination of the linear regression of the standard curve and the efficiency of the PCR reaction. Measurements with an efficiency < 95 % or > 105 % were discarded.

Table 4: qPCR primers.

Name	Primer type	Primer sequence	Chr	Chromosomal region	Organism	Ref
Arm cohesin low	Forward	GCCAAATCAAAC AAGGTCAC	VI	HXT10	<i>S. cerevisiae</i>	
	Reverse	TTGCAGTGA CTGG ATAACGA			<i>S. cerevisiae</i>	
Arm cohesin peak	Forward	CGTAACGCAGGG TTTAGAGG	VI	MET10- SMC2	<i>S. cerevisiae</i>	Gruber et al., (2006)
	Reverse	ATACATAGGCGC TGGTCGAA			<i>S. cerevisiae</i>	Gruber et al., (2006)
Pericentromeric cohesin	Forward	GTAGGCAAGATC CAAAGAAGCAC	VI	RPN11- SAD1	<i>S. cerevisiae</i>	
	Reverse	TTAATTGCCACTG AATTAACACCCG			<i>S. cerevisiae</i>	
Centromeric cohesin	Forward	ACGAACTTAAGG CCGCAGTA	VI	CEN6	<i>S. cerevisiae</i>	Gruber et al., (2006)
	Reverse	CTTCGACAGGTTC CATAACG			<i>S. cerevisiae</i>	Gruber et al., (2006)
Scc1 site	Forward	CTCAACAAAGTT GCCTAACTCG	I	CEN0a+13 kbp	<i>C. glabrata</i>	
	Reverse	CCGATCATGAAA GCAGAGTG	I		<i>C. glabrata</i>	

After passing the quality control, the IP / WCE enrichment was calculated by correcting the mean of the measured duplicates for the dilution factor and the volume of the IP or WCE sample, respectively, and calculation of the ratio. qPCR primers for a new locus

were established by testing a minimum of 4 primer combinations, using a standard dilution series with seven different concentrations. To be considered a suitable primer pair for qPCR the following criteria had to be met: PCR efficiency > 95 % and < 105 %, R<sup>2</sup> > 99 %. The melt curve must show only one distinct peak. No amplification must occur in the NTC, which could otherwise indicate self-priming.

### **Next-generation sequencing**

The sequencing library preparation was performed, using the Ovation Ultralow Library Systems Kit, NuGEN, San Carlos, USA. Sequencing was performed either on an Illumina HiSeq3000 platform, generating eight million reads per sample, with a read length of 150 bp, using a single-end protocol or on an Ion Proton System. Library preparation and sequencing was performed by the Max Planck Genome Center Cologne or by the Kim Nasmyth Group, Department of Biochemistry, Oxford University.

### **Bioinformatics**

#### **Short-read mapping**

Mapping of short reads obtained by sequencing of the ChIP-Seq libraries was performed using the web-based platform Galaxy (<https://usegalaxy.org/>). First, the quality control was performed, using the module FastQC. Subsequently, the alignment of the reads to the reference genomes was performed using the short-read aligner module Bowtie2. The *C. glabrata* genome was retrieved using the Candida genome database (<http://www.candidagenome.org/>). Mapping was performed in two rounds. First, all reads were mapped against the calibration and the experimental genome, whereas all unassigned reads were saved in a separate file. These unaligned reads were mapped in a second round against the other genome, generating a set of mapped reads, which are unique for the respective genome. The statistics of these mapping procedures were used to subsequently calibrated the obtained profiles. The retrieved SAM files were converted to Bam files using the module SAMTools. The ChIP-Seq profiles were visualized using the Integrated Genome Browser (IGB) (<http://bioviz.org/igb/>) (Freese et al., 2016).

### Calibration of ChIP-Seq profiles

The calibration of ChIP-Seq profiles was performed as described in Hu et al. (2015). Briefly, the occupancy ratio ( $OR_i$ ) is calculated as  $OR_i = (W_{Ci} * IP_{Xi}) / (W_{Xi} * IP_{Ci})$ , whereas  $W_{Ci}$  denotes the number of reads unique to the calibration genome in sample  $i$ ,  $W_{Xi}$  denotes the number of reads unique to the experimental genome in sample  $i$ ,  $IP_{Xi}$  denotes the number of reads assigned to the experimental genome in the IP fraction of sample  $i$  and  $IP_{Ci}$  denotes the number of reads assigned to the calibration genome in the IP fraction of sample  $i$ .  $OR_i$  is dimensionless and can be used to calculate the coefficient for calibration of the ChIP-Seq profiles. The coefficient is calculated by dividing the  $OR_i$  by the number of unique reads assigned to the experimental genome of sample  $i$ , followed by multiplication with the density data associated with each base.

### calChIP-Seq quantification

For quantification, we converted the calibrated ChIP-Seq data into text files containing the signal intensity for each base pair. We did this for all samples and all chromosomes. We then summed-up the signal intensity of all base pairs comprising the region of interest in the respective control sample, experimental sample, and untagged sample. This step is identical to integrating the ChIP-Seq profiles over the region of interest. Next, the signal sum of the region of interest of the control and experimental samples were subtracted from the signal sum of the same region in the untagged sample, to correct for artificial signal enrichment. Finally, we normalized the signal sum of each data point (each region of interest in each time point and each chromosome) to the highest signal value in the respective data set, to make the data comparable to other experimental data.

### Antibodies

Table 5: *Antibodies.*

<b>Indirect-immunofluorescence</b>	
Primary antibodies	
Anti-Tub1, rat, monoclonal, MCA78S (spindles)	Bio-Rad AbD Serotec, Munich, Germany
Anti-Tub4-C-6, rabbit, polyclonal (spindle pole bodies) (Matos et al., 2008)	Zachariae Lab

Anti-Human influenza hemagglutinin (HA), mouse, monoclonal, 12CA5	Zachariae Lab
Anti-c-myc, mouse, monoclonal, 9E10	Zachariae Lab
Secondary antibodies	
Alexa-Fluor 488 donkey anti-rat IgG, 2 mg/ml	Life technologies, Eugene, USA
Alexa-Fluor 488 goat anti-rabbit IgG, 2 mg/ml	Life technologies, Eugene, USA
Goat pAb to Ms IgG Cy3, 0.5 mg/ml	Abcam, Cambridge, UK
Goat pAb to Ms IgG Cy5, 0.5 mg/ml	Abcam, Cambridge, UK
<b>ChIP</b>	
Anti-Human influenza hemagglutinin (HA), rat, monoclonal, 3F10	Roche Diagnostics, Mannheim, Germany
Anti-Human influenza hemagglutinin (HA), mouse, monoclonal, 12CA5	Zachariae Lab
Anti-c-myc, mouse, monoclonal, 9E11	Zachariae Lab
Anti V5-Tag, mouse, monoclonal, MCA1360G	Bio-Rad AbD Serotec, Munich, Germany
<b>Western blotting</b>	
Anti-Rec8 serum, rabbit polyclonal, rabbit SA 4958 (Petronczki et al., 2006)	Zachariae Lab
Anti-Pgk1 mouse monoclonal, 1 mg/ml	Invitrogen, Carlsbad, USA
Anti-Dbf4-C rabbit polyclonal, rabbit C92C (Matos et al., 2008)	Zachariae Lab

## List of strains

Strain    Relevant genotype

21931 *MATa/MATalpha nap1::KanMx4 vps75::KanMx4 his3::HIS3p-GFP-TUB1-HIS3 leu2::URA3p-tetR-tdTomato::LEU2 ura3/ura3::tetOx224-URA3*

21937 *MATa/MATalpha his3::HIS3p-GFP-TUB1-HIS3 leu2::URA3p-tetR-tdTomato::LEU2 ura3/ura3::tetOx224-URA3*

25601 *MATa/MATalpha cdc20::CLB2p-CDC20::HphMX4 ura3:CUP1p-CDC20-URA3 HRR25-HIS3::hrr25-KanMX4 REC8ha3-LEU2::rec8::KanMX4*

29040 *MATa/MATalpha cdc20::CLB2p-CDC20::HphMX6 trp1::CUP1p-CDC20-TRP1 REC8ha3-URA3*

- 29041 *MATa/MATalpha cdc20::CLB2p-CDC20::HphMX6 trp1::CUP1p-CDC20-TRP1 sgo1::SCC1p-SGO1-KanMX4 REC8ha3-URA3*
- 29042 *MATa/MATalpha cdc20::CLB2p-CDC20::HphMX6 trp1::CUP1p-CDC20-TRP1*
- 29398 *MATa/MATalpha cdc20::CLB2p-CDC20::HphMX6 trp1::CUP1p-CDC20-TRP1 REC8ha3-URA3*
- 29399 *MATa/MATalpha cdc20::CLB2p-CDC20::HphMX6 trp1::CUP1p-CDC20-TRP1*
- 29565 *MATa/MATalpha SGO1ha3::KITRPI cdc20::CLB2p-CDC20::HphMX4 trp1::CUP1p-CDC20-TRP1*
- 30038 *MATa/MATalpha spo11::HIS3MX6 SGO1ha3::KITRPI cdc20::CLB2p-CDC20::HphMX4*
- 30040 *MATa/MATalpha rec8::KanMX4 spo11::HIS3MX6 SGO1ha3::KITRPI cdc20::CLB2p-CDC20::HphMX4*
- 30041 *MATa/MATalpha rec8::KanMX4 spo11::HIS3MX6 cdc20::CLB2p-CDC20::HphMX4*
- 30268 *MATa/MATalpha SGO1ha3::KITRPI cdc20::CLB2p-CDC20::HphMX4*
- 30270 *MATa/MATalpha SGO1ha3::KITRPI cdc5::SCC1p-CDC5-KanMX4 cdc20::CLB2p-CDC20::HphMX4*
- 30274 *MATa/MATalpha cdc20::CLB2p-CDC20::HphMX4*
- 30275 *MATa/MATalpha SGO1ha3::KITRPI rts1::NatMX4 cdc20::CLB2p-CDC20::HphMX4*
- 30276 *MATa/MATalpha SGO1ha3::KITRPI cdc5::SCC1p-CDC5-KanMX4 rts1::NatMX4 cdc20::CLB2p-CDC20::HphMX4*
- 30543 *MATa/MATalpha cdc20::CLB2p-CDC20::HphMX4 ura3::CUP1p-CDC20-URA3 Hrr25-HIS3::hrr25-KanMX4 REC8ha3-LEU2::rec8::KanMX4*
- 30544 *MATa/MATalpha cdc20::CLB2p-CDC20::HphMX4 ura3::CUP1p-CDC20-URA3 hrr25-as-HIS3::hrr25-KanMX4 REC8ha3-LEU2::rec8::KanMX4*

- 30545 *MATa/MATalpha cdc20::CLB2p-CDC20::HphMX4 ura3:CUP1p-CDC20-URA3 HRR25-HIS3::hrr25-KanMX4*
- 30904 *MATa/MATalpha SGO1ha3::KITRP1 cdc20::CLB2p-CDC20::HphMX4*
- 30905 *MATa/MATalpha spo11::HIS3MX6 SGO1ha3::KITRP1 cdc20::CLB2p-CDC20::HphMX4*
- 30906 *MATa/MATalpha SGO1ha3::KITRP1 bub1Δ::KIURA3 cdc20::CLB2p-CDC20::HphMX4*
- 30909 *MATa/MATalpha SGO1ha3::KITRP1 bub1Δ::KIURA3 cdc20::CLB2p-CDC20::HphMX4 rec8::KanMX4 spo11::HIS3MX6*
- 30910 *MATa/MATalpha cdc20::CLB2p-CDC20::HphMX4*
- 31309 *MATa/MATalpha cdc20::CLB2p-CDC20::KanMX6 REC8ha3-URA3*
- 31311 *MATa/MATalpha REC8ha3-URA3 cdc20::CLB2p-CDC20::KanMX6 cdc5::SCC1p-CDC5-KanMX4*
- 31313 *MATa/MATalpha spo11::HIS3MX6 SGO1ha3::KITRP1 cdc20::CLB2p-CDC20::HphMX4*
- 31314 *MATa/MATalpha spo11::HIS3MX6 SGO1ha3::KITRP1 cdc20::CLB2p-CDC20::HphMX4 scc4m35-HIS3*
- 31316 *MATa/MATalpha spo11::HIS3MX6 cdc20::CLB2p-CDC20::HphMX4*
- 32338 *MATa/MATspha Rec8-AID-9myc::HygroNT cdc20::CLB2p-CDC20::KanMX6 spo11::HIS3MX6 SGO1ha3::KITRP1*
- 32339 *MATa/MATalpha pCUP1-1-OsTIR1-9Myc-URA3 Rec8-AID-9myc::HygroNT cdc20::CLB2p-CDC20::KanMX6 spo11::HIS3MX6 SGO1ha3::KITRP1*
- 32340 *MATa/MATalpha Rec8-AID-9myc::HygroNT cdc20::CLB2p-CDC20::KanMX6 spo11::HIS3MX6*

## 5. Contributions

Several experiments presented in this thesis were performed with the help of other members of the Zachariae lab or in collaboration with the Kim Nasmyth Lab, Oxford University, UK. I would like to thank all the people involved and list their contributions.

Oleksi Lysak, Zachariae Lab, MPI of Biochemistry, Martinsried helped to perform the experiment shown in Figure 42, by preparing TCA extracts and running the western-blot.

Dr. Naomi Petela, Kim Nasmyth Lab, Oxford University, UK, performed the sequencing library preparation, operated the sequencer and mapped the obtained reads for the experiments presented in .Figure 17, Figure 23, Figure 36, Figure 45, Figure 49, Figure 50, Figure 51.

## 6. Acknowledgements

Many thanks to my supervisor, Dr. Wolfgang Zachariae, for accepting me as PhD Student in his lab and for supervising my work.

I would like to thank Prof. Dr. Marc Bramkamp for taking the effort of being the first referee and Prof. Dr. Peter Becker for being the co-referee of this work.

I would like to express my sincere gratitude to Prof. Dr. Marc Bramkamp, Prof. Dr. Stephan Gruber and Dr. Franz Herzog for being members of my Thesis Advisory Committee and for their advice and guidance.

Thanks to all other members of the Zachariae lab and all collaborators. My special thanks go to Dr. Naomi Petela, Kim Nasmyth Lab, Oxford University.

Many thanks to Dr. Assa Yeroslaviz of the MPI Core Facility, who was indispensable for setting-up the calibrated ChIP-Seq workflow.

Last but not least, I would like to express my special gratitude to Isabella Mathes, our lab technician, who was always very helpful and very dedicated to her work.

## 7. References

- Bausch, C., Noone, S., Henry, J.M., Gaudenz, K., Sanderson, B., Seidel, C., and Gerton, J.L. (2007). Transcription Alters Chromosomal Locations of Cohesin in *Saccharomyces cerevisiae*. *Mol. Cell. Biol.* *27*, 8522–8532.
- Bergerat, A., Massy, B. de, Gadelle, D., Varoutas, P.-C., Nicolas, A., and Forterre, P. (1997). An atypical topoisomerase II from archaea with implications for meiotic recombination. *Nature* *386*, 414.
- Berod, A., Hartman, B.K., and Pujol, J.F. (1981). Importance of fixation in immunohistochemistry: use of formaldehyde solutions at variable pH for the localization of tyrosine hydroxylase. *J. Histochem. Cytochem.* *29*, 844–850.
- Bishop, A.C., Ubersax, J.A., Petsch, D.T., Matheos, D.P., Gray, N.S., Blethrow, J., Shimizu, E., Tsien, J.Z., Schultz, P.G., Rose, M.D., et al. (2000). A chemical switch for inhibitor-sensitive alleles of any protein kinase. *Nature* *407*, 395–401.
- Blat, Y., and Kleckner, N. (1999). Cohesins Bind to Preferential Sites along Yeast Chromosome III, with Differential Regulation along Arms versus the Centric Region. *Cell* *98*, 249–259.
- Borrie, M.S., Campor, J.S., Joshi, H., and Gartenberg, M.R. (2017). Binding, sliding, and function of cohesin during transcriptional activation. *PNAS* *114*, E1062–E1071.
- Bortz, P.D.S., and Wamhoff, B.R. (2011). Chromatin Immunoprecipitation (ChIP): Revisiting the Efficacy of Sample Preparation, Sonication, Quantification of Sheared DNA, and Analysis via PCR. *PLOS ONE* *6*, e26015.
- Brar, G.A., Kiburz, B.M., Zhang, Y., Kim, J.-E., White, F., and Amon, A. (2006). Rec8 phosphorylation and recombination promote the step-wise loss of cohesins in meiosis. *Nature* *441*, nature04794.
- Buonomo, S.B.C., Clyne, R.K., Fuchs, J., Loidl, J., Uhlmann, F., and Nasmyth, K. (2000). Disjunction of Homologous Chromosomes in Meiosis I Depends on Proteolytic Cleavage of the Meiotic Cohesin Rec8 by Separin. *Cell* *103*, 387–398.
- Buonomo, S.B.C., Rabitsch, K.P., Fuchs, J., Gruber, S., Sullivan, M., Uhlmann, F., Petronczki, M., Tóth, A., and Nasmyth, K. (2003). Division of the Nucleolus and Its

- Release of CDC14 during Anaphase of Meiosis I Depends on Separase, SPO12, and SLK19. *Developmental Cell* 4, 727–739.
- Chambon, J.-P., Touati, S.A., Berneau, S., Cladière, D., Hebras, C., Groeme, R., McDougall, A., and Wassmann, K. (2013). The PP2A Inhibitor I2PP2A Is Essential for Sister Chromatid Segregation in Oocyte Meiosis II. *Current Biology* 23, 485–490.
- Chiang, T., Duncan, F.E., Schindler, K., Schultz, R.M., and Lampson, M.A. (2010). Evidence that Weakened Centromere Cohesion Is a Leading Cause of Age-Related Aneuploidy in Oocytes. *Current Biology* 20, 1522–1528.
- Chu, S., DeRisi, J., Eisen, M., Mulholland, J., Botstein, D., Brown, P.O., and Herskowitz, I. (1998). The transcriptional program of sporulation in budding yeast. *Science* 282, 699–705.
- Ciosk, R., Shirayama, M., Shevchenko, A., Tanaka, T., Toth, A., Shevchenko, A., and Nasmyth, K. (2000). Cohesin's Binding to Chromosomes Depends on a Separate Complex Consisting of Scc2 and Scc4 Proteins. *Molecular Cell* 5, 243–254.
- Clarke, A.S., Tang, T.T.-L., Ooi, D.L.-Y., and Orr-Weaver, T.L. (2005). POLO Kinase Regulates the *Drosophila* Centromere Cohesion Protein MEI-S332. *Developmental Cell* 8, 53–64.
- Clift, D., and Marston, A.L. (2011). The Role of Shugoshin in Meiotic Chromosome Segregation. *Cytogenet Genome Res* 133, 234–242.
- Darwiche, N., Freeman, L.A., and Strunnikov, A. (1999). Characterization of the components of the putative mammalian sister chromatid cohesion complex. *Gene* 233, 39–47.
- Dobie, K.W., Kennedy, C.D., Velasco, V.M., McGrath, T.L., Weko, J., Patterson, R.W., and Karpen, G.H. (2001). Identification of Chromosome Inheritance Modifiers in *Drosophila melanogaster*. *Genetics* 157, 1623–1637.
- Freese, N.H., Norris, D.C., and Loraine, A.E. (2016). Integrated genome browser: visual analytics platform for genomics. *Bioinformatics* 32, 2089–2095.
- Gandhi, R., Gillespie, P.J., and Hirano, T. (2006). Human Wapl Is a Cohesin-Binding Protein that Promotes Sister-Chromatid Resolution in Mitotic Prophase. *Current Biology* 16, 2406–2417.

- Gietz, D., St Jean, A., Woods, R.A., and Schiestl, R.H. (1992). Improved method for high efficiency transformation of intact yeast cells. *Nucleic Acids Res* 20, 1425.
- Gillespie, P.J., and Hirano, T. (2004). Scc2 Couples Replication Licensing to Sister Chromatid Cohesion in *Xenopus* Egg Extracts. *Current Biology* 14, 1598–1603.
- Goldstein, A.L., and McCusker, J.H. (1999). Three new dominant drug resistance cassettes for gene disruption in *Saccharomyces cerevisiae*. *Yeast* 15, 1541–1553.
- Gómez, R., Valdeolmillos, A., Parra, M.T., Viera, A., Carreiro, C., Roncal, F., Rufas, J.S., Barbero, J.L., and Suja, J.A. (2007). Mammalian SGO2 appears at the inner centromere domain and redistributes depending on tension across centromeres during meiosis II and mitosis. *EMBO Rep* 8, 173–180.
- Grömping, U. (2014). R Package FrF2 for Creating and Analyzing Fractional Factorial 2-Level Designs. *Journal of Statistical Software*; Vol 56 (2014).
- Gruber, S., Haering, C.H., and Nasmyth, K. (2003). Chromosomal Cohesin Forms a Ring. *Cell* 112, 765–777.
- Gruber, S., Arumugam, P., Katou, Y., Kuglitsch, D., Helmhart, W., Shirahige, K., and Nasmyth, K. (2006). Evidence that Loading of Cohesin Onto Chromosomes Involves Opening of Its SMC Hinge. *Cell* 127, 523–537.
- Guacci, V., Koshland, D., and Strunnikov, A. (1997). A Direct Link between Sister Chromatid Cohesion and Chromosome Condensation Revealed through the Analysis of MCD1 in *S. cerevisiae*. *Cell* 91, 47–57.
- Gullerova, M., and Proudfoot, N.J. (2008). Cohesin Complex Promotes Transcriptional Termination between Convergent Genes in *S. pombe*. *Cell* 132, 983–995.
- Haering, C.H., and Gruber, S. (2016). SnapShot: SMC Protein Complexes Part I. *Cell* 164, 326-326.e1.
- Haering, C.H., Löwe, J., Hochwagen, A., and Nasmyth, K. (2002). Molecular Architecture of SMC Proteins and the Yeast Cohesin Complex. *Molecular Cell* 9, 773–788.
- Haering, C.H., Farcas, A.-M., Arumugam, P., Metson, J., and Nasmyth, K. (2008). The cohesin ring concatenates sister DNA molecules. *Nature* 454, nature07098.

- Hamant, O., Golubovskaya, I., Meeley, R., Fiume, E., Timofejeva, L., Schleiffer, A., Nasmyth, K., and Cande, W.Z. (2005). A REC8-Dependent Plant Shugoshin Is Required for Maintenance of Centromeric Cohesion during Meiosis and Has No Mitotic Functions. *Current Biology* *15*, 948–954.
- Head, S.R., Komori, H.K., LaMere, S.A., Whisenant, T., Van Nieuwerburgh, F., Salomon, D.R., and Ordoukhanian, P. (2014). Library construction for next-generation sequencing: Overviews and challenges. *Biotechniques* *56*, 61-passim.
- Herbert, M., Kalleas, D., Cooney, D., Lamb, M., and Lister, L. (2015). Meiosis and Maternal Aging: Insights from Aneuploid Oocytes and Trisomy Births. *Cold Spring Harb Perspect Biol* *7*.
- Hinshaw, S.M., Makrantonis, V., Kerr, A., Marston, A.L., and Harrison, S.C. (2015). Structural evidence for Scc4-dependent localization of cohesin loading. *ELife* *4*, e06057.
- Hinshaw, S.M., Makrantonis, V., Harrison, S.C., and Marston, A.L. (2017). The Kinetochores Receptor for the Cohesin Loading Complex. *Cell* *171*, 72-84.e13.
- Holland, A.J., Fachinetti, D., Han, J.S., and Cleveland, D.W. (2012). Inducible, reversible system for the rapid and complete degradation of proteins in mammalian cells. *PNAS* *109*, E3350–E3357.
- Horsfield, J.A., Anagnostou, S.H., Hu, J.K.-H., Cho, K.H.Y., Geisler, R., Lieschke, G., Crosier, K.E., and Crosier, P.S. (2007). Cohesin-dependent regulation of Runx genes. *Development* *134*, 2639–2649.
- Hu, B., Itoh, T., Mishra, A., Katoh, Y., Chan, K.-L., Upcher, W., Godlee, C., Roig, M.B., Shirahige, K., and Nasmyth, K. (2011). ATP Hydrolysis Is Required for Relocating Cohesin from Sites Occupied by Its Scc2/4 Loading Complex. *Curr Biol* *21*, 12–24.
- Hu, B., Petela, N., Kurze, A., Chan, K.-L., Chapard, C., and Nasmyth, K. (2015). Biological chromodynamics: a general method for measuring protein occupancy across the genome by calibrating ChIP-seq. *Nucleic Acids Res* *43*, e132.
- Huang, H., Feng, J., Famulski, J., Rattner, J.B., Liu, S.T., Kao, G.D., Muschel, R., Chan, G.K.T., and Yen, T.J. (2007). Tripin/hSgo2 recruits MCAK to the inner centromere to correct defective kinetochores attachments. *J Cell Biol* *177*, 413–424.

- Ishiguro, T., Tanaka, K., Sakuno, T., and Watanabe, Y. (2010). Shugoshin–PP2A counteracts casein-kinase-1-dependent cleavage of Rec8 by separase. *Nature Cell Biology* *12*, 500–506.
- Ito, H., Fukuda, Y., Murata, K., and Kimura, A. (1983). Transformation of intact yeast cells treated with alkali cations. *J. Bacteriol.* *153*, 163–168.
- Kanke, M., Nishimura, K., Kanemaki, M., Kakimoto, T., Takahashi, T.S., Nakagawa, T., and Masukata, H. (2011). Auxin-inducible protein depletion system in fission yeast. *BMC Cell Biology* *12*, 8.
- Katis, V.L., Galova, M., Rabitsch, K.P., Gregan, J., and Nasmyth, K. (2004). Maintenance of Cohesin at Centromeres after Meiosis I in Budding Yeast Requires a Kinetochores-Associated Protein Related to MEI-S332. *Current Biology* *14*, 560–572.
- Katis, V.L., Lipp, J.J., Imre, R., Bogdanova, A., Okaz, E., Habermann, B., Mechtler, K., Nasmyth, K., and Zachariae, W. (2010). Rec8 Phosphorylation by Casein Kinase 1 and Cdc7-Dbf4 Kinase Regulates Cohesin Cleavage by Separase during Meiosis. *Developmental Cell* *18*, 397–409.
- Kawashima, S.A., Tsukahara, T., Langeegger, M., Hauf, S., Kitajima, T.S., and Watanabe, Y. (2007). Shugoshin enables tension-generating attachment of kinetochores by loading Aurora to centromeres. *Genes Dev.* *21*, 420–435.
- Kawashima, S.A., Yamagishi, Y., Honda, T., Ishiguro, K., and Watanabe, Y. (2010). Phosphorylation of H2A by Bub1 Prevents Chromosomal Instability Through Localizing Shugoshin. *Science* *327*, 172–177.
- Keeney, S., Giroux, C.N., and Kleckner, N. (1997). Meiosis-Specific DNA Double-Strand Breaks Are Catalyzed by Spo11, a Member of a Widely Conserved Protein Family. *Cell* *88*, 375–384.
- Kerrebrock, A.W., Moore, D.P., Wu, J.S., and Orr-Weaver, T.L. (1995). Mei-S332, a drosophila protein required for sister-chromatid cohesion, can localize to meiotic centromere regions. *Cell* *83*, 247–256.
- Kiburz, B.M., Reynolds, D.B., Megee, P.C., Marston, A.L., Lee, B.H., Lee, T.I., Levine, S.S., Young, R.A., and Amon, A. (2005). The core centromere and Sgo1 establish a 50-kb cohesin-protected domain around centromeres during meiosis I. *Genes Dev* *19*, 3017–3030.

- Kitajima, T.S., Kawashima, S.A., and Watanabe, Y. (2004). The conserved kinetochore protein shugoshin protects centromeric cohesion during meiosis. *Nature* *427*, 510–517.
- Kitajima, T.S., Hauf, S., Ohsugi, M., Yamamoto, T., and Watanabe, Y. (2005). Human Bub1 Defines the Persistent Cohesion Site along the Mitotic Chromosome by Affecting Shugoshin Localization. *Current Biology* *15*, 353–359.
- Kitajima, T.S., Sakuno, T., Ishiguro, K., Iemura, S., Natsume, T., Kawashima, S.A., and Watanabe, Y. (2006). Shugoshin collaborates with protein phosphatase 2A to protect cohesin. *Nature* *441*, 46–52.
- Klein, F., Mahr, P., Galova, M., Buonomo, S.B.C., Michaelis, C., Nairz, K., and Nasmyth, K. (1999). A Central Role for Cohesins in Sister Chromatid Cohesion, Formation of Axial Elements, and Recombination during Yeast Meiosis. *Cell* *98*, 91–103.
- Kogut, I., Wang, J., Guacci, V., Mistry, R.K., and Megee, P.C. (2009). The Scc2/Scc4 cohesin loader determines the distribution of cohesin on budding yeast chromosomes. *Genes Dev* *23*, 2345–2357.
- Kugou, K., and Ohta, K. (2009). Genome-Wide High-Resolution Chromatin Immunoprecipitation of Meiotic Chromosomal Proteins in *Saccharomyces cerevisiae*. In *Meiosis*, (Humana Press), pp. 285–304.
- Kuliev, A., Cieslak, J., and Verlinsky, Y. (2005). Frequency and distribution of chromosome abnormalities in human oocytes. *CGR* *111*, 193–198.
- Lee, J., Kitajima, T.S., Tanno, Y., Yoshida, K., Morita, T., Miyano, T., Miyake, M., and Watanabe, Y. (2008). Unified mode of centromeric protection by shugoshin in mammalian oocytes and somatic cells. *Nat. Cell Biol.* *10*, 42–52.
- Lee, J.Y., Dej, K.J., Lopez, J.M., and Orr-Weaver, T.L. (2004). Control of Centromere Localization of the MEI-S332 Cohesion Protection Protein. *Current Biology* *14*, 1277–1283.
- Lengronne, A., Katou, Y., Mori, S., Yokobayashi, S., Kelly, G.P., Itoh, T., Watanabe, Y., Shirahige, K., and Uhlmann, F. (2004). Cohesin relocation from sites of chromosomal loading to places of convergent transcription. *Nature* *430*, 573–578.
- Lengronne, A., McIntyre, J., Katou, Y., Kanoh, Y., Hopfner, K.-P., Shirahige, K., and Uhlmann, F. (2006). Establishment of Sister Chromatid Cohesion at the *S. cerevisiae* Replication Fork. *Molecular Cell* *23*, 787–799.

- Lister, L.M., Kouznetsova, A., Hyslop, L.A., Kalleas, D., Pace, S.L., Barel, J.C., Nathan, A., Floros, V., Adelfalk, C., Watanabe, Y., et al. (2010). Age-Related Meiotic Segregation Errors in Mammalian Oocytes Are Preceded by Depletion of Cohesin and Sgo2. *Current Biology* 20, 1511–1521.
- Liu, H., Jia, L., and Yu, H. (2013a). Phospho-H2A and Cohesin Specify Distinct Tension-Regulated Sgo1 Pools at Kinetochores and Inner Centromeres. *Current Biology* 23, 1927–1933.
- Liu, H., Rankin, S., and Yu, H. (2013b). Phosphorylation-enabled binding of SGO1–PP2A to cohesin protects sororin and centromeric cohesion during mitosis. *Nature Cell Biology* 15, 40–49.
- Lopez-Serra, L., Lengronne, A., Borges, V., Kelly, G., and Uhlmann, F. (2013). Budding Yeast Wapl Controls Sister Chromatid Cohesion Maintenance and Chromosome Condensation. *Current Biology* 23, 64–69.
- Lopez-Serra, L., Kelly, G., Patel, H., Stewart, A., and Uhlmann, F. (2014). The Scc2–Scc4 complex acts in sister chromatid cohesion and transcriptional regulation by maintaining nucleosome-free regions. *Nature Genetics* 46, 1147.
- Marston, A.L., Lee, B.H., and Amon, A. (2003). The Cdc14 Phosphatase and the FEAR Network Control Meiotic Spindle Disassembly and Chromosome Segregation. *Developmental Cell* 4, 711–726.
- Marston, A.L., Tham, W.-H., Shah, H., and Amon, A. (2004). A Genome-Wide Screen Identifies Genes Required for Centromeric Cohesion. *Science* 303, 1367–1370.
- Martin, R.H., and Rademaker, A. (1990). The frequency of aneuploidy among individual chromosomes in 6,821 human sperm chromosome complements. *Cytogenet. Cell Genet.* 53, 103–107.
- Matos, J., Lipp, J.J., Bogdanova, A., Guillot, S., Okaz, E., Junqueira, M., Shevchenko, A., and Zachariae, W. (2008). Dbf4-Dependent Cdc7 Kinase Links DNA Replication to the Segregation of Homologous Chromosomes in Meiosis I. *Cell* 135, 662–678.
- Melby, T.E., Ciampaglio, C.N., Briscoe, G., and Erickson, H.P. (1998). The Symmetrical Structure of Structural Maintenance of Chromosomes (SMC) and MukB Proteins: Long, Antiparallel Coiled Coils, Folded at a Flexible Hinge. *The Journal of Cell Biology* 142, 1595–1604.

- Michaelis, C., Ciosk, R., and Nasmyth, K. (1997). Cohesins: Chromosomal Proteins that Prevent Premature Separation of Sister Chromatids. *Cell* *91*, 35–45.
- Misulovin, Z., Schwartz, Y.B., Li, X.-Y., Kahn, T.G., Gause, M., MacArthur, S., Fay, J.C., Eisen, M.B., Pirrotta, V., Biggin, M.D., et al. (2008). Association of cohesin and Nipped-B with transcriptionally active regions of the *Drosophila melanogaster* genome. *Chromosoma* *117*, 89–102.
- Molnar, M., Bähler, J., Sipiczki, M., and Kohli, J. (1995). The *rec8* gene of *Schizosaccharomyces pombe* is involved in linear element formation, chromosome pairing and sister-chromatid cohesion during meiosis. *Genetics* *141*, 61–73.
- Nakajima, Y., Tyers, R.G., Wong, C.C.L., Yates, J.R., Drubin, D.G., and Barnes, G. (2009). Nbl1p: A Borealin/Dasra/CSC-1-like Protein Essential for Aurora/Ipl1 Complex Function and Integrity in *Saccharomyces cerevisiae*. *Mol. Biol. Cell* *20*, 1772–1784.
- Nasmyth, K., and Haering, C.H. (2009). Cohesin: Its Roles and Mechanisms. *Annual Review of Genetics* *43*, 525–558.
- Natsume, T., Müller, C.A., Katou, Y., Retkute, R., Gierliński, M., Araki, H., Blow, J.J., Shirahige, K., Nieduszynski, C.A., and Tanaka, T.U. (2013). Kinetochores Coordinate Pericentromeric Cohesion and Early DNA Replication by Cdc7-Dbf4 Kinase Recruitment. *Molecular Cell* *50*, 661–674.
- Nishimura, K., Fukagawa, T., Takisawa, H., Kakimoto, T., and Kanemaki, M. (2009). An auxin-based degron system for the rapid depletion of proteins in nonplant cells. *Nat Meth* *6*, 917–922.
- Ocampo-Hafalla, M.T., and Uhlmann, F. (2011). Cohesin loading and sliding. *J Cell Sci* *124*, 685–691.
- Ocampo-Hafalla, M., Muñoz, S., Samora, C.P., and Uhlmann, F. (2016). Evidence for cohesin sliding along budding yeast chromosomes. *Open Biology* *6*, 150178.
- Oelschlaegel, T., Schwickart, M., Matos, J., Bogdanova, A., Camasses, A., Havlis, J., Shevchenko, A., and Zachariae, W. (2005). The Yeast APC/C Subunit Mnd2 Prevents Premature Sister Chromatid Separation Triggered by the Meiosis-Specific APC/C-Ama1. *Cell* *120*, 773–788.

- O'Geen, H., Echipare, L., and Farnham, P.J. (2011). Using ChIP-Seq Technology to Generate High-Resolution Profiles of Histone Modifications. In *Epigenetics Protocols*, (Humana Press), pp. 265–286.
- Okaz, E., Argüello-Miranda, O., Bogdanova, A., Vinod, P.K., Lipp, J.J., Markova, Z., Zagoriy, I., Novak, B., and Zachariae, W. (2012). Meiotic Prophase Requires Proteolysis of M Phase Regulators Mediated by the Meiosis-Specific APC/C<sup>Ama1</sup>. *Cell* *151*, 603–618.
- Orr-Weaver, T.L. (1999). The Ties that Bind: Localization of the Sister-Chromatid Cohesin Complex on Yeast Chromosomes. *Cell* *99*, 1–4.
- Park, P.J. (2009). ChIP-seq: advantages and challenges of a maturing technology. *Nat Rev Genet* *10*, 669–680.
- Pauli, A., van Bommel, J.G., Oliveira, R.A., Itoh, T., Shirahige, K., van Steensel, B., and Nasmyth, K. (2010). A Direct Role for Cohesin in Gene Regulation and Ecdysone Response in *Drosophila* Salivary Glands. *Current Biology* *20*, 1787–1798.
- Petronczki, M., Siomos, M.F., and Nasmyth, K. (2003). Un Ménage à Quatre: The Molecular Biology of Chromosome Segregation in Meiosis. *Cell* *112*, 423–440.
- Petronczki, M., Matos, J., Mori, S., Gregan, J., Bogdanova, A., Schwickart, M., Mechtler, K., Shirahige, K., Zachariae, W., and Nasmyth, K. (2006). Monopolar Attachment of Sister Kinetochores at Meiosis I Requires Casein Kinase 1. *Cell* *126*, 1049–1064.
- Rabitsch, K.P., Petronczki, M., Javerzat, J.-P., Genier, S., Chwalla, B., Schleiffer, A., Tanaka, T.U., and Nasmyth, K. (2003). Kinetochores Recruitment of Two Nucleolar Proteins Is Required for Homolog Segregation in Meiosis I. *Developmental Cell* *4*, 535–548.
- Rabitsch, K.P., Gregan, J., Schleiffer, A., Javerzat, J.-P., Eisenhaber, F., and Nasmyth, K. (2004). Two Fission Yeast Homologs of *Drosophila* Mei-S332 Are Required for Chromosome Segregation during Meiosis I and II. *Current Biology* *14*, 287–301.
- Rankin, S. (2015). Complex elaboration: making sense of meiotic cohesin dynamics. *FEBS J* *282*, 2426–2443.
- Resnick, T.D., Satinover, D.L., MacIsaac, F., Stukenberg, P.T., Earnshaw, W.C., Orr-Weaver, T.L., and Carmena, M. (2006). INCENP and Aurora B Promote Meiotic Sister

- Chromatid Cohesion through Localization of the Shugoshin MEI-S332 in *Drosophila*. *Developmental Cell* *11*, 57–68.
- Riedel, C.G., Katis, V.L., Katou, Y., Mori, S., Itoh, T., Helmhart, W., Gálová, M., Petronczki, M., Gregan, J., Cetin, B., et al. (2006). Protein phosphatase 2A protects centromeric sister chromatid cohesion during meiosis I. *Nature* *441*, 53–61.
- Roberts, B.T., Farr, K.A., and Hoyt, M.A. (1994). The *Saccharomyces cerevisiae* checkpoint gene BUB1 encodes a novel protein kinase. *Mol. Cell. Biol.* *14*, 8282–8291.
- Rosbach, D., and Sclafani, R.A. (2016). Role of DDK in Replication Initiation. In *The Initiation of DNA Replication in Eukaryotes*, (Springer, Cham), pp. 279–296.
- Ruchaud, S., Carmena, M., and Earnshaw, W.C. (2007). Chromosomal passengers: conducting cell division. *Nat Rev Mol Cell Biol* *8*, 798–812.
- Salah, S.M., and Nasmyth, K. (2000). Destruction of the securin Pds1p occurs at the onset of anaphase during both meiotic divisions in yeast. *Chromosoma* *109*, 27–34.
- Salic, A., Waters, J.C., and Mitchison, T.J. (2004). Vertebrate Shugoshin Links Sister Centromere Cohesion and Kinetochore Microtubule Stability in Mitosis. *Cell* *118*, 567–578.
- Sherman, F. (1991). Getting started with yeast. *Methods Enzymol.* *194*, 3–21.
- Sjögren, C., and Nasmyth, K. (2001). Sister chromatid cohesion is required for postreplicative double-strand break repair in *Saccharomyces cerevisiae*. *Current Biology* *11*, 991–995.
- Stigler, J., Çamdere, G.Ö., Koshland, D.E., and Greene, E.C. (2016). Single-Molecule Imaging Reveals a Collapsed Conformational State for DNA-Bound Cohesin. *Cell Reports* *15*, 988–998.
- Sullivan, M., Hornig, N.C.D., Porstmann, T., and Uhlmann, F. (2004). Studies on Substrate Recognition by the Budding Yeast Separase. *J. Biol. Chem.* *279*, 1191–1196.
- Sumara, I., Vorlaufer, E., Gieffers, C., Peters, B.H., and Peters, J.-M. (2000). Characterization of Vertebrate Cohesin Complexes and Their Regulation in Prophase. *The Journal of Cell Biology* *151*, 749–762.

- Sumara, I., Vorlaufer, E., Stukenberg, P.T., Kelm, O., Redemann, N., Nigg, E.A., and Peters, J.-M. (2002). The dissociation of cohesin from chromosomes in prophase is regulated by Polo-like kinase. *Mol. Cell* *9*, 515–525.
- Tanaka, T., Cosma, M.P., Wirth, K., and Nasmyth, K. (1999). Identification of Cohesin Association Sites at Centromeres and along Chromosome Arms. *Cell* *98*, 847–858.
- Tanco, M., Viles, E., Ilzarbe, L., and Álvarez, M.J. (2007). Manufacturing Industries Need Design of Experiments (DoE). Proceedings of the World Congress on Engineering. WCE , July 2 - 4, 2007, London, U.K. *Vol II*.
- Tang, Z., Sun, Y., Harley, S.E., Zou, H., and Yu, H. (2004). Human Bub1 protects centromeric sister-chromatid cohesion through Shugoshin during mitosis. *PNAS* *101*, 18012–18017.
- Tang, Z., Shu, H., Qi, W., Mahmood, N.A., Mumby, M.C., and Yu, H. (2006). PP2A Is Required for Centromeric Localization of Sgo1 and Proper Chromosome Segregation. *Developmental Cell* *10*, 575–585.
- Tóth, A., Rabitsch, K.P., Gálová, M., Schleiffer, A., Buonomo, S.B.C., and Nasmyth, K. (2000). Functional Genomics Identifies Monopolin: A Kinetochores Protein Required for Segregation of Homologs during Meiosis I. *Cell* *103*, 1155–1168.
- Uhlmann, F., Lottspeich, F., and Nasmyth, K. (1999). Sister-chromatid separation at anaphase onset is promoted by cleavage of the cohesin subunit Scc1. *Nature* *400*, 21831.
- Uhlmann, F., Wernic, D., Poupart, M.-A., Koonin, E.V., and Nasmyth, K. (2000). Cleavage of Cohesin by the CD Clan Protease Separin Triggers Anaphase in Yeast. *Cell* *103*, 375–386.
- W Y Miyazaki, and Orr-Weaver, and T.L. (1994). Sister-Chromatid Cohesion in Mitosis and Meiosis. *Annual Review of Genetics* *28*, 167–187.
- Wach, A., Brachat, A., Pöhlmann, R., and Philippsen, P. (1994). New heterologous modules for classical or PCR-based gene disruptions in *Saccharomyces cerevisiae*. *Yeast* *10*, 1793–1808.
- Waizenegger, I.C., Hauf, S., Meinke, A., and Peters, J.-M. (2000). Two Distinct Pathways Remove Mammalian Cohesin from Chromosome Arms in Prophase and from Centromeres in Anaphase. *Cell* *103*, 399–410.

- Watanabe, Y., and Nurse, P. (1999). Cohesin Rec8 is required for reductional chromosome segregation at meiosis. *Nature* *400*, 461–464.
- Xu, Z., Cetin, B., Anger, M., Cho, U.S., Helmhart, W., Nasmyth, K., and Xu, W. (2009). Structure and Function of the PP2A-Shugoshin Interaction. *Molecular Cell* *35*, 426–441.
- Yamagishi, Y., Sakuno, T., Shimura, M., and Watanabe, Y. (2008). Heterochromatin links to centromeric protection by recruiting shugoshin. *Nature* *455*, 251–255.
- Yao, Y., and Dai, W. (2012). Shugoshins function as a guardian for chromosomal stability in nuclear division. *Cell Cycle* *11*, 2631–2642.
- Yu, H.-G., and Koshland, D. (2005). Chromosome Morphogenesis: Condensin-Dependent Cohesin Removal during Meiosis. *Cell* *123*, 397–407.
- Zachariae, W. (2004). Destruction with a Box: Substrate Recognition by the Anaphase-Promoting Complex. *Molecular Cell* *13*, 2–3.
- Zhang, L., Ward, J.D., Cheng, Z., and Dernburg, A.F. (2015). The auxin-inducible degradation (AID) system enables versatile conditional protein depletion in *C. elegans*. *Development* *142*, 4374–4384.
- Zuin, J., Franke, V., IJcken, W.F.J. van, Sloot, A. van der, Krantz, I.D., Reijden, M.I.J.A. van der, Nakato, R., Lenhard, B., and Wendt, K.S. (2014). A Cohesin-Independent Role for NIPBL at Promoters Provides Insights in CdLS. *PLOS Genetics* *10*, e1004153.

## 8. Appendix

	-	+	Center point
tFix (min)	8	20	14
tShear (min)	20	40	30
Cell density (%)	33%	100%	67%
Power (Watts)	100	200	150
Duty factor (%)	5	15	10
cFix (%)	2	4	3
Cycles/burst	133	266	200
Buffer	self-mixed	TrueChIP	

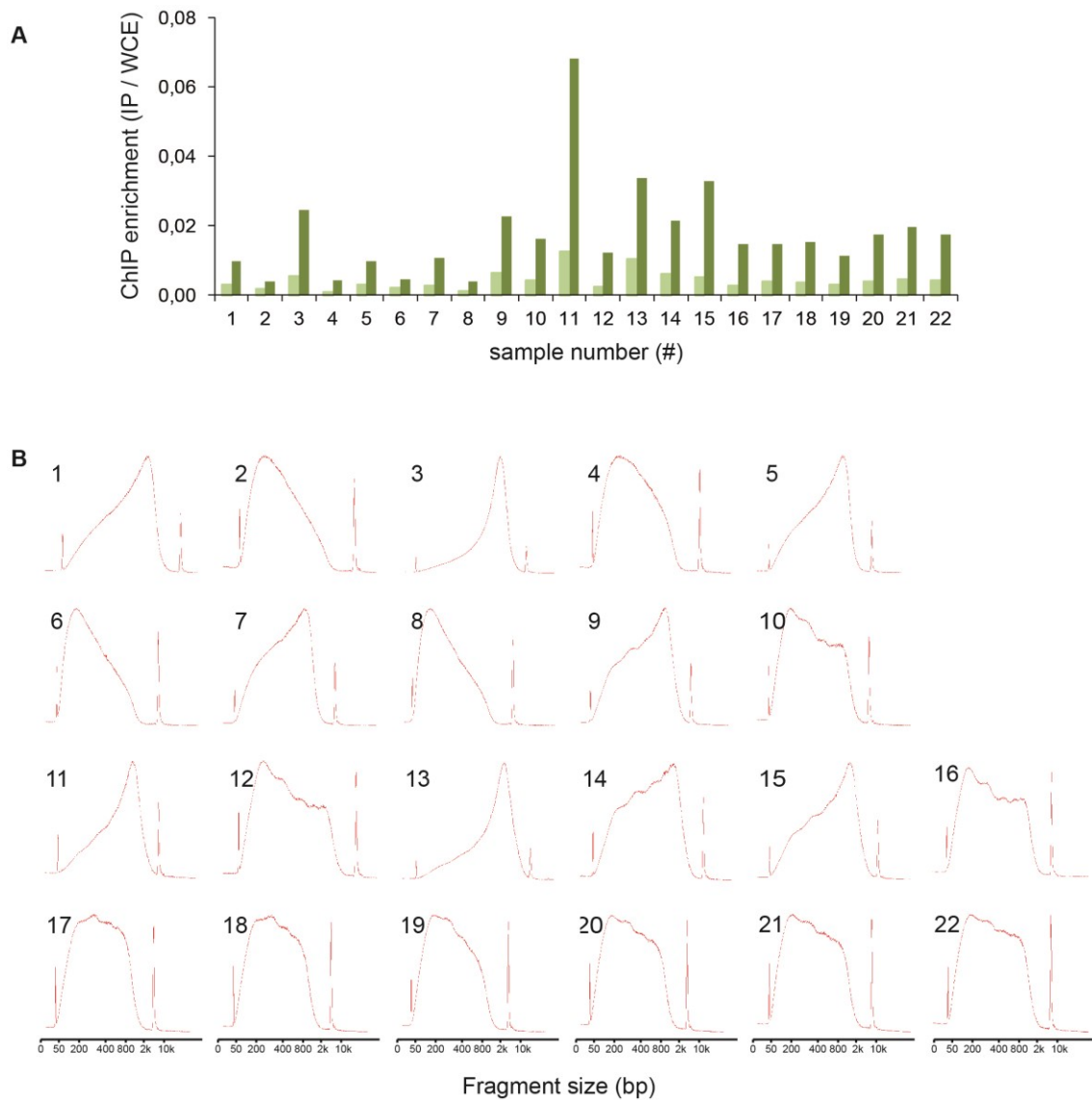
Sample #	tFix	tShear	Density	Power	Duty	cFix	Cycles	Buffer
1	8	20	33%	100	5	2	133 self-mixed	
2	20	20	33%	100	15	4	266 self-mixed	
3	8	40	33%	100	15	4	133 TrueChIP	
4	20	40	33%	100	5	2	266 TrueChIP	
5	8	20	100%	100	15	2	266 TrueChIP	
6	20	20	100%	100	5	4	133 TrueChIP	
7	8	40	100%	100	5	4	266 self-mixed	
8	20	40	100%	100	15	2	133 self-mixed	
9	8	20	33%	200	5	4	266 TrueChIP	
10	20	20	33%	200	15	2	133 TrueChIP	
11	8	40	33%	200	15	2	266 self-mixed	
12	20	40	33%	200	5	4	133 self-mixed	
13	8	20	100%	200	15	4	133 self-mixed	
14	20	20	100%	200	5	2	266 self-mixed	
15	8	40	100%	200	5	2	133 TrueChIP	
16	20	40	100%	200	15	4	266 TrueChIP	
17	14	30	67%	150	10	3	200 self-mixed	
18	14	30	67%	150	10	3	200 self-mixed	
19	14	30	67%	150	10	3	200 TrueChIP	
20	14	30	67%	150	10	3	200 TrueChIP	

Appendix Figure A 1: *Experimental plan for a 2-level fractional factorial design with resolution IV. Upper table shows the two values for each of the eight input factors. The lower table shows the combination of the input factor values for each of the 16 runs and the two center points in such a way that the design matrix is orthogonal.*

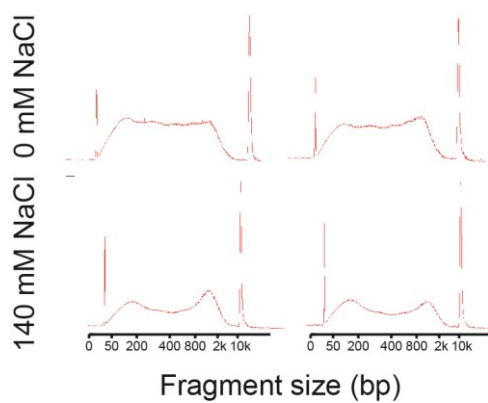
	-	+	Center point
tShear (min)	10	30	20
c(NaCl) for IP	80	200	140
Protease inhibs	100X	100X, Comp, Pepstat	
tFix (min)	5	35	20
Power (Watts)	100	100	100
Cell density (%)	50	50	50
Cycles/burst	200	200	200
cFix (%)	3	3	3
Duty factor (%)	10	10	10

Sample #	tShear	c(NaCl) for IP	Protease inhibs	tFix
1	10	80	100X	5
2	30	80	100X	5
3	10	200	100X	5
4	30	200	100X	5
5	10	80	100X, Comp, Pepstat	5
6	30	80	100X, Comp, Pepstat	5
7	10	200	100X, Comp, Pepstat	5
8	30	200	100X, Comp, Pepstat	5
9	10	80	100X	35
10	30	80	100X	35
11	10	200	100X	35
12	30	200	100X	35
13	10	80	100X, Comp, Pepstat	35
14	30	80	100X, Comp, Pepstat	35
15	10	200	100X, Comp, Pepstat	35
16	30	200	100X, Comp, Pepstat	35
17	20	140	100X	20
18	20	140	100X	20
19	20	140	100X	20
20	20	140	100X, Comp, Pepstat	20
21	20	140	100X, Comp, Pepstat	20
22	20	140	100X, Comp, Pepstat	20

*Appendix Figure A 2: Experimental plan for a 2-level full factorial design. The upper table shows the two values for each of the input factors. For this design, only four input factors were altered. The lower table shows the combination of the input factor values for each of the 16 runs and the two center points in such a way that the design matrix is orthogonal.*



*Appendix Figure A 3: Measured values of the output factors “ChIP-qPCR” and “Shearing” after realization of the full factorial design, comprising 16 runs and two sets of triplicates. (A) ChIP-qPCR values for 22 samples. For each sample the values of two different loci were measured in duplicates. The y-axis denotes the enrichment in the immunoprecipitation samples (IP) over the whole cell extract samples (WCE). Samples 1 to 16 are the experimental runs with changing input parameter values. Samples 17 to 22 define the center points. (B) Bioanalyzer profiles of the same 22 samples show the chromatin fragment size distributions after shearing on a Covaris water bath sonicator. The horizontal axis on the small diagrams denotes the fragment size in base pairs.*



*Appendix Figure A 4: Effect of the shearing buffer salt concentration on the chromatin fragment size distribution after sonication. The horizontal axis on the small Bioanalyzer diagrams denotes the fragment size in base pairs.*

